HERON is jointly edited by:
STEVIN-LABORATORY of the faculty of Civil Engineering, Delft University of Technology, Delft, The Netherlands
and
TNO BUILDING AND CONSTRUCTION RESEARCH. Rijswijk (ZH), The Netherlands
HERON contains contributions based mainly on research work performed in these laboratories on strength of materials, structures and materials science.

ISSN 0046-7316

This publication has been issued in close co-operation with the Netherlands Technology Foundation (STW)

Secretary:
J. G. M. van Mier
Stevinweg 1
P.O. Box 5048
2600 GA Delft, The Netherlands
Tel. 0031-15-784578
Fax 0031-15-611465
Telex 38151 BUTUD

HERON vol. 38 1993 no. 2

Contents

EXPERIMENTAL AND NUMERICAL ANALYSIS OF FRACTURE PROCESSES IN CONCRETE

Erik Schlangen

Publication in HERON since 1970

Acknowledgements

The research reported was carried out at the Stevin Laboratory of the Civil Engineering Department of Delft University of Technology.
I would like to express my gratitude to my supervisor Dr. Jan Van Mier for his guidance and fruitful discussions throughout the research.
I am also grateful for the help of Professor J. C. Walraven, who contributed his valuable comments.
Furthermore I would like to thank all the colleagues of the Concrete Structures Group and the Measurements and Instrumentation Group for their help and support in the various parts of this research. I am particularly indebted to Mr. Allard Elgersma for his expert help in performing all the experiments with great precision.
I would also like to thank Dr. H. J. Herrmann and co-workers from HLRZ KFA, Jülich, Germany, for the inspiring discussions about fracture simulations and Dr. C. Moukarzel for providing the input data for the random lattice.
The financial support provided by the Dutch Technology Foundation (STW grant DCT 81.1491) is gratefully acknowledged. The additional financial support by the "Stichting Professor Bakkerfonds" is also highly appreciated. The research was carried out under the auspices of CUR research committee A 30 "Concrete Mechanics".

Summary

A combined experimental and numerical approach is adopted to investigate fracture processes in concrete. The experimental programme focuses on the failure of concrete subjected to mixed mode I and II loading. The influence of shear load on the nucleation and propagation of cracks in concrete is studied by means of four-point-shear tests on single and double edge notched beams. A numerical model for simulating fracture is developed in which the heterogeneous microstructure of concrete is implemented. The model is used to carry out simulations of different fracture experiments.

In Chapter 1 of this report the subject of the investigation is clarified. Chapter 2 deals with a summary of research regarding tensile fracture and combined tensile and shear fracture of concrete. An overview of different types of experiments is given. Furthermore numerical models and simulations of fracture tests are discussed. The experiments conducted in the present investigation are described in Chapter 3. Beam specimens with one or two notches, made of different concrete mixes are loaded in four-point-shear. All experiments are carried out under displacement control using a closed loop hydraulic system. In the developed test set-up experiments can be carried out either with freely rotating or fixed supports. The results of the various experiments are presented in Chapter 4. The experimental outcome is presented by means of crack patterns, different load-deformation curves and details of cracks obtained with an optical microscope. In Chapter 5 the numerical model is explained. Different ways of implementing heterogeneity are presented. The determination of the various input parameters is discussed. Simulations of different types of experiments are presented in Chapter 6, i.e. uniaxial tensile tests, four-point-shear tests, pull-out of anchor bolts and mixed mode tests on plate specimens. The last chapter includes a discussion of the results and a summary of the conclusions.

The main conclusion derived from the experimental part of this investigation is that fracture in concrete is a mode I mechanism, even if the external loading on a specimen is a combination of tensile and shear. The numerical model developed has proved able to predict fracture in concrete quite accurately. Simulations with the model increase insight into the fracture mechanism.

Symbols

The following symbols are used in this report

A	cross-sectional area
a	notch depth
b	specimen depth
c	distance between the two middle supports
CMOD	crack mouth opening displacement
CMSD	crack mouth sliding displacement
con8	normal weight concrete with maximum aggregate size of 8 mm
con16	normal weight concrete with maximum aggregate size of 16 mm
D, D_{max}	diameter
d	specimen depth
DEN	double edge notched
DIANA	finite element program, developed by TNO Building and Construction Research
E	Young's modulus
E_A, E_B, E_M	Young's modulus aggregate, bond, matrix
F	normal force
F_1, F_2	forces
F_{pre}	prescribed force
f_b	bending strength
f_c	compressive strength (150 mm cubes)
f_{spl}	splitting tensile strength (150 mm cubes)
f_t	tensile strength
$f_{t,A}, f_{t,B}, f_{t,M}$	tensile strength aggregate, bond, matrix
fcon	fibre reinforced concrete
G_f	fracture energy
h	beam height
hcp	hardened cement paste
hsc	high strength concrete
k	confinement
l	specimen length, beam length
LVDT	linear variable differential transducer
lytag	lytag lightweight concrete
$M_{i,j}$	bending moment
P	load
P_{pre}	prescribed external load
P_s	compressive shear load
RILEM	Réunion Internationale des Laboratoires d'Essais et de Recherches sur les Matériaux et les Constructions
SEN	single edge notched
t	speciment width

u_{pre}	prescribed nodal displacement
W	elastic section modulus ($= b * h^2/6$)
α	parameter
β	scaling factor, shear retention factor
γ	parameter
δ_1, δ_2	displacement, axial deformation
$\delta_s, \delta_{s,1}, \delta_{s,2}$	lateral deformation
σ_1, σ_2	stress
$\sigma_t, \sigma_{t,1}, \sigma_{t,2}$	tensile stress

Experimental and Numerical Analysis of Fracture Processes in Concrete

1 Introduction

In practice, structures made of concrete are full of cracks. The strength of concrete is mainly determined by the tensile strength, which is about 10 % of the compressive strength. Because of this, reinforcement (mostly steel) is used to increase the carrying capacity of the material and to control the development of cracks if concrete is loaded in tension. However for designing concrete structures, knowledge is required about the strength of the concrete material and about the process of fracture growth that takes place in the concrete. In this chapter the subject of this research, which deals with a particular part of fracture research in concrete, will be clarified. Furthermore a short summary of the contents of this report will be given.

1.1 *State of fracture research for concrete*

Concrete structures that fail, already show a large number of large and small cracks before their maximum carrying capacity is reached. The failure of concrete can be characterized by the nucleation and propagation of cracks until final collapse. The loading on a structure that leads to fracture can be of any kind. Cracks appear due to mechanical loading but shrinkage or temperature changes may also lead to cracking. However the concept of fracture mechanics has not yet been developed to the point where it is used as a design tool for concrete structures. The basics of fracture mechanics theory has been available since the beginning of this century, Griffith (1920). The question that (concrete fracture) researchers have tried to answer in the last decades is whether the application of fracture mechanics, which can be used to describe fracture growth in homogeneous brittle materials, can be extended to heterogeneous materials such as concrete.
In fracture mechanics three basic modes of loading on a crack are distinguished, see Figure 1.1. These three modes are described as opening mode (mode I), shearing mode (mode II) and tearing mode (mode III). Any arbitrary load in three-dimensional space can be expressed, at least in a linear theory, as a superposition of these three modes. For more details about the theory of fracture mechanics the reader is referred to textbooks, see for instance Broek (1984).

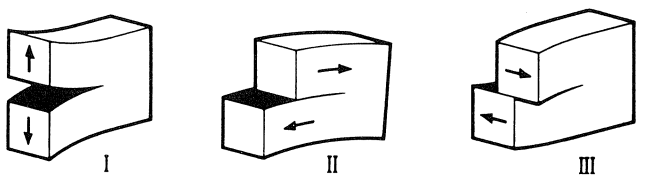

Fig. 1.1 Three modes of loading.

Experimental fracture studies for concrete mainly focus on deriving values to describe stress-strain curves for different modes, or combinations of modes. The resulting stress-strain relations are used as input for numerical models to simulate fracture problems. Examples of mode I and mixed mode I and II fracture studies in concrete will be discussed in Chapter 2. Mixed mode I and III are, among others, studied by Tokatly et al. (1989) and Arslan et al. (1991).

In recent years, concrete structures have become increasingly more sophisticated. Cementitious materials are now used under extreme conditions. It is essential that the behaviour of a material can be accurately predicted. This aim however, can only be achieved through a better understanding of the complete material. This means that knowledge is required about the structure of hardened cement paste, the behaviour of the composite of aggregate particles embedded in the matrix and also about the macroscopically observed behaviour in real structures. Wittmann (1983) proposed a hierarchic system of three different levels on which modelling of concrete can be applied. The models on the different levels should be interrelated in a systematic way, or more precisely models on a given level are based on the results of the previous level. The three levels are shown in Figure 1.2: (a) the micro level, which is concerned with the structure of the hardened cement paste; (b) the meso level, which deals with pores, inclusions, cracks and interfaces, and (c) the macro level, which is related to the structural element. In many investigations, as in this report, only two levels are considered if fracture of concrete is studied, i.e. the meso level (then called micro level) and the macro level.

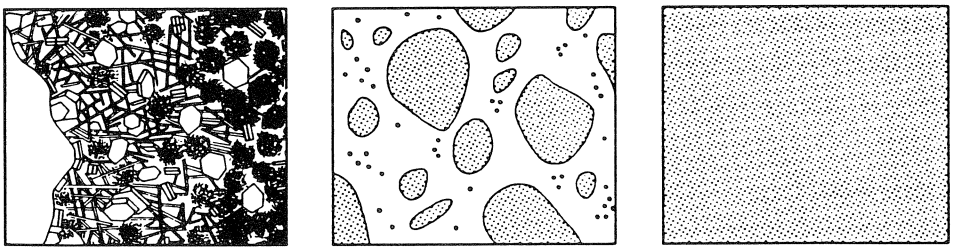

micro level meso level macro level

Fig. 1.2 Three level approach according to Wittmann (1983).

1.2 *Goal of research*

This investigation focuses on the mixed mode I and II fracture behaviour of concrete. It is not the purpose to extract nice relations which can be implemented into numerical codes; the intention is to find explanations why the fracture process is as it is.

In fracture studies the following procedure is often adopted. Measure the behaviour of a material in an experiment. Implement this behaviour in a computer code. Try to simulate fracture in experiments and real structures. However this will only give good results if the same experiment from which the behaviour is measured is simulated. For

the simulations of other experiments and real structures good predictions can be only obtained if the experiment from which the behaviour is derived is representative for the material. Moreover no geometrical factors should influence the measured results.
The procedure that should be followed in the author's opinion: carry out experiments in order to find a physical explanation for the observed phenomena and to increase the knowledge about the fracture behaviour in a material. Use this newly gained knowledge to develop numerical tools which can be used to simulate the behaviour.
This procedure is not new but has already proved successful in many applications. Below an old example recently used by Goldberg(1989) is included. It deals with a different subject. However, it reflects the developments in fracture mechanics research for concrete in recent years.

When man wanted to fly, he first turned to natural example - the bird - to develop his early notions of how to accomplish this difficult task. Notable failures by Daedalus and numerous bird-like contraptions (ornithopters) at first pointed in the wrong direction, but eventually, persistence and the abstraction of the appropriate knowledge (lift over an airfoil) resulted in successful glider and powered flight.

A second reason why an explanation of the fracture process is necessary is for the development of new materials, see Van Mier et al. (1991) and Schlangen & Van Mier (1992e). Especially in the case of concrete, it is important to know which steps have to be taken to improve the material. A further question regarding this is how the material properties and the fracture process of concrete will change if different types of aggregate particles are used in the concrete mix.
To achieve the above described abstraction of appropriate knowledge in order to find an explanation for fracture processes in concrete, a combined experimental and numerical approach is adopted. Both approaches are described in this report. Chapter 2 includes a discussion of research regarding mode I and mixed mode fracture in concrete conducted by others. In Chapter 3 the experimental approach followed in this investigation is presented. The results of the experiments are sketched in Chapter 4. The numerical micro mechanical model developed for a better understanding of fracture processes is explained in Chapter 5. Simulations of mode I and mixed mode I and II fracture problems are discussed in Chapter 6. Finally conclusions are drawn in Chapter 7.

2 What is already known

In this chapter a survey of literature will be given regarding fracture processes in concrete. This summary of research carried out by others is far from complete, and is coloured by the author's view. For a more extensive and objective overview the reader is referred to textbooks, journals and a large number of conference proceedings published recently about the subject. It should also be mentioned that because of the large amount of research that is going on in this field the opinions and knowledge are continuously changing. This overview therefore consists of a mixture of old and fresh

knowledge (in this context old means older than the start (1989) of this research). Since mixed-mode fracture is often seen as an extension of mode I fracture, the first paragraph deals with mode I fracture behaviour. The next item is the experimental treatment of mixed mode problems. Finally various numerical models will be discussed.

2.1 *Mode I fracture behaviour*

2.1.1 Fracture models

When studying fracture, concrete is mostly considered to be a homogeneous material. Thus fracture is studied on a macro level as described in Chapter 1. In that case the linear elastic fracture mechanics concept valid for homogeneous materials is not sufficient to describe the fracture process in concrete, because of the heterogeneity of the material which causes crack growth that consists of macro- and microcracks. Therefore non-linear fracture mechanics is introduced for the analysis of crack propagation in concrete structures on a macro level, where concrete is assumed to be homogeneous. Such an approach (Fictitious Crack Model) was first introduced by Hillerborg et al. (1976). A similar model (Crack Band Model) based on approximately the same principle has been developed by Bažant & Oh (1983).
The stress-strain curve of concrete loaded in tension shows an ascending branch, a peak which is called the tensile strength, and a descending branch or softening branch. The post-peak behaviour can only be measured if a stiff servo-controlled testing machine is available. Experiments have shown that beyond the peak, localisation of deformations (here defeormation means elongation of the specimen) in a small region of the test specimen occurs. According to the Fictitious Crack Model, the behaviour of concrete under tensile loading can be devided into a stress-strain relation for the uncracked part of the specimen and a stress-crack opening relation for the crack itself, see Figure 2.1. In the Crack Band Model, the crack is smeared out over a zone of a certain width instead of using one localised crack.
In the above, the softening behaviour of concrete subjected to a tensile load is discussed. However in compression a comparable behaviour is observed. Here also localisation occurs, see Van Mier (1984) and Vonk (1992).

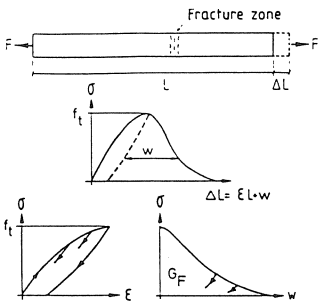

Fig. 2.1 Basics of the Fictitious Crack Model (Hillerborg et al. (1976)).

2.1.2 Definition of fracture parameters

The non-linear fracture models discussed in the previous paragraph are implemented in many codes for simulating fracture in concrete on a macro level, where concrete is assumed to be homogeneous. The softening behaviour measured in tension is then considered to be a material property. This behaviour has to be derived from a stable displacement controlled uniaxial tensile test. The parameters that define the first part of the measured response are: the initial stiffness E of the material and the tensile strength f_t. For the second part of the response, the softening curve, a definition of the shape should be introduced. Hordijk (1991) proposed the following equation which was fitted from experimental results:

$$\sigma/f_t = \{1 + (c_1 * w/w_c)^3\} * \exp(-c_2 * w/w_c) - w/w_c * (1 + c_1^3) * \exp(-c_2) \qquad (2.1)$$

where f_t is the tensile strength of the material, w_c is the maximum crack opening when no stress is transferred any more (at the end of the tail of the tensile softening diagram), and c_1 and c_2 are two empirical constants. From the post-peak diagram of Figure 2.1 the fracture energy G_f can be determined. G_f represents the area under the curve ($G_f = \int \sigma \, dw$). The various parameters are assumed to be material properties. They change if a different concrete composition is used.

However, many researchers are doubtful about the assumption that the above mentioned parameters are really material properties. Difficulties that appear if the material properties (on a macro level) are to be measured are summarised in Van Mier (1992). The first problem that arises is which test should be used to measure the response. To derive the tensile properties a stable *direct* tensile test has to be performed. A uniform stress field should be applied to the cracking plane and the stress field should stay uniform during the fracture process. However in a heterogeneous material, the cracks will not be uniformly distributed, which also results in a non-uniform stress field. In addition, the test from which the parameters are to be derived should be representative for what happens in a real structure. However the stress field in a real structure made of a heterogeneous material will always be non-uniform.

Different experiments have been proposed and adopted for deriving the tensile properties. An overview of different uniaxial tensile tests is given in Hordijk(1989). To measure the softening curve from a uniaxial tensile test, a stable test should be performed in displacement control. For this a servo-controlled machine is required. Because of the localisation of fracture which takes place in a small zone, arrangements have to be made to ensure that the crack propagates inside the measurement zone. For this the specimen can be notched or given a dog bone shape, for instance. The measuring length must be small in order to get a continuously increasing deformation. For longer measuring lengths a snap back behaviour will take place as shown in Figure 2.2, see also Hordijk (1991). To perform a stable test Schorn & Berger-Böcker (1989) used unnotched specimens with several displacement transducers glued on the surface covering the entire length of the specimen. A fast system was used to switch between the signals of the transducers in such a way that the transducer with the most increasing deformation was used as feed back signal.

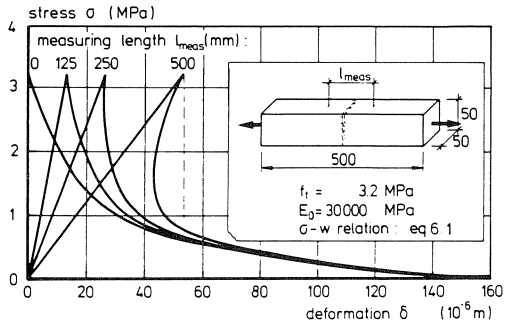

Fig. 2.2 Stress-deformation relation as influenced by measuring length (Hordijk (1991)).

In the experiments the boundary conditions are important, as was recognised first for experiments on concrete by Van Mier (1986). Uniaxial tensile tests between hinges are performed by Daerga (1992), for instance. Tests between fixed end platens are among others performed by Hordijk(1991). Both approaches lead to a different fracture mechanism. If freely rotating supports are used, the crack will start opening at one side and will gradually propagate to the other side. Using fixed supports again, the cracks start on one side. If the crack has traversed part of the specimen a bending moment will occur in the specimen which causes crack growth starting on the opposite side. Recently Carpinteri & Ferro (1993) proposed a test method with three actuators in which it is possible to obtain a more uniform opening of the crack. With this system the deformation measured at four corners of a specimen is kept constant. This means that part of the specimen with a length equal to the measuring length of the transducers opens uniformly. The measuring length is therefore very important in this case. Yet this procedure does not imply that the crack opens completely uniformly, because inside the measuring area (between the measuring points) non-uniform opening can and will still take place, as shown in Van Mier et al. (1993). Here simulations are carried out with the lattice model that will be explained in Chapter 5. Only the boundaries of the measuring area are kept parallel. An easier test to determine the fracture energy is proposed by RILEM TC-50 FMC (1985), i.e. a three-point-bending test on notched beams. For this geometry a correction method was recently proposed by Guinea et al.(1992), Planas et al.(1992) and Elices et al. (1992) in order to derive the fracture energy without having the effects of bulk energy dissipation, experimental procedures and size effects. However some assumptions made in this method are doubtful and it is not clear if this method is also valid for different types of experiments. Another test geometry used by Brühwiler (1988) for determining the fracture energy is the wedge splitting test. However, as all the different test geometries give different results the question arises: which one should be chosen?

A further problem already mentioned above is the size effect on tensile strength and fracture energy. The size effect on fracture energy is shown in Figure 2.3. These values are the result of a round robin by means of three point bending tests for determining the

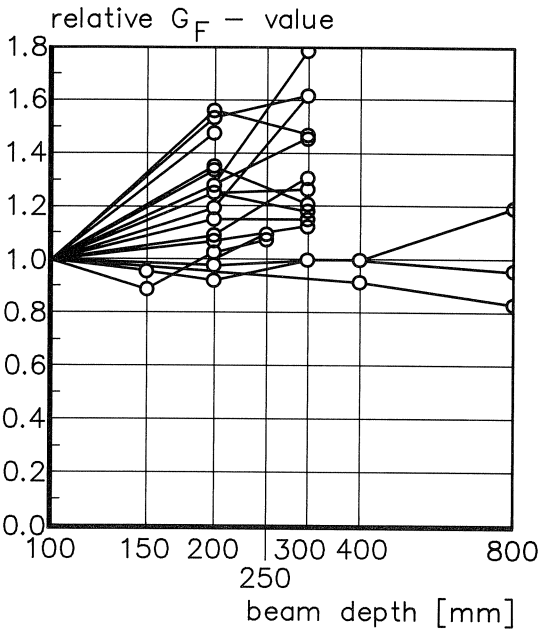

Fig. 2.3 Size effect in G_f (Hillerborg (1985)).

fracture energy. The G_f values reported by different laboratories are plotted against the beam depth of the specimen used. The determination of the fracture energy will be further discussed in paragraph 4.1.2.

2.1.3 Discussion of softening

There is a great deal of confusion about the physical explanation of the softening behaviour of concrete. The classical "explanation" is based on an analogy with the Dugdale-Barenblatt model for plastic metals. The fracture process zone is then considered to be a zone of discontinuous microcracking ahead of a continuous macrocrack as described by Mindess (1991). Many investigators have focused on proving the existence of this fracture process zone.

Two other explanations for the softening behaviour will be discussed here, i.e. friction between the crack faces and crack face bridging.

The first explanation is an aggregate interlock type phenomenon which was introduced by Walraven (1980) to study the effect of sliding between crack faces. Duda (1991) presented a grain model to explain the softening behaviour in tension that is based on the friction that occurs if aggregates are pulled out of the cement matrix. It is *assumed* that stress transfer between both crack surfaces is possible as long as the crack width perpendicular to the load is less than the effective roughness r at the contact surface, see Figure 2.4.

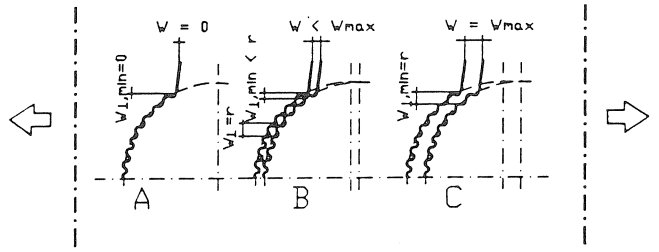

Fig. 2.4 Crack development at the interface between concrete and aggregate (Duda (1991)).

A more physically-based explanation for the softening behaviour of concrete is given by Van Mier (1990). Observations in fracture experiments showed a mechanism, i.e. crack face bridging, that can be found in all kinds of materials and on different scales, see Bremaecker & Svensson (1990). Van Mier (1990) adapted two approaches, i.e. a vacuum impregnation technique and an optical microscopy technique, for measuring the crack extension in uniaxial tensile tests on single edge notched specimens, see also paragraph 6.1. The main conclusions from the tests were the following. In the steep part of the load-average crack opening diagram, a macroscopic crack structure traverses the specimens cross-section. At larger crack openings (> 50 μm) the specimen is completely cracked. The remaining stress-transfer occurs through crack face bridging. The crack face bridges are found to develop mainly around aggregate particles with a higher stiffness than the surrounding matrix. Figure 2.5 shows an example of crack face bridging as found in experiments by using the impregnation technique. In Figure 2.6 the failure of a crack face bridge observed with a long distance microscope during the test is shown. The mechanism of crack face bridging is confirmed numerically by using micromechanical models, see Chapter 6 and Vonk (1992).

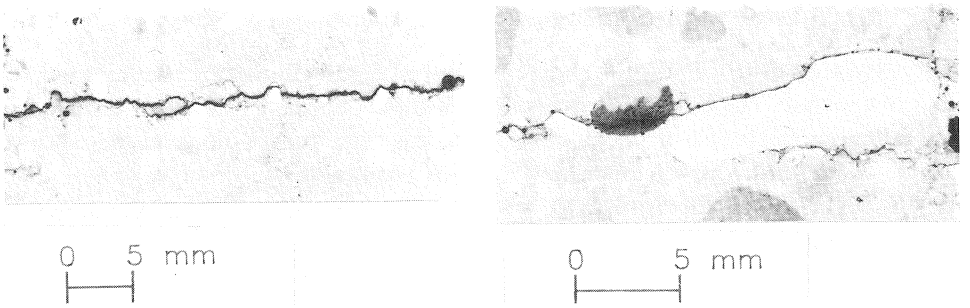

Fig. 2.5 Crack face bridging observed with a vacuum impregnation technique (Van Mier (1990)).

The size effect on tensile strength and fracture energy can probably be explained by the heterogeneous microstructure. As discussed before localisation of the cracks occurs in a small zone. The width of this zone depends on the aggregate size, which also defines the size of the crack face bridges. If the specimen size is changed, the ratio between aggregate size and specimen depth also changes. This of course leads to size effects.

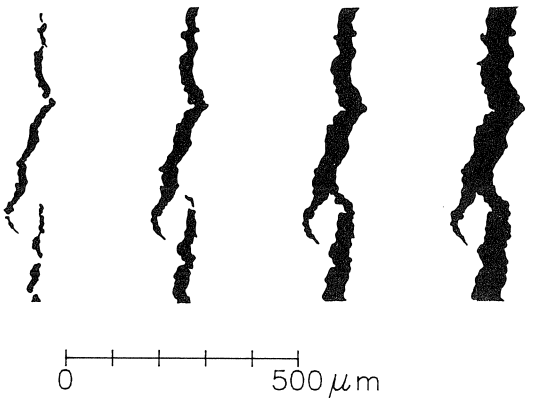

Fig. 2.6 Crack face bridging observed with optical microscope.

2.2 *Experimental treatment of the mixed mode fracture problem*

2.2.1 Various test procedures

There are two different ways in which the mixed mode fracture problem is studied. Both procedures try to investigate the influence of the shear loading on the fracture process. In the first case fracture propagation is studied when a crack tip is subjected to mixed mode loading. The second case focuses on the determination of material properties and the fracture extension of a partially cracked material loaded by a combination of tension and shear.

Examples of the first approach are four-point-shear geometries, three-point-bending beams with an eccentric placed notch and the pull-out of anchor bolts. The four-point-shear geometries will be discussed in the next paragraph. Eccentric notched beams are among others tested by Jenq & Shah (1987), see Figure 2.7, and by Swartz et al. (1988), see Figure 2.8. The main conclusion of these investigations was that mode I fracture parameters can be used as a first approximation to model mixed mode situations, but if the amount of shear stress is high compared to the tensile stress, shear friction and aggregate interlock effects can no longer be neglected.

The pull-out of anchor bolts has been investigated by many researchers. The test can be carried out as an axi-symmetric case or a plane stress case. The interpretation of axi-symmetric tests is difficult because of the complicated fracture patterns that occur, i.e. pull-out of a cone and radial cracking. The plane stress case was the subject of a round

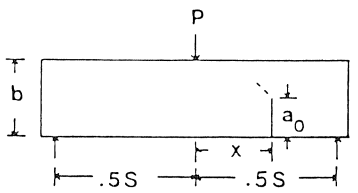

Fig. 2.7 Geometry used by Jenq & Shah (1987).

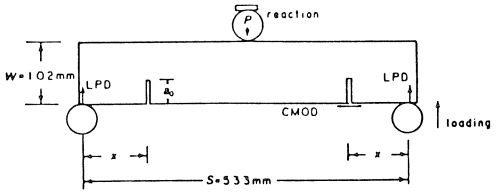

Fig. 2.8 Geometry used by Swartz et al. (1988).

robin analysis and was studied numerically and experimentally. The conclusions presented by different authors in Elfgren (1991) varied from "the mixed mode problem can be analysed with mode I parameters alone", to "mode II parameters have to be included". The resulting conclusion of the contribution of the Stevin Laboratory to the round robin was that the mechanism that takes place is a mode I fracture mechanism, see Vervuurt et al. (1993) and Chapter 6.

For the testing of the shear capacity of a partially cracked material, investigations were undertaken by Keuser (1989), Hassanzadeh (1992), and Nooru-Mohamed (1992).

Hollow cylindrical specimens, Figure 2.9, were adopted by Keuser (1989). The upper and lower part of the specimen were glued in a steel holder. The specimen was pre-cracked in tension to a desired crack opening. Thereafter an axial tension and a torsional moment were applied simultaneously. The conclusion arrived at from this investigation was that mixed mode situations cannot be described with mode I fracture parameters alone. However mode I and mode II stress-displacement relations can be described independently from each other.

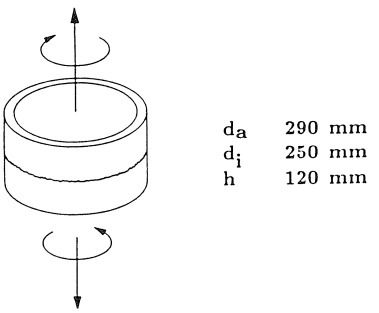

Fig. 2.9 Hollow cylindrical specimen adopted by Keuser (1989).

Hassanzadeh (1992) used grooved cube specimens, see Figure 2.10, to study the mixed mode fracture problem. The aim of the research was to find the variations of the normal and shear stresses as a function of both normal and shear displacements inside the fracture process zone. One of the conclusions was that if different load paths are followed, different shapes of the stress-displacement curve are found.

The experiments carried out by Nooru-Mohamed (1992) are similar to the experiments by Hassanzadeh(1992) discussed above. However the test method was more sophisti-

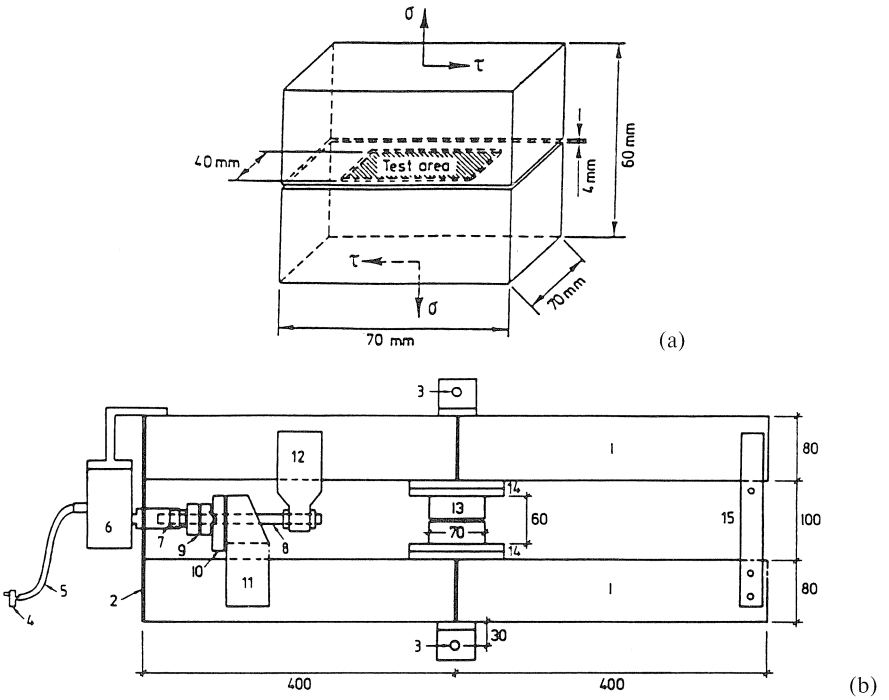

Fig. 2.10 Quadratic prism or cube geometry for mixed mode testing (a) and loading machine (b), Hassanzadeh (1992).

cated and a greater variety of load-paths were investigated. The machine used (Figure 2.11) consists of two independent loading frames with two hydraulic systems for displacement controlled testing. The loading procedure in both directions is completely automatic and computer-controlled whereas in the testing machine of Hassanzadeh (1992), shear displacement is applied manually. Some of the experiments are discussed in Chapter 6. The most important result is the path dependency observed in the tests. It is concluded that for extending the mode I crack models discussed in the first part of this chapter to mixed mode problems this path dependency has to be taken into account. A further conclusion was that the applicability of the conventional aggregate interlock theories at small crack openings is questionable. When the crack openings are relatively small, the shear transfer mechanism is not only governed by aggregate interlock but also by secondary cracking.

2.2.2 Four-point-shear

The four-point-shear geometry was first proposed by Iosipescu (1967) to test the ultimate strength for pure shear loading for metals and welded joints. If a beam specimen is loaded in four-point-shear, a zone is created where high shear stresses exist and where bending stresses are not dominant, see Figure 2.12.

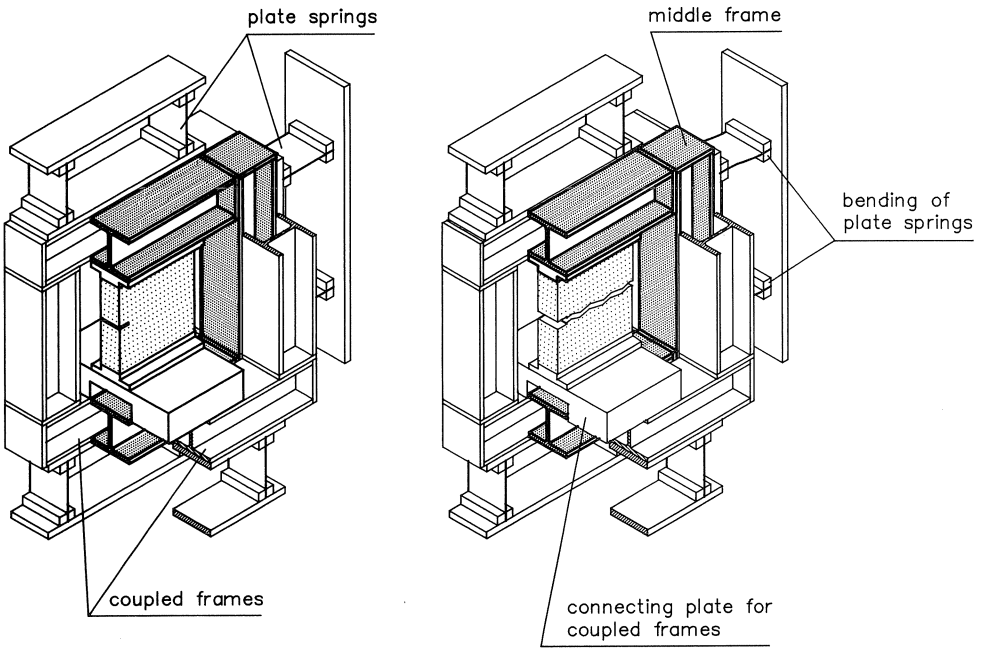

Fig. 2.11 Mixed mode loading machine used by Nooru-Mohamed (1992).

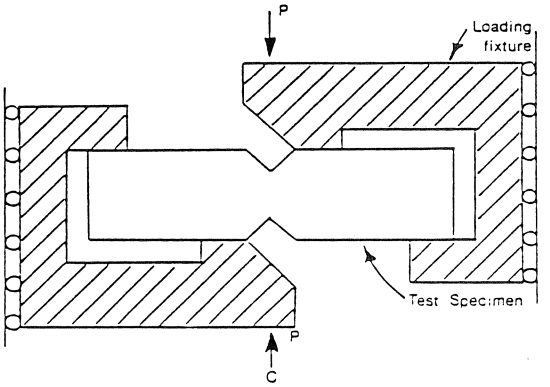

Fig. 2.12 Four-point-shear principle used by Kumosa & Hull (1987).

For concrete this type of geometry was first adapted by Arrea & Ingraffea (1982). In contradiction to the specimens and geometry used by Iosipescu, to test concrete single edge notched beams were chosen and roller bearings were used at the supports, see Figure 2.13. At the tip of the notch a high shear stress is created. Yet if the crack starts to propagate from the notch it grows away from the shear zone and opens further in mode I. In order to study shear fracture of concrete, Bažant & Pfeiffer(1985) proposed a double-edge-notched beam geometry as shown in Figure 2.14. The zone between the middle loading points is taken very narrow to ensure high shear stresses. The experiments were

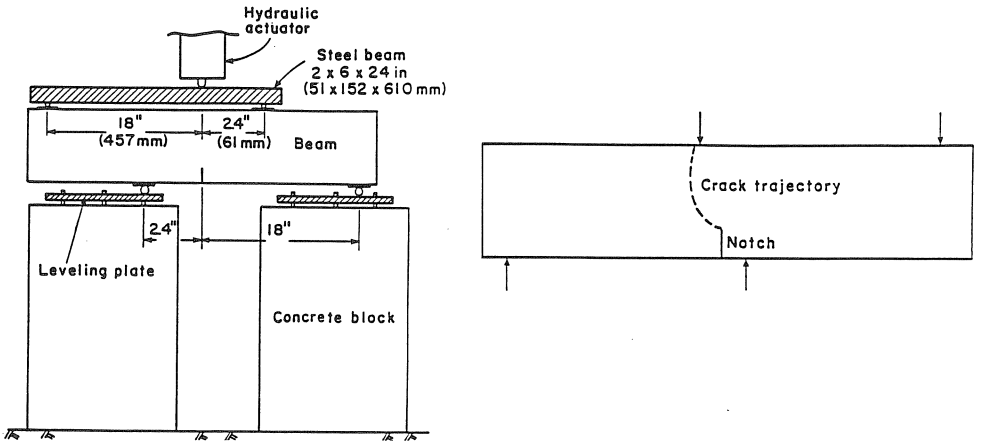

Fig. 2.13 Single-edge-notched beam used by Arrea & Ingraffea (1982).

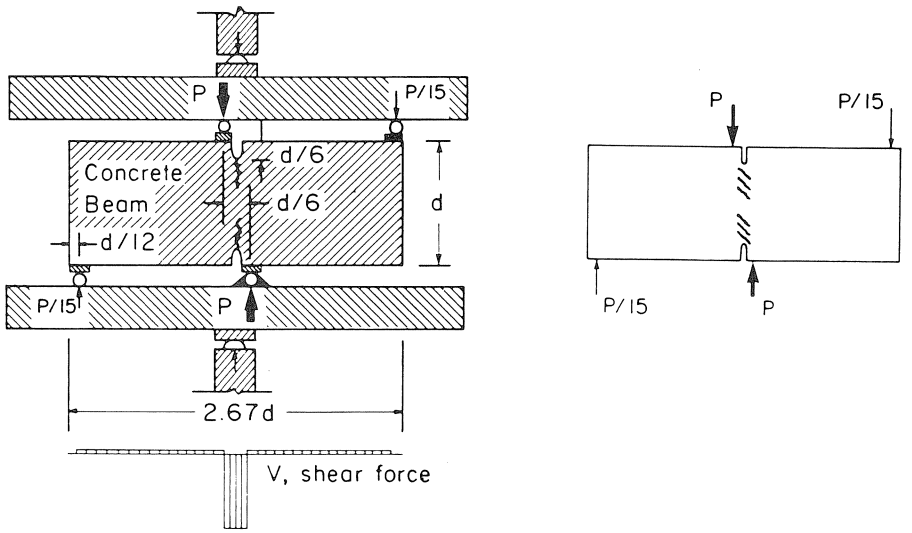

Fig. 2.14 Double-edge-notched beam used by Bažant & Pfeiffer (1985).

carried out at constant displacement rate of the piston. This implies that the deformation in the actuator is controlled, which corresponds to a load control testing. Therefore, the final failure may have been of a dynamic nature. Bažant & Pfeiffer (1985) concluded from their tests that shear fracture exists and that the mode II fracture energy is thirty times larger than the mode I fracture energy. Finally, the direction of crack propagation is not mode I, but a direction where the energy release rate for the entire structure is maximised. It was *assumed* that at first inclined tensile microcracks (under an angle of approximately 45°) formed in the shear zone, which were later connected by shearing. In a macroscopic sense this was described as shear (mode II) failure. Simulations of these experiments will be presented in paragraph 2.3.3. The experiments were

repeated and numerical simulations were carried out with a micromechanical model in the present investigation and will be further discussed in the following chapters.
The same geometry as used by Bažant & Pfeiffer was adapted by Melin (1989) to study cracking in a PMMA material. The crack patterns obtained in this investigation differ from the tests on the concrete beams, see Figure 2.15.

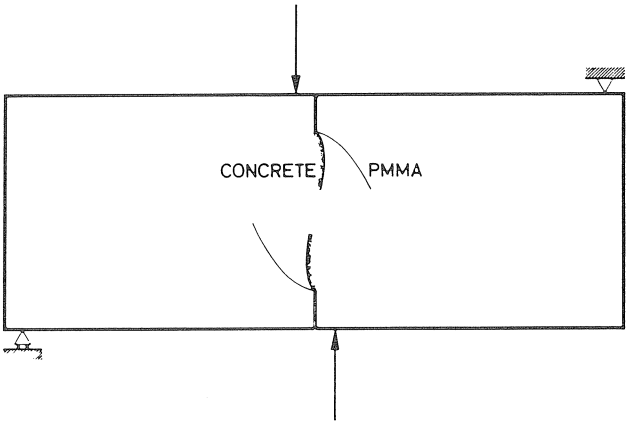

Fig. 2.15 Fracture mechanism observed by Melin (1989).

Davies (1991) used the four-point-shear tests to study dynamic fracture. In this case one single crack between the notches is observed. The cracking was explosive as soon as the peak load was reached. The same probably occurred in the tests of Bažant & Pfeiffer.
In the machine used by Swartz & Taha (1987) for four-point-shear tests on double-edge-notched beams, it was possible to apply an additional axial force. The testing scheme is shown in Figure 2.16. It was concluded from the failure mode that the fracture was due to tensile deformation and not to shear deformation. In the tests two curved cracks were observed. If an axial compressive force was applied, those two cracks (cracks no 1) were arrested and final failure was due to splitting (crack no 2), see Figure 2.17.

2.2.3 Four-point-shear, Round Robin proposal RILEM

RILEM committee 89-FMT (Fracture Mechanics of Concrete, Test Methods) studied the mixed mode fracture process. After examining the results published in literature a few questions still remained unanswered. In summary these questions are:
- Is the crack growth only governed by a mode I deformation mechanism?
- Do aggregate interlock and friction play a role?
- Does mixed mode fracture energy exist?
- What influence does the loading sequence have on crack propagation?

It was decided to start a round robin using the four-point-shear test on single edge notched beams. The proposed loading scheme is shown in Figure 2.18. In this report experiments performed according to the round robin proposal will be presented. However the way the load is applied to the specimen is different.

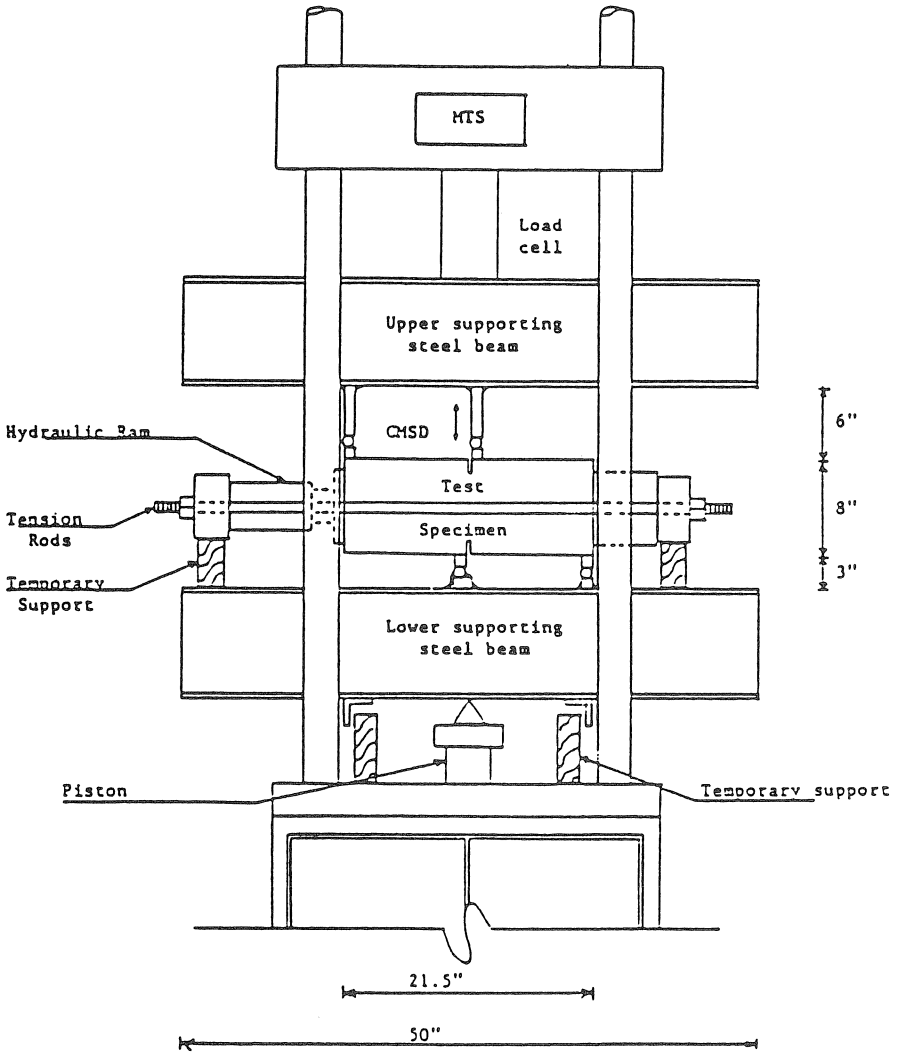

Fig. 2.16 Testing geometry used by Swartz & Taha (1987).

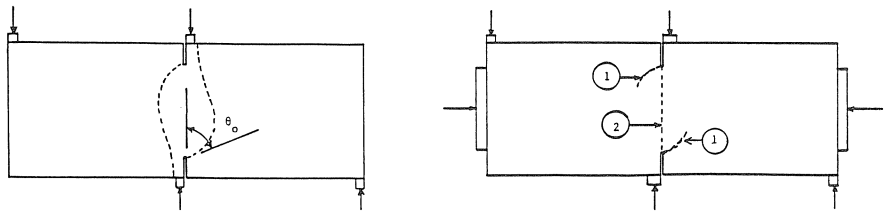

(a) (b)

Fig. 2.17 Crack patterns observed by Swartz & Taha (1987), no axial force (a) and with axial force (b).

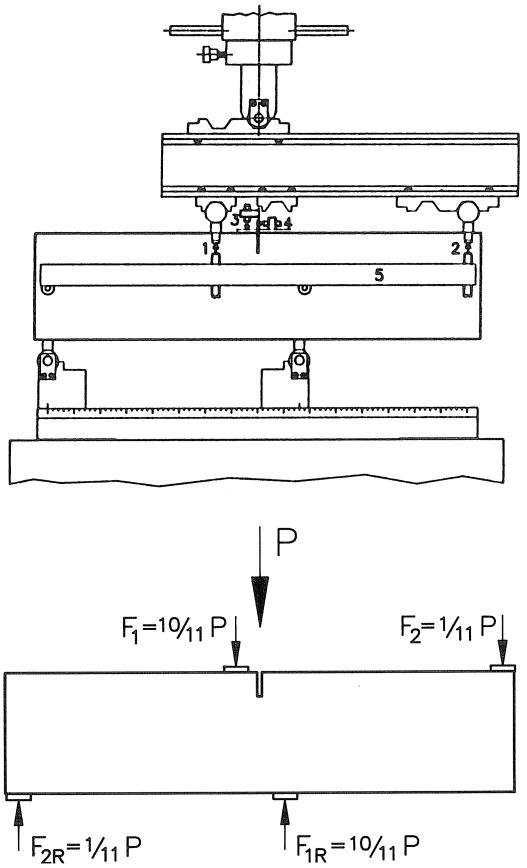

Fig. 2.18 Geometry proposed four round robin by RILEM (Carpinteri et al. (1989)).

The first results published were the outcome of a joint research programme between ENEL-CRIS-Milano and Politecnico di Torino. The conclusions in the papers presented by this group in recent years contradict each other. In their first publication, Ballatore et al. (1988) concluded that the fracture toughness of concrete is defined by the unique parameter G_f, even for mixed mode problems. The crack patterns observed are shown in Figure 2.19. In the smaller beam size a different failure mechanism was observed, i.e. a curved "mixed mode" crack and a flexural crack. In Carpinteri et al. (1989) and Carpinteri et al. (1990), a difference in mode I and mixed mode fracture energy was reported. Mixed mode fracture energy resulted to be higher than mode I fracture energy, about 19% for a concrete with maximum aggregate size of 10 mm and about 33% with the largest aggregates equal to 20 mm. With decreasing beam size the difference between mode I and mixed mode fracture energy increases, from about 19% for large (specimen depth is 300 mm) to about 31% for small specimens (specimen depth is 200 mm). In a paper (Carpinteri et al.(1991)) that was published after the first results of the experiments of this research were presented, Schlangen & Van Mier

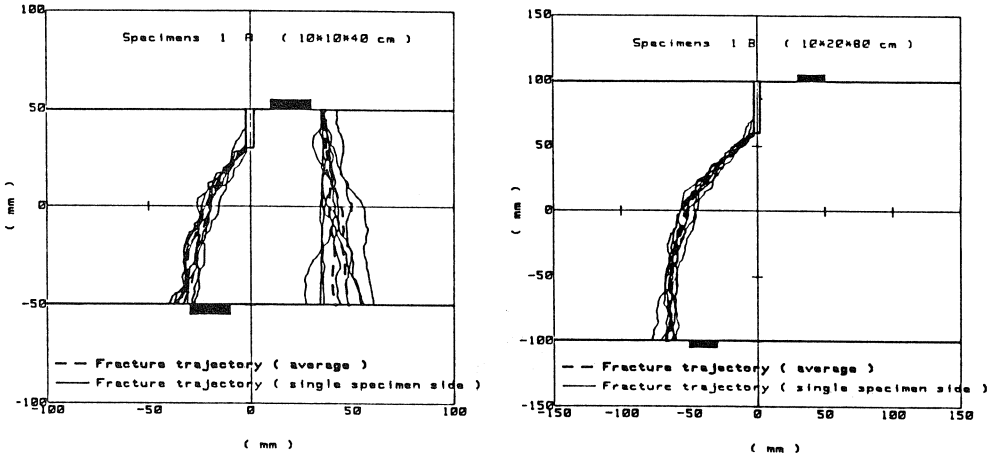

Fig. 2.19 Crack patterns observed by Carpinteri et al. (1989).

(1990, 1991a), again the opposite conclusions were drawn, i.e. fracture toughness of the material is measured by a unique parameter even for mixed mode condition.

2.3 *Numerical models for simulating fracture*

2.3.1 Homogeneous models

To study fracture problems in concrete the finite element method is a tool which is generally used. The finite element method was developed to describe the material as a continuum. In continuum macro mechanical models the material is mostly assumed to be homogeneous and the non linearity is implemented by using the measured softening behaviour. Two main approaches can be distinguished in the concrete mechanics world, i.e. the discrete approach on the one hand and the smeared crack approach, damage and non-local models on the other hand.
In the first approach (the discrete approach) each crack is modelled separately. Two different methods have to be distinguished. In one case the crack is modelled a priori (this means that the crack path must be known in advance), see Figure 2.20 (Rots(1988)). The second case makes use of remeshing techniques, see for instance Ingraffea & Saouma(1985). Based on the calculated stress in the continuum the direction of crack propagation is predicted and a new mesh configuration is generated, usually with a refined part around the crack tip (Figure 2.21), Carpinteri et al. (1992). In both cases the crack is not immediately stress-free as it appears, but a stress-crack opening relation which the opening crack should follow is implemented. The stress-crack opening relation has to be measured in experiments as described in paragraph 2.1.2. In the models the mode I stress-crack opening relation is implemented and in addition sometimes the mode II shear stress-sliding displacement relation. These properties must be material parameters. The problems arising when these parameters are measured have already been discussed in paragraph 2.1.2.

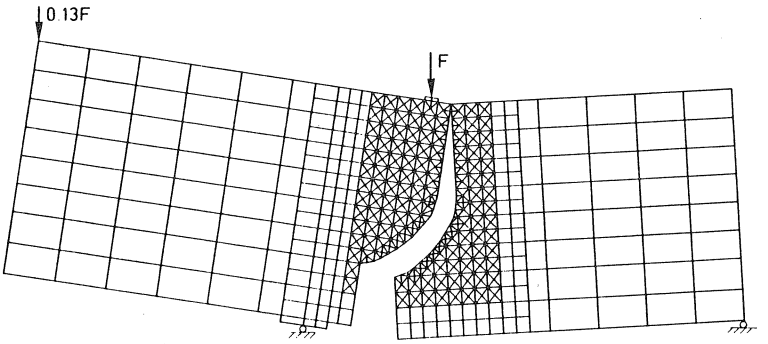

Fig. 2.20 Discrete crack approach, Rots (1988).

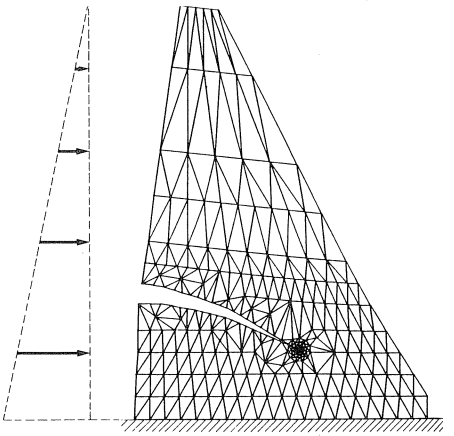

Fig. 2.21 Discrete crack approach with remeshing technique (Carpinteri et al. (1992)).

In the second approach fracture is not simulated as a line-crack but as a zone of cracks with a certain width. One of the concepts often used is the smeared crack approach, see for instance Rots (1988). In this approach the softening behaviour of the cracking material is implemented by means of a stress-strain relation for the elements where the cracking occurs. For the stress-strain relation again the measured response from an experiment is taken. Reduction in shear stiffness can be implemented by means of a shear retention factor, Rots (1988). The width of the band in which cracking will occur has to be defined and is often related to the maximum aggregate size in the concrete, Bažant & Oh (1983). In general the direction of the crack is fixed as soon as it initiates. Therefore more sophisticated models are developed to allow rotation of cracks during the fracture process, see for instance Rots (1988). A disadvantage of the smeared crack approach, however, is that the outcome depends on the size and alignment of the mesh. To overcome the problems outlined above the development of non-local models and gradient models has recently become a trend, see for instance Sluys (1992). It has been showed that with these models softening can be implemented in continuum models

without getting effects due to mesh size and mesh alignment. However it is not yet known if these models can be used in all loading cases. De Borst & Mühlhaus (1991) showed for instance that in their model the Cosserat continuum does not produce correct results if only tensile loading is involved. The rotational degrees of freedom are only activated under shear loading.
A comparable approach involves the use of local and non-local damage models. In these models the formation of cracks is obtained by reducing the elastic moduli as a function of one or more damage parameters, which represents the state of damage due to crack formation, see for instance Mazars (1984). The damage parameters can also be chosen following a probabilistic approach. In that case this type of model also belongs to the heterogeneous models discussed in the next paragraph, see Mazars (1984) and Carmeliet & Hens (1992).
All the above mentioned models have their own numerical difficulties. In the past many efforts have been directed to the way in which the models should be implemented into computer codes. On of the problems was how to produce correctly converged solutions. Furthermore effects from the chosen mesh configuration had to be avoided. These efforts have proved to be successful. Yet, the question arises as to whether the basic assumption that is made for all these models is true. Softening of concrete has to be a material property, or at least the heterogeneous material concrete must have well defined material properties. Since there is not a general agreement about the validation of this assumption, see paragraph 2.1, the author feels more drawn to models that treat concrete as a heterogeneous material. Those type of models are discussed in the next paragraph.

2.3.2 Heterogeneous models

In heterogeneous models the concrete is not treated as a homogeneous material, but heterogeneity is implemented directly by modelling the microstructure of the material or indirectly by using statistical distributions of material properties. Usually the size of the sample or the structure that is simulated with the heterogeneous models is smaller compared to the size of the problems studied with homogeneous models, because of the larger computer times needed, in particular if the microstructure is implemented. Different types of models where the heterogeneity is implemented are used, i.e. continuum models and non-continuum models.
An example of a continuum model where heterogeneity is implemented following a stochastic approach is the model of Rossi & Richer (1987). The heterogeneity is introduced on a local scale of the material, considering that cracks are created within the concrete with different energy dissipations on the spatial distribution of constituents and initial defects. Continuum models in which the heterogeneity is implemented using a generated grain structure, see Figure 2.22, have been developed among others by Roelfstra et al. (1985), Vonk et al. (1991), Wang et al. (1992). All three examples are models to simulate fracture in concrete. In the models strong and stiff elements, representing aggregate particles, are embedded in weaker (matrix) elements,

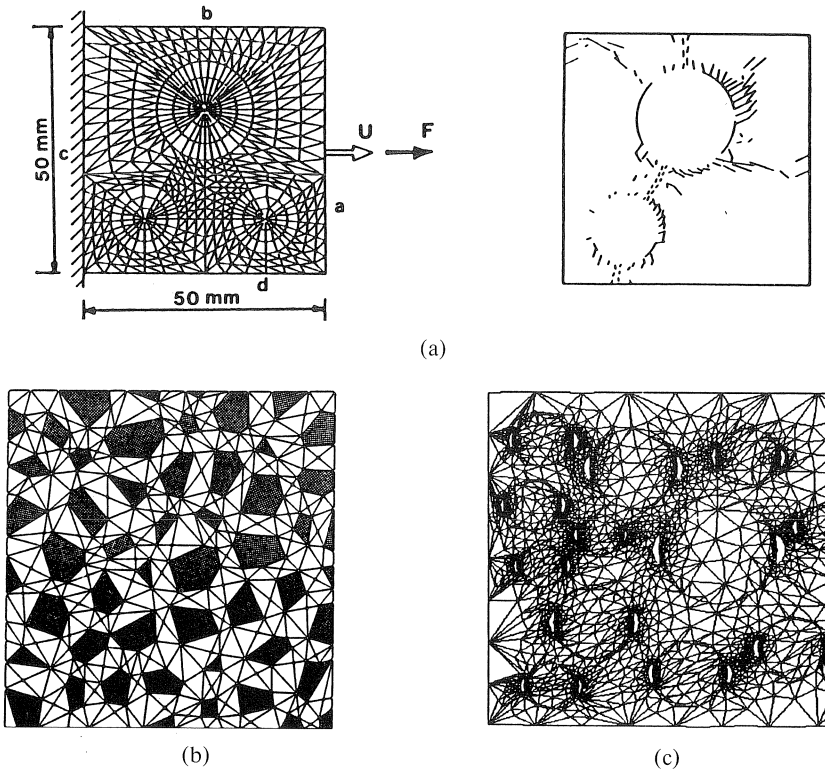

Fig. 2.22 Continuum models with generated grain structure, (a) Roelfstra et al. (1985), (b) Vonk et al. (1991) and (c) Wang et al. (1992).

see Figure 2.22. The model of Roelfstra et al. (1985) is able to simulate three dimensional fracture processes. To obtain the correct load-displacement response, softening is implemented as discussed in the previous paragraph. In the model developed by Vonk et al. (1991) the Distinct Element method (Cundall & Strack (1979)) is used. Here also softening is implemented. This model has proved to be very powerful in simulating compression tests, but tensile tests have been successfully simulated as well. Wang et al. (1992) have used a finite element code in which crack growth is modelled using Linear Elastic Fracture Mechanics.

Another group of models for simulating fracture in materials which has also received much attention in the past years in theoretical physics, are lattice type models. In a lattice type model the material is schematized as a network of truss (hinged nodes) or beam (fixed nodes) elements. Crack growth is obtained by removing elements which exceed their tensile strength. A model with truss elements is used by Meakin et al. (1989) for simulating shrinkage cracks in clay, see Figure 2.23a. Termonia et al. (1985) simulated fracture in polymer fibres with a truss model, see Figure 2.23b. Herrmann (1991) used a square lattice with beam elements to simulate fracture in disordered

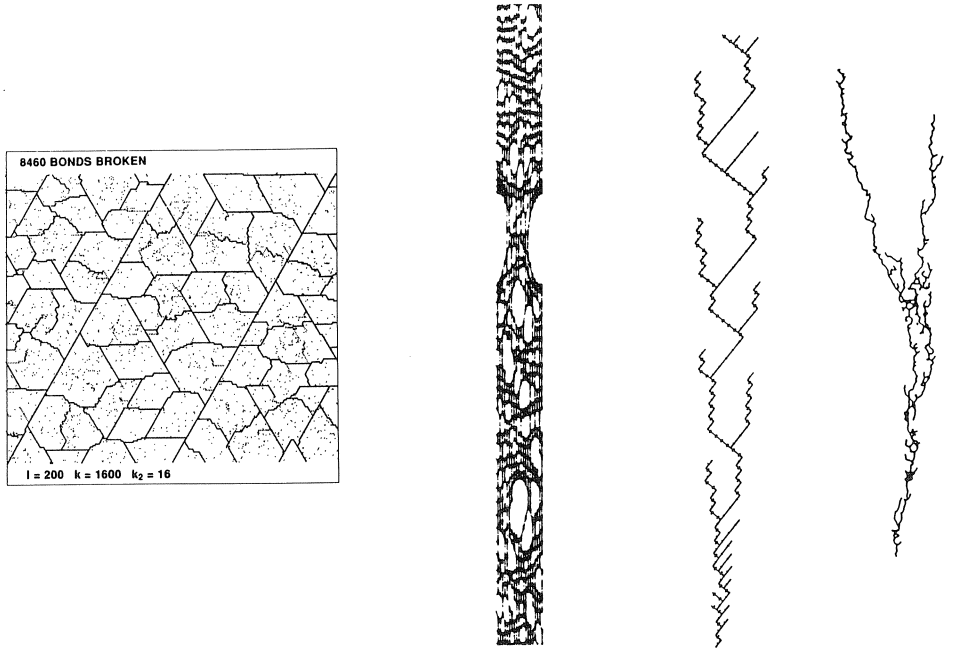

(a) (b) (c)

Fig. 2.23 Lattice models used for simulating cracking in clay (a) by Meakin et al. (1989), fracture in polymer fibres (b) by Termonia et al. (1985) and disordered media (c) by Herrmann (1991).

media in which heterogeneity was implemented by a variation of strengths, see Figure 2.23c. Arbabi & Sahimi (1989) carried out three dimensional simulations using a network with truss elements.

To simulate fracture in concrete only lattices with truss elements are used. Burt & Dougill (1977) and Berg & Svensson (1991) used random lattices in which the elements crossed each other, see Figure 2.24. This makes the visualization of the crack growth difficult. The heterogeneity was implemented by a variation of strength of the lattice elements. Rocha & Riera (1991), Shorn & Rode (1987) and Bažant et al. (1990) used networks with truss elements in which the heterogeneity is implemented by using a grain structure. However in the latter ones softening was implemented in the elements. However most of these lattice type models are used to simulated basic problems such as tension or shear on a simple square or prismatic mesh. Only the principle of crack simulations with such an approach is discussed. In Chapters 5 and 6 a similar model using beam elements are presented and simulations of more complicated experiments are described.

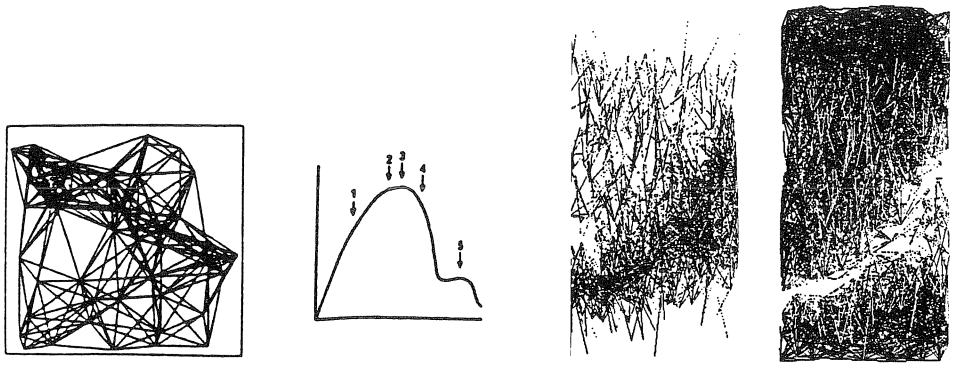

(a) (b)

Fig. 2.24 Random lattices used by (a) Burt & Dougill (1977) and (b) Berg & Svensson (1992).

2.4 *Simulations of four-point-shear test*

The four-point-shear tests discussed in paragraph 2.2.2. are simulated by many researchers using continuum models. In this section some of these simulations will be discussed and compared with the experiments. The first example that is simulated is the four-point-shear test on single edge notched beams carried out by Arrea & Ingraffea (1982). In Figure 2.25 simulations performed by Arrea & Ingraffea (1982), De Borst (1986), Rots (1992) and Alfaiate et al. (1992) are compared.
In these four simulations different models are used. Area & Ingraffea (1982) used a discrete approach with remeshing technique. Softening and aggregate interlock were

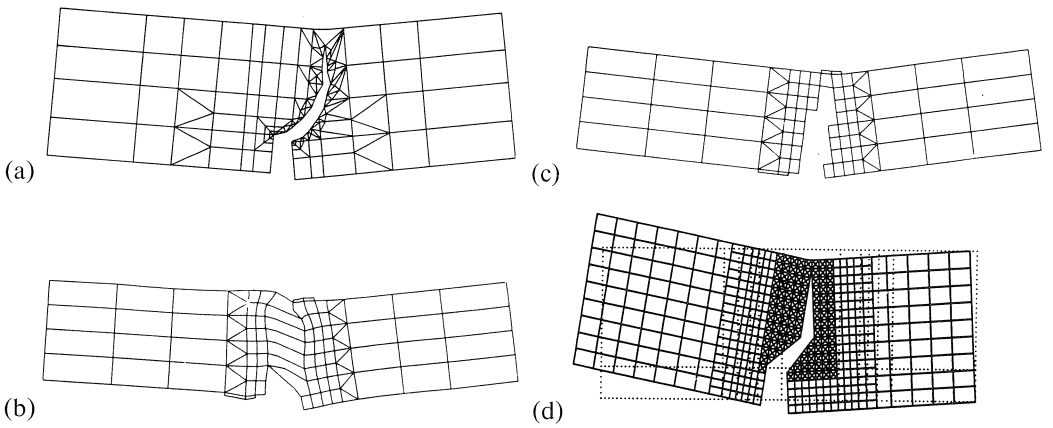

(a) (c) (b) (d)

Fig. 2.25 Crack patterns observed in four-point-shear beam by Area & Ingraffea (1982) (a), De Borst (1986) (b), Rots (1992) (c) and Alfaiate et al. (1992) (d).

taken into account. A fixed smeared crack model was used by De Borst (1986). It can be seen that the crack follows the direction of the mesh (Figure 2.25b). De Borst (1986) claimed that an excellent match with the experimentally found load-displacement curve was obtained. However the author feels doubt about this, since the crack pattern is wrong the load-displacement curve *cannot* be correct. Rots (1992) adopted a smeared crack approach with removal of elements to overcome stress-locking effects. Again the cracks follow the mesh lines, which results in the wrong crack pattern. Alfaiate et al. (1992) used a discrete crack approach with a predefined crack. The maximum load obtained in this simulation was too low, which Alfaiate et al. (1992) explained by the fact that no aggregate interlock was included in the model. In this report experimental and numerical results will be presented which lead to opposite conclusions, i.e. aggregate interlock is not imported in this four-point-shear problem.
The single-edge-notched beam used for the round robin is simulated by Carpinteri et al. (1990). A discrete approach with remeshing technique was adopted. A correct crack pattern is obtained as shown in Figure 2.26. However softening which was implemented was assumed to be a material property. The validation of this assumption has already been discussed in paragraph 2.1.2.

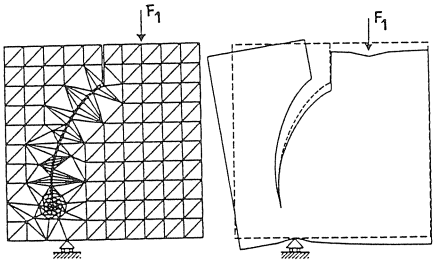

Fig. 2.26 Crack pattern simulated by Carpinteri et al. (1990) in single-edge-notched beam used for round robin organised by RILEM TC 89 FMT.

The double-edge-notched beams tested by Bažant & Pfeiffer (1985) are simulated among others by Ingraffea & Panthaki (1985), Rots et al. (1987) and Swartz & Taha (1987). Ingraffea & Panthaki (1985) concluded from their simulations that the final failure which occurs in this beam is a tensile splitting failure, rather than a shear failure. The crack pattern is shown in Figure 2.27a. At first two curved cracks start at the two notches, followed by a straight (splitting) crack between the notches, which started in the centre of the beam. Rots et al. (1987) found that first two cracks start at both notches, but after reaching the peak load one crack continues and finally grows together with the crack at the opposite notch, see Figure 2.27b. To obtain this asymmetric behaviour an imperfection was introduced at one notch. Swartz & Taha (1987) (Figure 2.27c) found two curved cracks in their simulations. No imperfection was implemented and the material was assumed to be homogeneous. However, the curvature of the cracks which was found in these simulations was larger than found in the other simulations and closer to the experimental curves observed in this study, see Chapter 4.

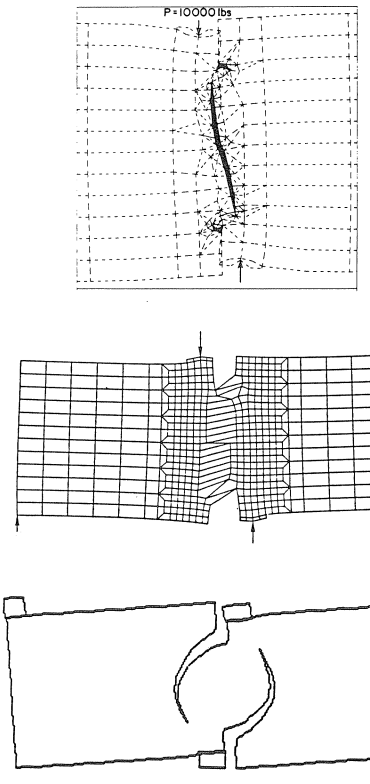

(a) (b) (c)

Fig. 2.27 Crack pattern in double-edge-notched beams simulated by Ingraffea & Panthaki (1985) (a) and Rots et al. (1987) (b) and Swartz & Taha (1987) (c).

3 Experimental procedure

In this chapter the development of the test set-up will be discussed. Subsequently an outline of the test control and measurement technique will be given. Furthermore the materials, specimens and determination of strength results are considered. Finally a summary of the test series performed is given.

3.1 *Test set-up*

3.1.1 First design

In experiments boundary conditions are of great importance. The way specimens are supported can influence the complete fracture mechanism. To obtain the desired distribution of the loads in the four-point-shear tests as described in Figures 2.18 and 3.1, i.e. 10/11 of the total load at the middle support and 1/11 at the outer support, rollers and hinges are required as boundary conditions at the loading points. It was expected that in the loading scheme proposed by RILEM (Carpinteri et al. (1989), see also paragraph 2.2.3.), where the specimens are loaded in compression, friction would occur at the

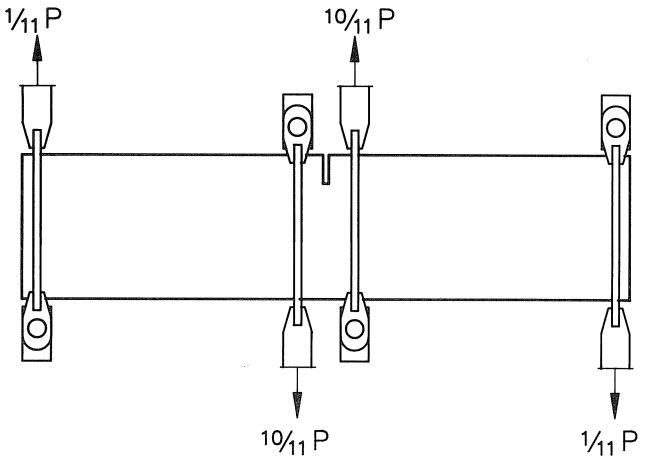

Fig. 3.1 Load-distribution in SEN-beams.

loading points. This friction leads to the introduction of horizontal forces, which will influence the stress distribution in the specimen.
Therefore a test rig was developed in which both the supporting fixtures can be changed and the distribution of the loads can be measured, Schlangen & Van Mier (1990, 1991a). A steel beam is used to distribute the load from the hydraulic actuator (Figure 3.2a).

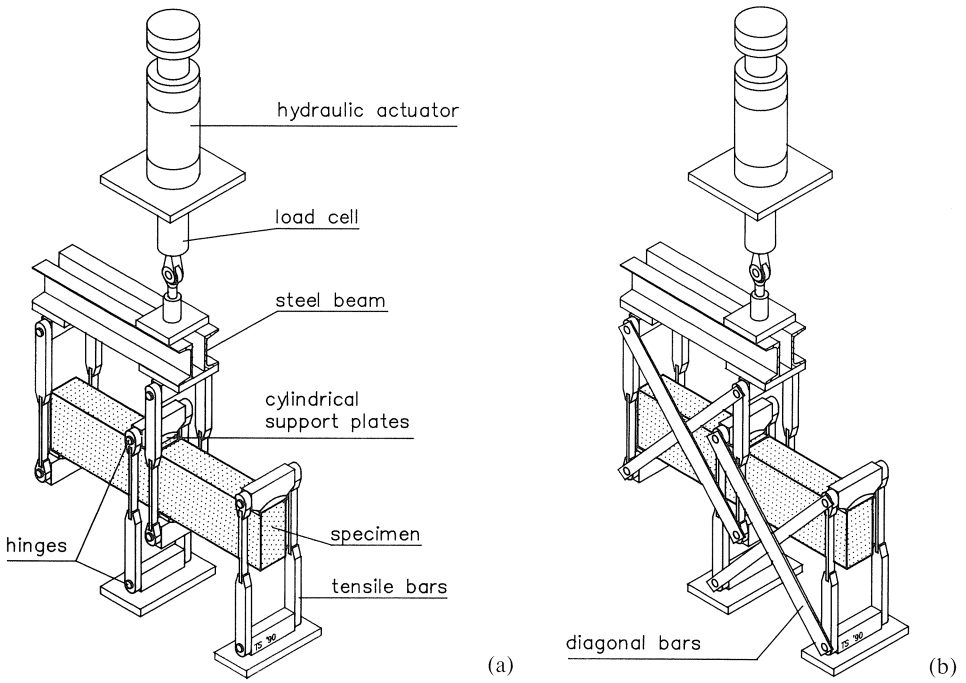

Fig. 3.2 Initially designed loading machine with freely rotating supports (a) and fixed supports (b).

The weight of the steel beam was balanced using a contra-weight attached, by means of a wire guided over a wheel, at the end of the beam, see Figure 3.3. The loads are introduced into the specimen via double-hinged tensile bars. The reaction loads are again transferred by means of double-hinged tensile bars to a very stiff steel frame. The loads in the tensile bars are measured by means of strain gauges glued onto the pendulum bars. The pendulum bars at the outer side are given a smaller cross section and a lower stiffness compared to the bars in the middle, to obtain an equal elongation of the bars. At the supports the specimens are glued to the supporting blocks to ensure a perfect transmission of the loads. The supporting blocks are connected by hinges to the pendulum bars. Also in the direction perpendicular to the beam axis rotation of the beams is possible through the use of cylindrical support plates.
To study the influence of friction, the supports can be fixed by mounting diagonal bars to the loading frame, see Figure 3.2b. In the case of fixed supports the rotation of the supporting blocks is also restricted.

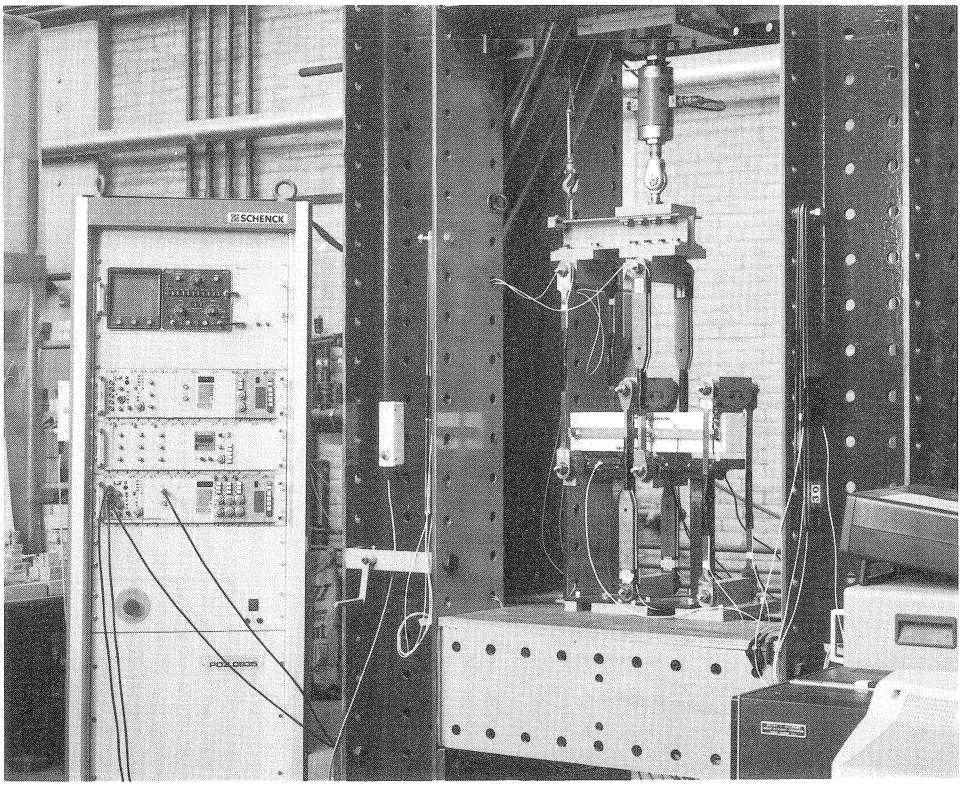

Fig. 3.3 Photograph of first loading frame containing a small specimen.

3.1.2 Later improvements in set-up

As the results obtained with the test set-up described in the previous section were not completely satisfactory some improvements were made. From the distribution of the loads in the pendulum bars it can be seen that eccentricities are present in the machine, Schlangen & Van Mier (1990, 1991) and paragraph 4.1.1. This can either be caused by the way the weight of the steel beam is balanced or by the fact that the supports at the bottom are fixed to the stiff frame or by friction in the supports. To overcome these problems the machine was changed. First at the bottom an additional steel beam was placed. This steel beam was attached to the stiff frame by a hinge, completely identical to the one at the top of the loading frame, see Figure 3.4. The hinges were now placed in the centre of the steel beam. Although this is still not the centre of gravity of the system, rotation of the beam is easier. The next improvement was the balancing of the steel beam. Now both the steel beam at the top and at the bottom are longer and the weights are balanced with weights attached directly to the beams.
The resulting loading frame is far from stiff and besides this, it is unstable. Nevertheless stable fracture test are possible, with a constant load distribution. Performing tests was possible only when there were no eccentricities. This means that the set-up would give a warning if the eccentricities were too large: testing becomes simply impossible.

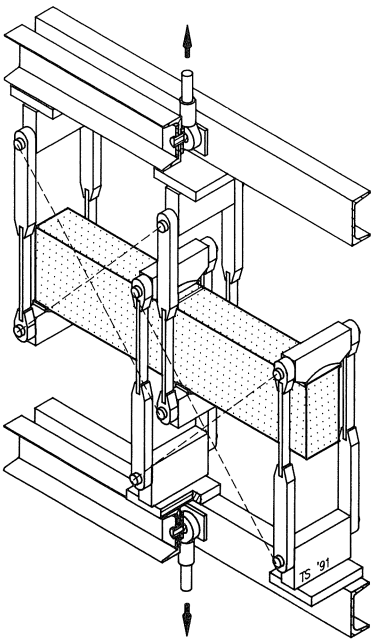

Fig. 3.4 New symmetric machine.

3.1.3 Changing frame for testing double-edge-notched beams

Some years ago Bažant & Pfeiffer (1985, 1986) claimed that true macroscopic shear (mode II) fracture occurred in their shear tests on double-edge-notched beams. Because these observations contradict the findings in the experiments on the single-edge-notched beams described in paragraph 4.1. it was decided to repeat the tests. Only a small change was required in the machine to make it suitable for the experiments on the double-edge-notched beams.

The distribution of the loads is different and the shear zone in the middle is narrower, see Figure 3.5a and Van Mier et al. (1992). Two beam sizes were tested, i.e. $d = 150$ mm and $d = 300$ mm. For the small size it was necessary to change the position of the middle pendulum bars as shown in Figure 3.5b. Experiments were carried out both with freely rotating and fixed supports. Figure 3.6 shows a picture of the set-up with the diagonal bars mounted to the frame.

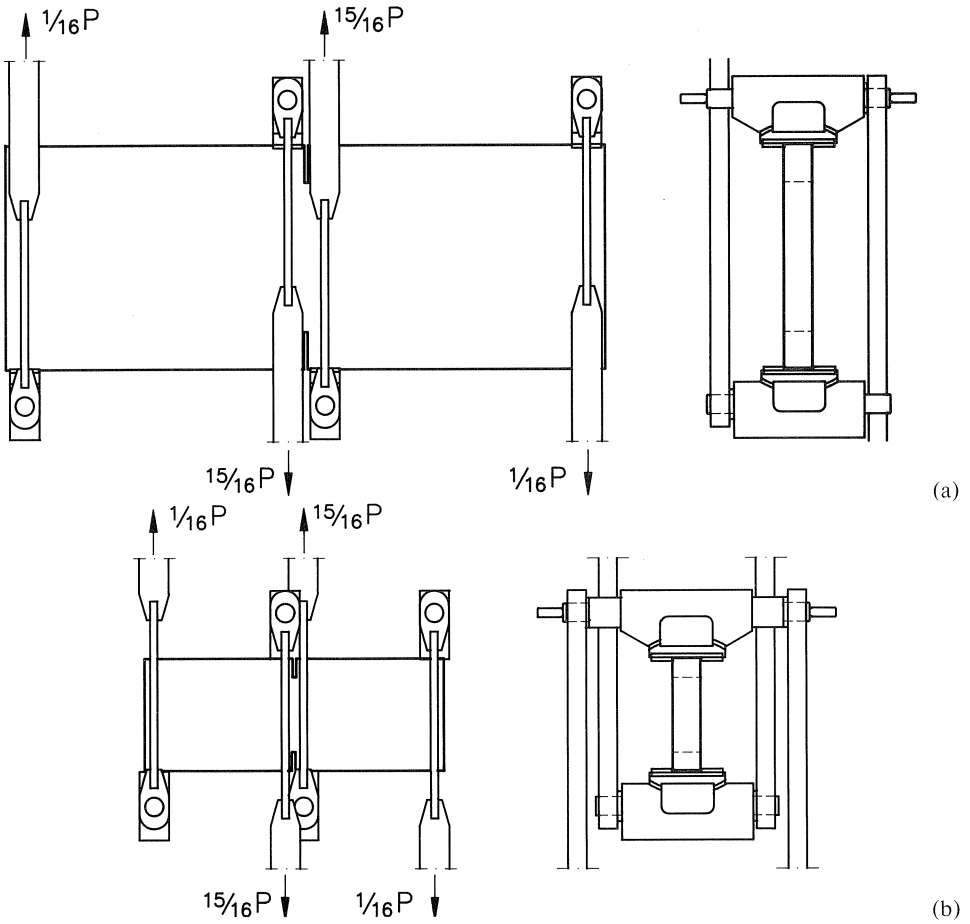

Fig. 3.5 Distribution of loads for tests on large DEN-beams (a); Placement of pendulum bars for small specimens (b).

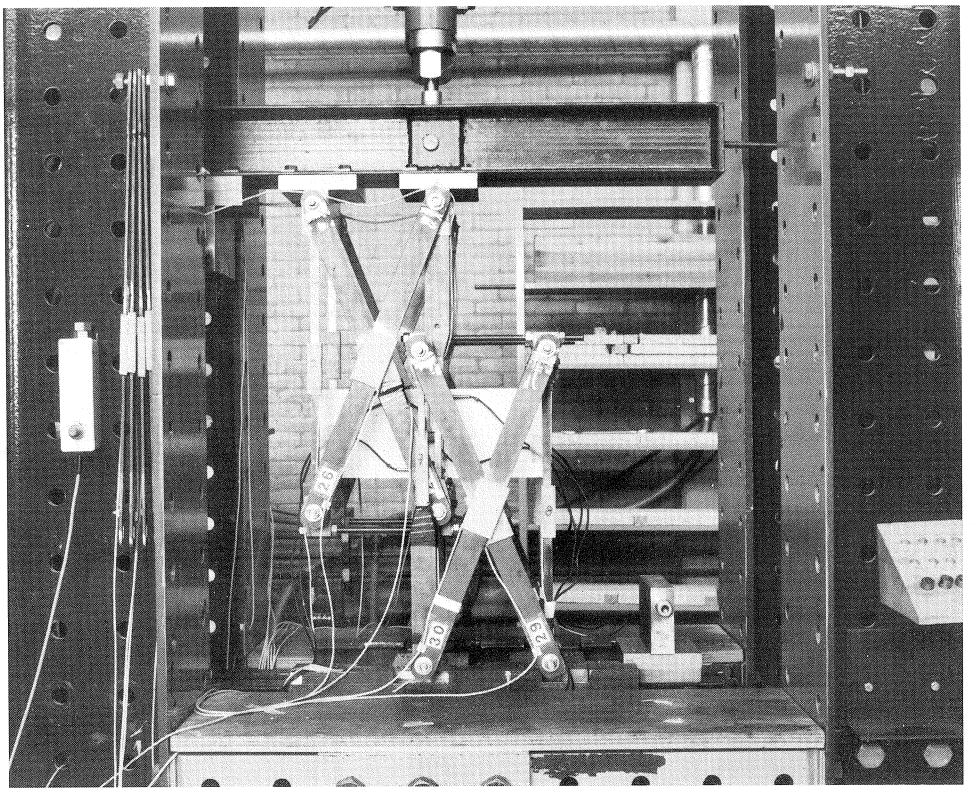

Fig. 3.6 Photograph of newly designed machine with fixed supports and small DEN specimen.

3.2 *Test control and measurement technique*

All the experiments were carried out under displacement control. Displacements measured on the surface of the specimen (see paragraph 3.3.) were used as a feed-back signal in the closed loop servo control. First of all, the specimens were loaded in load control up to a certain level, after which the circuit was changed to deformation control. The applied deformation rate was in all the tests approximately 0.1 μm/s. The hydraulic actuator used in the tests has a maximum loading capacity of 100 kN in compression and tension. The maximum stroke of the actuator was 100 mm. The applied load was measured by means of a load cell, see Figure 3.2a. For test control a Schenck regulation system (type POZ) was used.

Deformations on the surface of the specimen, the applied load and the load-distribution in the pendulum bars were measured with two different systems. In the first test series a Keithley Scanner (model 705) and Digital Multimeter (Model 195) were used. Later a new apparatus was designed and built by the instrumentation and measurement group of the Stevin Laboratory. With this new data acquisition system a shorter scan time was possible (40 channels in 1 second). The data were stored with a PC. The dis-

placements for the feed-back signal were measured with LVDTs (Sangamo type A6GH, linear stroke $\pm$ 1 mm). Other displacements on the specimen surface were measured with clip gauges designed in the Stevin Laboratory. On these clip gauges (Figure 3.7) strain gauges are glued in a full wheatstone-bridge. On the pendulum bars and the diagonal bars strain gauges were glued in a full bridge configuration to determine the forces in the bars.

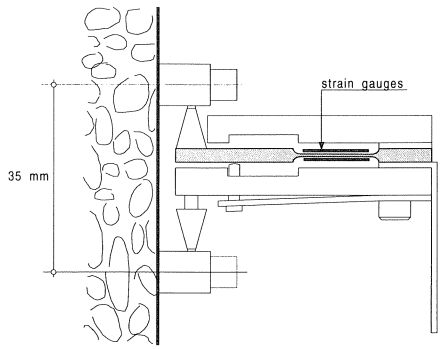

Fig. 3.7 Clip gauges used for measurements of local deformations.

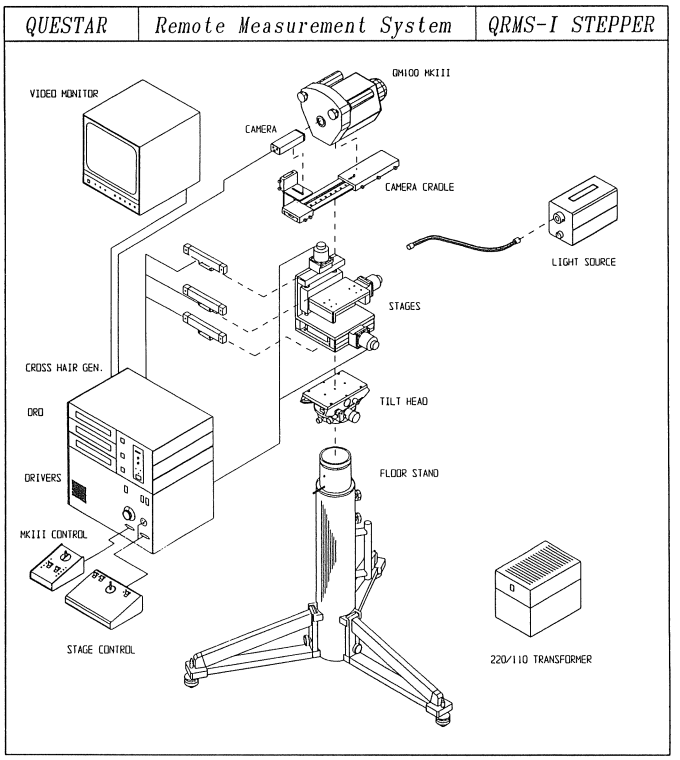

Fig. 3.8 Questar remote measurement system.

To study the crack propagation process a long-distance microscope was used. The microscope (Questar QM-100) can enlarge a part of the specimen. The resolution of the microscope is 1.1 μm The distance from the surface of the specimen is about 150 mm, which makes it possible to make real time observations from the propagating crack without disturbing the experiment. The microscope is mounted on a tilt head (see Figure 3.8) which can move in three orthogonal directions with stepper motors. On the back of the microscope a ccd video camera (Sony XC-77CE, 756 * 581 pixels) is fixed. The video signal can either be stored with a video recorder and printed afterwards or directly printed with a video printer (Seikosha VP-3500). The system has since been upgraded to allow for digital storage of the pictures and automated scanning of the surface.

3.3 *Materials used and beam specimens tested*

For the tests on the SEN beams, in each batch two large beams of size 840 * 260 * 100 mm^3 and two small beams of size 440 * 160 * 100 mm^3 were casted. After two days of casting the specimens were demoulded and cured under water. After 14 days the beams were sawn to the required size as shown in Figure 3.9. After sawing, the specimens were again placed in a fresh water basin. After 28 days of casting the specimens were removed from the water and left in the laboratory to dry until testing. In addition to the beam specimens, specimens for tensile and compressive tests were casted to obtain strength parameters. These tests will be discussed in the next paragraph.

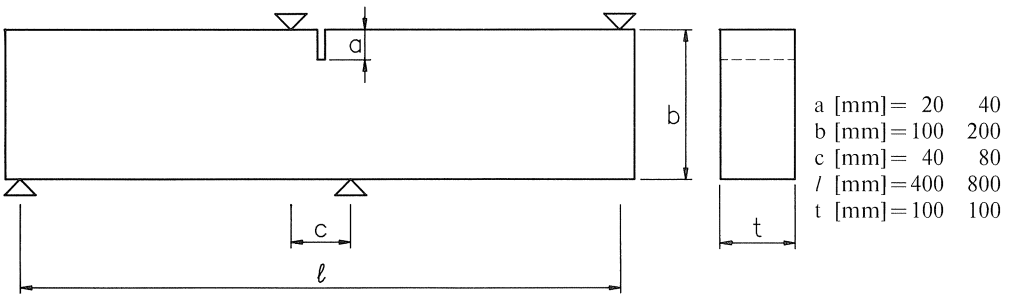

Fig. 3.9 Geometry of SEN beams tested.

Two sizes of the DEN beams were tested, viz. $d = 150$ and $d = 300$ mm (see Figure 3.10). The specimens were sawn from larger beams, 500 * 200 * 37.5 and 900 * 350 * 37.5 mm^3 respectively. The curing of the specimens was the same as for the SEN beams. In the investigation different concrete types are used. The mix designs for the different materials are listed in Table 3.1. The different concretes are: normal weight concrete with maximum aggregate size of 8 mm (con8), a normal weight concrete with maximum aggregate size of 16 mm (con16), a high strength concrete (hsc), a lytag lightweight concrete (lytag), a fibre reinforced concrete (fcon) and a hardened cement paste (hcp). The names between brackets will be used in the rest of this report to refer to these

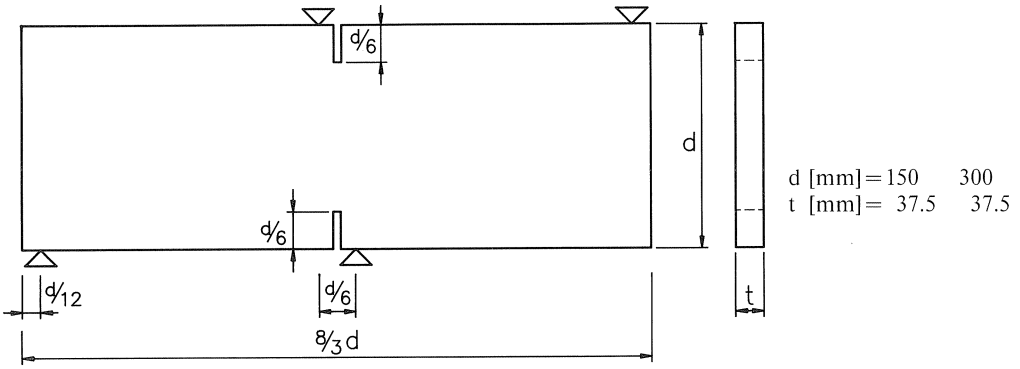

Fig. 3.10 Geometry of DEN beams tested.

Table 3.1 Mix designs and strength results for different concretes

	con8	con16	lytag	hsc	fcon	hcp
Cement PC-B[1]	375	375	330	350	375	979
Microsilica[2]	-	-	-	35	-	-
w/c-ratio	0.5	0.5	0.34	0.37	0.5	0.4
Superplast. Melment	-	-	5	14	7.5	12
River gravel						
16-8 mm	-	457	-	609	-	-
8-4 mm	540	365	-	431	540	-
2-4 mm	363	256	79	304	363	-
1-2 mm	272	256	158	216	272	-
.5-1 mm	272	202	158	151	272	-
.25- .5 mm	234	165	237	107	234	-
.125-.25 mm	127	128	158	95	127	822
Lytag[3] 12-8 mm	-	-	484	-	-	-
Lytag 8-4 mm	-	-	264	-	-	-
Steel fibres, type Dramix OL 25/.5	-	-	-	-	157[4]	-
28 day strength						
f_c [MPa]	46.6	50.1	55.8	81.9	46.5	66.9
f_{spl} [MPa]	3.1	3.38	3.8	4.6	3.9	-
f_b [MPA]	-	-	-	-	-	11.8
Tensile strength (from uniaxial tensile tests)[5]						
f_t [MPa]	3.44	3.10	3.74	3.86	2.98	1.79

[1] all quantities are given in kg/m^3, except the w/c-ratio which is the ratio by weight
[2] solid solution only
[3] the lytag aggregates were saturated in water before casting. The given values are inclusive of 15% and 14% water for the 4-8 mm and 8-12 mm grading respectively
[4] quantity = 2% of total volume
[5] tested at same age as beam specimens

materials. For the SEN beams all six different concretes were used; for the DEN beams only the con8 concrete was used.

For the SEN-beams displacements on the specimen are measured with LVDTs and clip gauges at the positions plotted in Figure 3.11a, b. The clip gauges are placed in the zone where the curved crack is expected to grow. However, also in the zone where a flexural crack is found by Carpinteri et al. (1989) deformations are measured. The LVDTs measuring δ_1 and δ_2 are fixed on a reference bar which is glued on the concrete beam as shown in Figure 3.11c. As feed-back signal the average (front and back) deformation δ_2 is used, which measures the displacement of the support on the right-hand side with respect to the two supports where the load is applied (actually with respect to the two points in the centre axis of the beam where the reference bar is glued on the concrete beam), see Figure 3.11c.

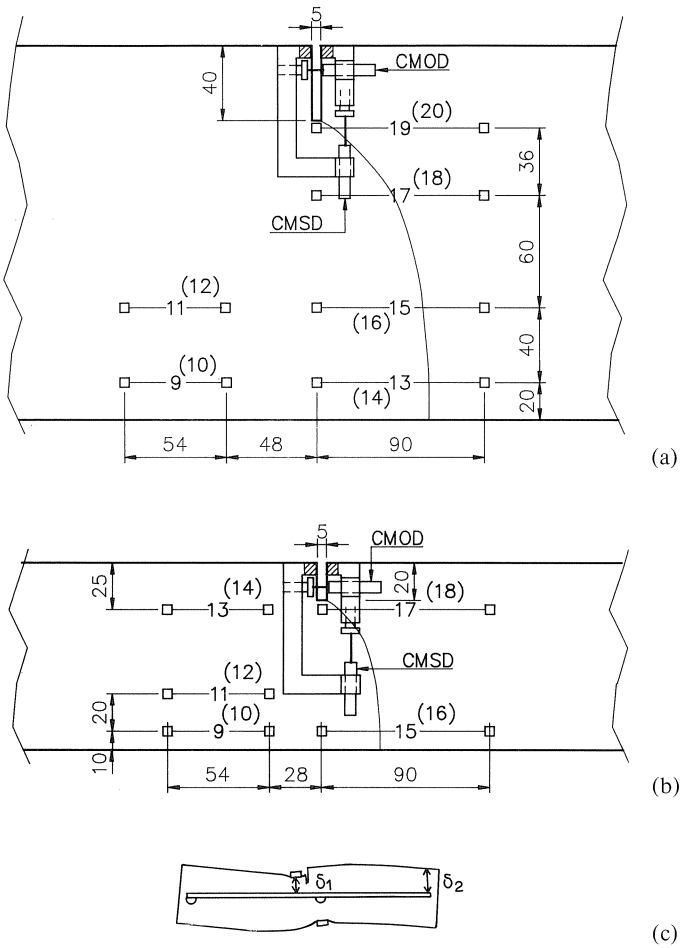

Fig. 3.11 Deformations measured on large (a) and small (b) SEN beams; Reference bar and LVDTs measuring δ_1 and δ_2 (c).

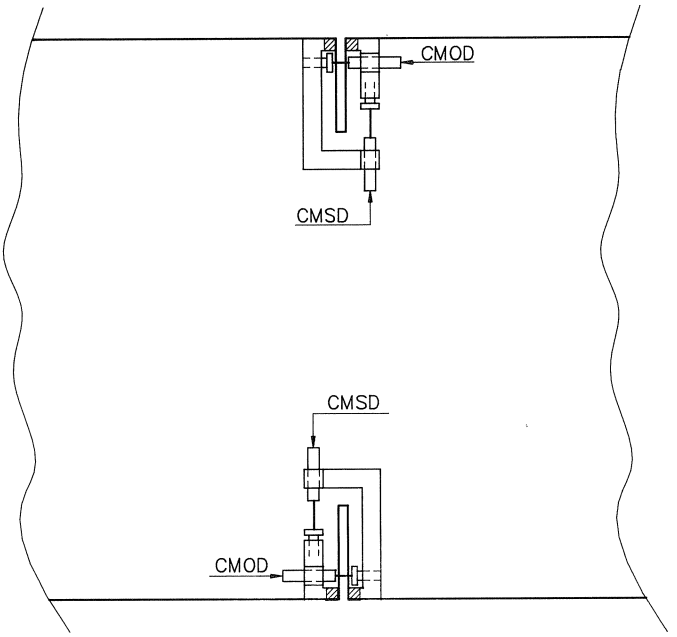

Fig. 3.12 Deformations measured in tests on DEN beams.

In the tests on the DEN beams the average value of the crack mouth opening displacement (CMOD) and the crack mouth sliding displacement (CMSD) at the top and bottom notch on the front of the specimen is used as feed-back signal, see Figure 3.12.

3.4 *Uniaxial tensile tests and determination of strength results*

In addition to the beam tests uniaxial tensile tests were carried out on specimens of the same material. Prismatic specimens were sawn from plates of size $300 * 300 * 50$ mm^3. For each batch three specimens, see Figure 3.13a, were tested. The prisms were loaded in deformation control using a closed loop hydraulic system. The machine is described in detail in Hordijk (1991), see also Figure 3.13b. The specimens are glued in the machine between fixed end platens. The test control was over four LVDTs mounted at the front and rear of the specimen as shown in Figure 3.13a. The tensile tests were performed at the same age of the specimens as the beam specimens. For each material type a stress deformation curve is plotted in Figure 4.19. In Table 3.1 the average tensile strength f_t is included for each material.
In each batch six cubes (150 mm) were casted to determine the compressive strength and the splitting tensile strength. These tests were carried out according to the Dutch codes at an age of 28 days. For the hcp, the strength was determined from small prismatic specimens of size $40 * 40 * 160$ mm^3. After failing these beams in three-point-bending, the two remaining specimen halves were loaded in compression (loading area $40 * 40$ mm^2). The strength results are included in Table 3.1.

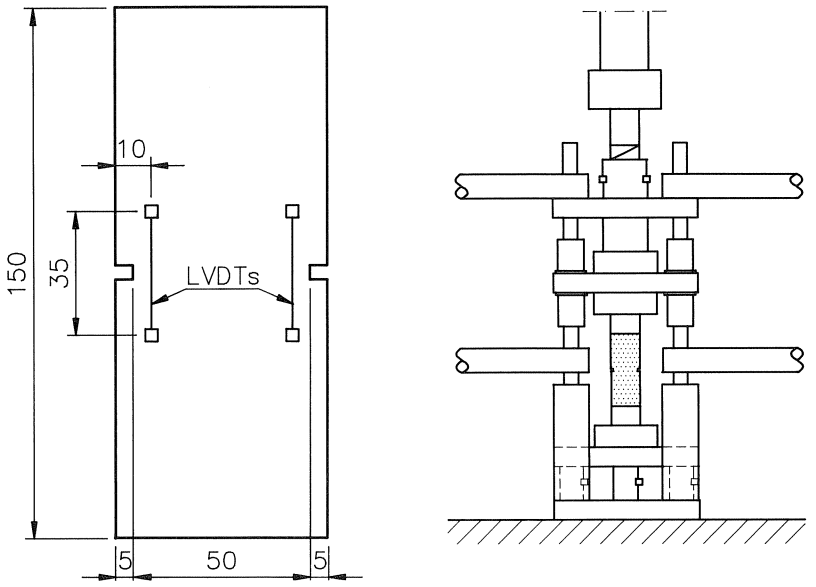

(a) (b)

Fig. 3.13 Uniaxial tensile tests: specimen (a) and testing machine (b).

3.5 *Test Series*

A large number of batches were casted for testing the SEN specimens. The first specimens were used to test the machine and to find the correct feed-back signal to control the test. Thereafter con8 and con16 SEN-beams were tested in the first designed machine. After changing the machine to the new symmetric set-up, a series of trial tests was performed on con8 specimens. For the different concretes lytag, fcon and hcp specimens from two batches were always tested. For the hsc only one specimens from one batch were tested. For the DEN specimens five batches of con8 only were casted. The different test series and the age at testing of the beams are listed in Table 3.2.

Table 3.2 Test series performed

number of batches	specimen type	type of concrete	age of testing [days]	test set-up
8	SEN	con8 (trial)	-	a-symmetric
6	SEN	con8	45–65	a-symmetric
6	SEN	con16	45–65	a-symmetric
3	SEN	con8 (trial)	-	symmetric
4	SEN	con8	77–96	symmetric
1	SEN	hsc	92–98	symmetric
2	SEN	lytag	77–100	symmetric
2	SEN	fcon	77–105	symmetric
2	SEN	hcp	89–104	symmetric
5	DEN	con8	31–43	symmetric

4 Experimental results

In paragraph 3.5. an overview is given of the four-point-shear experiments carried out in the test set-up developed in the Stevin Laboratory. In this chapter the experimental results are discussed. The first paragraph of this chapter deals with the fracture mechanism observed in the single-edge-notched beams made of normal weight concrete. Subsequently the results of the experiments on SEN beams are presented for different concrete mixes. The results for DEN beams are described in paragraph 4.3. A discussion of the experimental results and a comparison with experiments and simulations of four-point-shear beams presented in Chapter 2 concludes this chapter.

4.1 *Four-point-shear; SEN beams*

4.1.1 Description of fracture process

In the previous chapter it has already been explained that the test set-up was changed several times during the experimental program. The main improvement that was realized is changing the machine to a completely symmetric one. In this paragraph the experiments on SEN beams made of normal weight concrete (con8) will be discussed. A comparison will be made of the results of the beams tested in the old a-symmetric and the new symmetric machine. First the experiments with freely rotating supports are discussed. The following paragraphs focus on the influence of friction in the supports and on the determination of fracture energy.

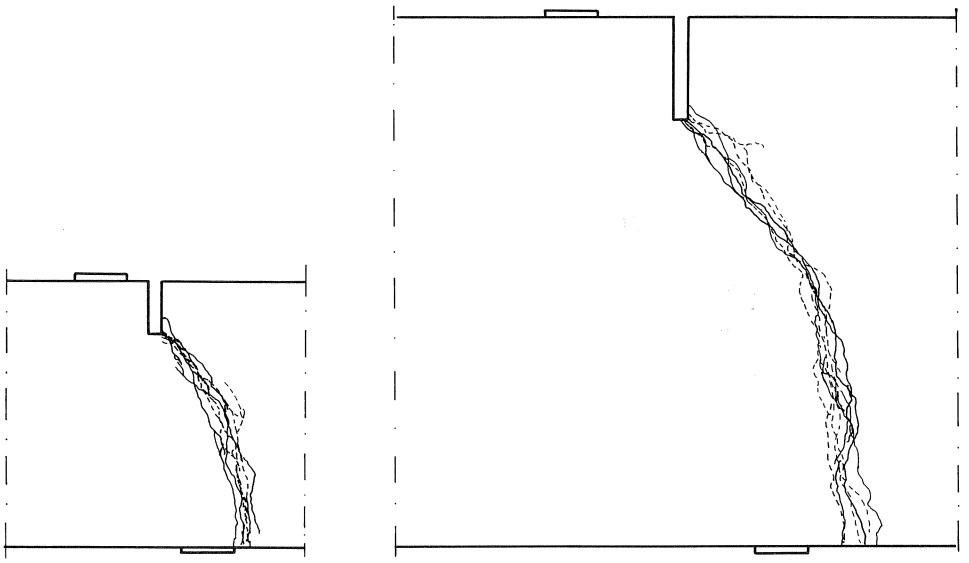

Fig. 4.1 Experimental crack patterns in three small (a) and three large (b) SEN beams loaded between freely rotating supports.

The main difference between the results obtained in the old and the new machine is the distribution of the loads; the failure mechanisms are not affected and are completely identical. The crack in both the large and the small beams starts at the notch and propagates to the opposite support as shown in Figure 4.1, where the cracks in three small and large specimens are plotted. In the theoretical case the distribution of the loads F_1/F_2 and F_{1R}/F_{2R} (see Figure 2.18) should be equal to 10. Yet eccentricities in the machine or in the specimen and friction in the supports (see paragraph 4.1.4. and Schlangen & Van Mier (1990,1991a)) disturb this value. In Figure 4.2 the distribution of loads is plotted versus the deformation δ_2 for two tests in the old (one test with the notch at the top and one at the bottom side of the beam) and one in the new machine. In the experiments carried out in the new machine the range of the LVDTs was changed to be able to measure larger deformations. In the plot it can be seen that in the new symmetric machine the distribution remains constant for a longer time, as compared to the distribution of loads in the a-symmetric machine. This difference can be explained

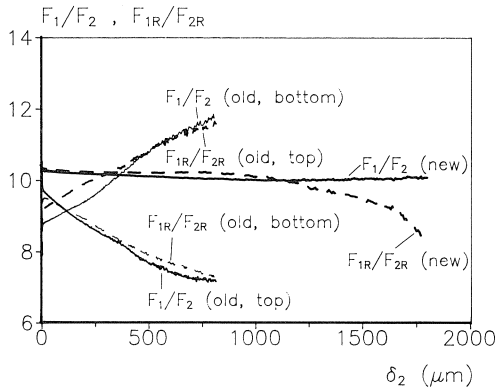

Fig. 4.2 Distribution of loads versus deformation δ_2 in two tests (one with the notch at the top and one at the bottom of the beam) in the old a-symmetric machine and one test in the new symmetric machine.

from the mechanism that takes place. Figure 4.3a shows the situation in the a-symmetric machine is shown. If the crack starts to grow, the amount of load that will be transferred to the smallest part of the beam will decrease. Note that only one force acts on this part of the beam. The two action loads will be transferred through the largest part of the beam directly to the supporting pendulum bar in the middle, as shown in Figure 4.3a. Due to this mechanism the ratio of the action loads F_1/F_2 will decrease and the ratio of the reaction loads F_{1R}/F_{2R} will increase if the notch is at the top of the beam. In the case the notch is at the bottom, the deviation of the ratios is reversed as can be seen in Figure 4.2. In the new symmetric machine the situation is different, see Figure 4.3b. Here the ratio of the reaction loads is forced to stay constant and equal to 10, because the pendulum bars in the middle and at the side are connected by the steel beam at the bottom which is supported by a hinge. However, at the end of the plot (large deformation), the distribution also deviates in the new machine. For large values of the

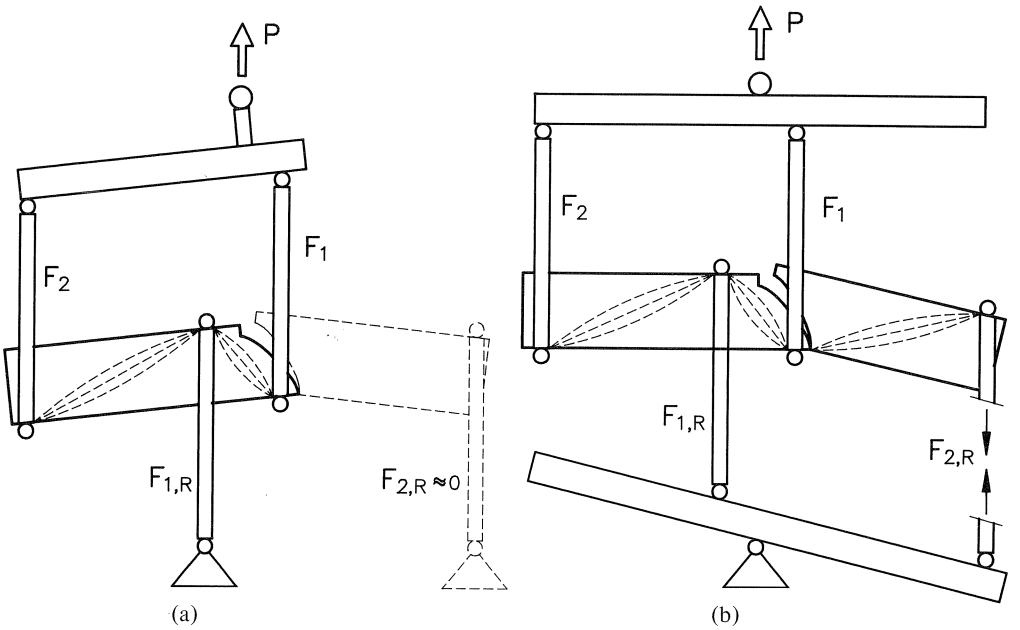

Fig. 4.3 Mechanism in four-point-shear beam in old (a) and new (b) machine.

displacement δ_2 the total load and thus the load in the pendulum bars, especially the bars at the outer side of the beam, is low. The error that is made in the measurements is large because also the weight of the specimen itself and the machine are relatively more important if the applied load is small.

Several displacements on the specimen are measured in the experiments as explained in Chapter 3. In Figure 4.4b the total load P is plotted versus the deformation δ_2 for three tests on small beams and three tests on large beams in the new machine. The

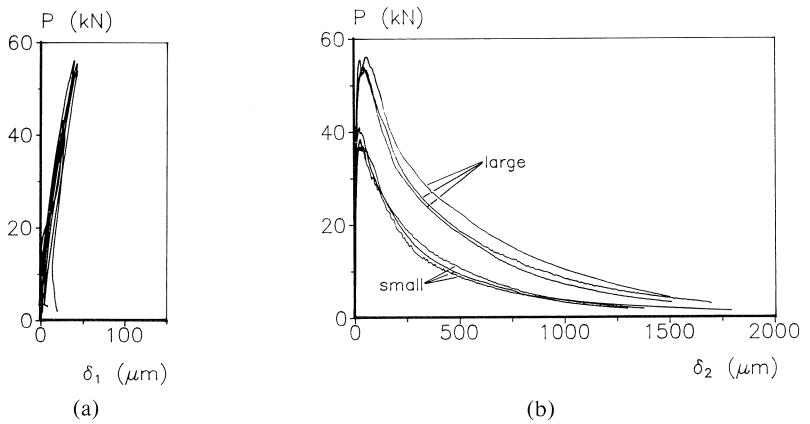

Fig. 4.4 Total load P versus deformation δ_1 (a) and δ_2 (b) for three large beams and three small beams.

LVDTs measuring δ_1 show only an elastic deformation and will unload after peak load, see Figure 4.4a. The crack mouth opening and sliding displacements are shown in Figure 4.5. For the displacements, the average deformation of the front and the back side is always plotted. It can be seen that the scatter is small. This is the consequence of using a machine which is actually unstable. Only if there were no eccentricities could the test be carried out successfully as explained in Chapter 3.

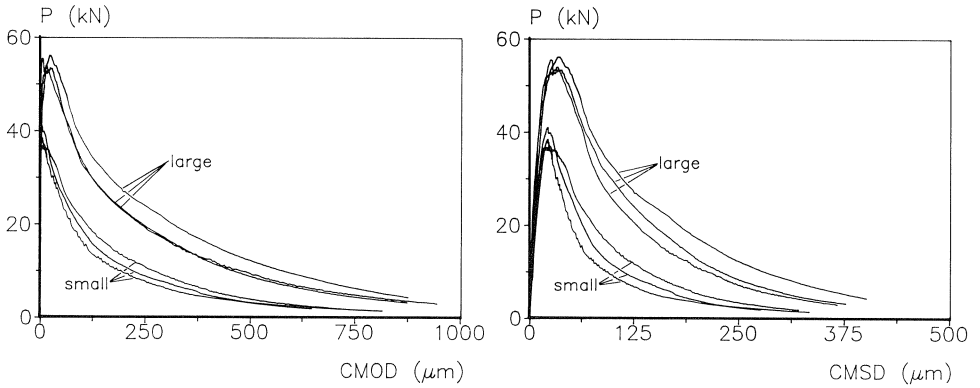

Fig. 4.5 Total load P versus CMOD (a) and CMSD (b) for three large beams and three small beams.

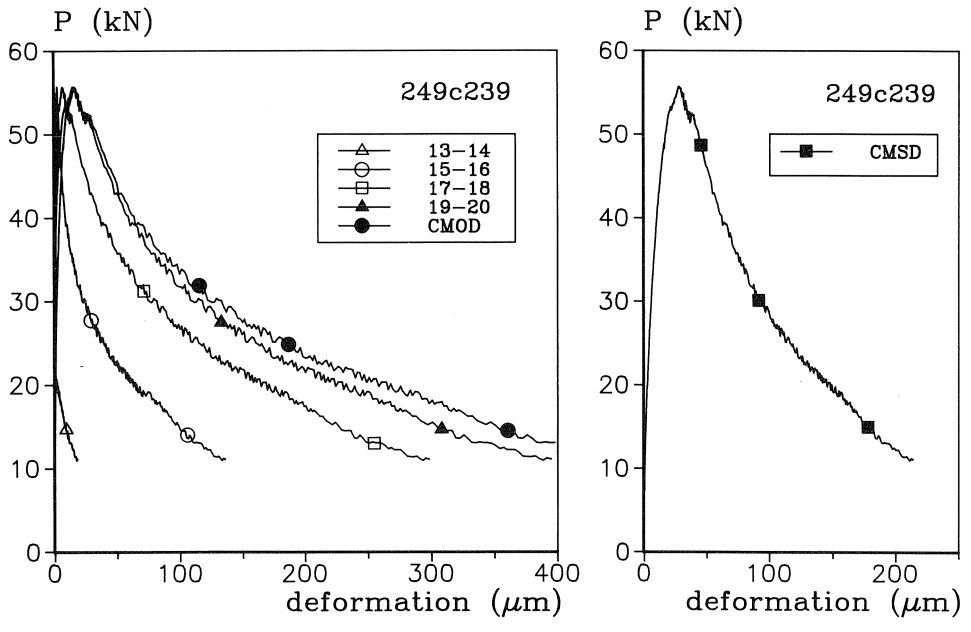

Fig. 4.6 Total load P versus local deformations.

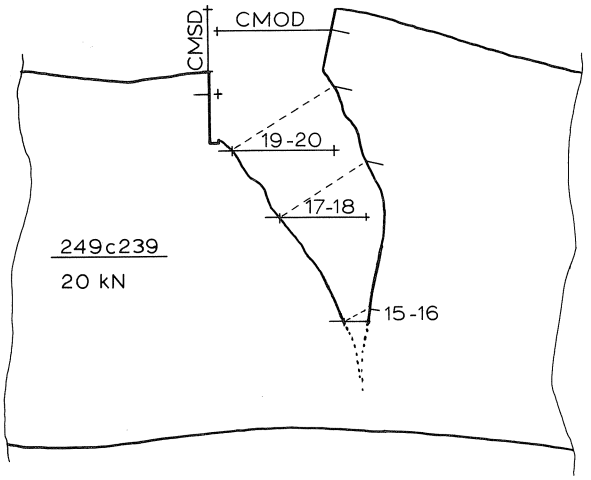

Fig. 4.7 Construction of open crack.

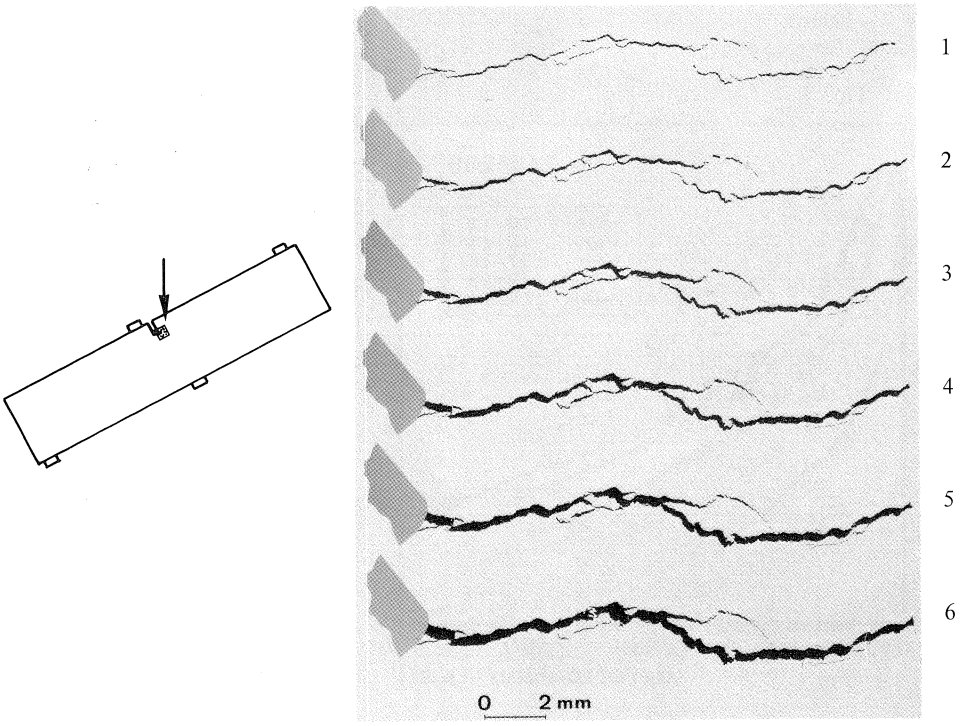

Fig. 4.8 Crack development studied with a long distance microscope.

The crack opens at the notch side of the beam and propagates to the opposite support. The opening of the crack can be seen from the measurements of the local deformations on the specimen surfaces (Figure 4.6). In Figure 4.7 for one experiment the open crack is constructed from these local deformations. This is done at the stage in the descending branch where the load is 20 kN. First, the left beam half with the final crack pattern for this particular test is drawn. At the places where the extensometers are fixed on the specimen, a horizontal line is plotted starting at the left crack surface with a length corresponding to the measured deformation (note that the deformations are enlarged in the Figure to be able to see any crack opening). For CMSD a vertical line is plotted. The right beam half with the same crack curvature is drawn starting at the top of the beam, because this point is defined by CMSD and CMOD. The horizontal distance between the points on the right surface at the positions where the local deformations are measured and the corresponding points on the left crack surface has to be equal to the length of the respective horizontal lines plotted. The results indicate that the crack opens perpendicular to the crack surfaces (see the dashed lines in the plot).
The crack opening is also studied during the test by means of a long distance microscope. In Figure 4.8 the crack development at the notch tip in a large specimen is plotted. At six stages in the load-displacement curve, see Figure 4.9, the area at the notch is scanned with the microscope. Note that the tests are not stopped during scanning. The time needed to obtain each of the six figures is indicated with the thick lines in Figure 4.9. Each crack is constructed from a large number of photos. From these cracks it can also be seen that the crack opens perpendicular to the crack faces and that there is no sliding. Further it can be concluded that the crack is not continuous but that there are a large number of crack face bridges of different sizes. The same was observed in uniaxial tensile tests by Van Mier (1990) as explained in Chapter 2.

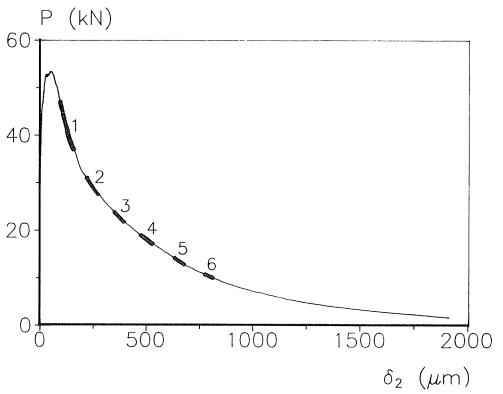

Fig. 4.9 Load-displacement curve of a crack detection test; the numbers correspond to the various stages of crack growth in Figure 4.8.

4.1.2 Determination of fracture energy

To get an idea of the difference in crack growth between mode I and mixed mode I and II, fracture energy obtained from both experiments is often compared. In the proposal

for the round robin by RILEM 89 FMT, one of the objectives was to measure the fracture energy in the beam tests and compare these G_f values with the fracture energy obtained from mode I tests. The problems that arise if the fracture energy is to be determined from experiments have already been shortly discussed in Chapter 2. Here the procedure followed for deriving the fracture energy from the uniaxial tensile tests and the four-point-shear tests performed in this investigation will be explained.
The three main problems to be tackled are sketched in Figure 4.10. The first question is whether pre-peak cracking has to be taken into account, area A_1 in Figure 4.10. Furthermore, the tests are stopped at a certain deformation and it is not known how the tail of the curve should be extended, area A_2. The next problem is the exact zero load. A small error in the zero load can already give a non-negligible error in fracture energy, area A_3. Comparable remarks were already made by Petersson (1981), Hordijk (1991) and Elices et al. (1992).

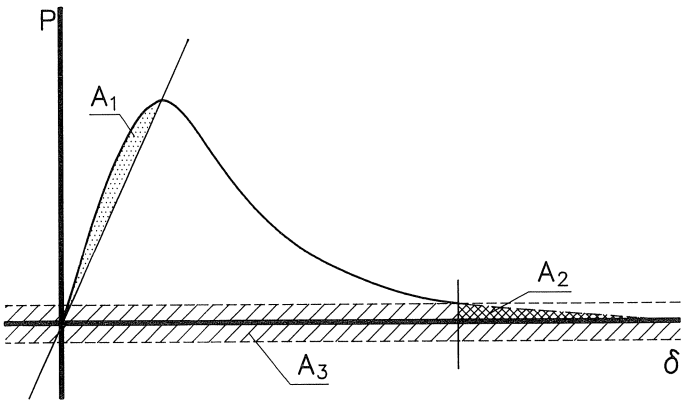

Fig. 4.10 Determination of fracture energy from load-displacement response.

In Table 4.1 G_f-values for both uniaxial tensile tests and four-point-shear tests are given. Results are shown for two different concretes (con8 and con16). The values are the average of at least six experiments, see also Schlangen & Van Mier (1991a). The four-point-shear tests are performed in the old machine. Both tests with the notch at the top and bottom side are included. For the tensile tests the complete area under the σ-δ curve is taken into account (δ is the average signal of 4 LVDTs with a measuring length of 35 mm, see Figure 3.13). Thus, pre-peak cracking also is included in the G_f-value. The curve is cut off at a deformation of 150 μm.
Carpinteri et al. (1989) proposed the following method to obtain the fracture energy from the four-point-shear tests. The fracture energy should be calculated by adding the area under the F_1-δ_1 and F_2-δ_2 curves and dividing the total by the area of the curved crack. For the forces F_1 and F_2 the measured values should be taken, see Schlangen & Van Mier (1991a). If these forces are taken as constant and equal to 10/11 and 1/11 of the total load P, as done by Carpinteri et al. (1989, 1990), the fracture energy is overestimated. The tests of the Italian group were later repeated. Now the distribution of the

Table 4.1 Fracture energy (and standard deviation) determined from mode I and mixed mode I and II tests.

d_{max}	beam size	mixed mode I+II G_f	mode I G_f
8	small	125.6 (7.4)	115.1 (8.3)
8	large	132.1 (29.6)	
16	small	127.8 (22.1)	125.4 (11.5)
16	large	144.6 (18.7)	

loads was measured. The results of these tests (Ferrara (1991)) confirmed the conclusion that the fracture energy is overestimated when a constant distribution of the loads is assumed. The values in Table 4.1 are derived from the F_{2R}-δ_2 curve for tests with the notch at the top and from the F_2-δ_2 curve for tests with the notch at the bottom of the beam. The area under the F_{1R}-δ_1 (and F_1-δ_1) curve is equal to zero as shown in Figure 4.11. The total area under the curve is taken. The tail of the curves is extended until the x-axis is crossed by taking the tangent of the curve.

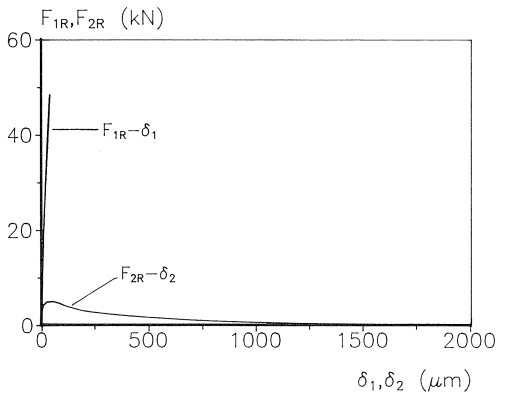

Fig. 4.11 F_{1R}-δ_1 and F_{2R}-δ_2 curves in four-point-shear test.

The difference between the fracture energy derived from the uniaxial tensile tests and the beam tests is small. This supports the conclusion made in the previous paragraph that the fracture mechanism in the four-point-shear tests is caused by mode I opening only. What can be concluded is that G_f for the 16 mm concrete is larger than for the 8 mm concrete, which confirms measurements by others for mode I (e.g. Petersson (1981)). Furthermore the fracture energy seems size-dependent, which is probably caused by crack interface grain bridging. The bridges will probably be larger not only when larger aggregates are used but also when the absolute length of the crack increases, i.e. for larger specimen size. More energy is needed to break larger bridges. It should be mentioned that for a good comparison between G_f-values found with different test procedures and G_f-values found by different researchers, the effects described above are important sources of errors and should be eliminated. However, it is the author's opinion that the fracture energy also depends on the fracture mechanism

that takes place. Since the fracture mechanism for concrete is different in different tests, the fracture energy cannot be a material property.

4.1.3 Numerical study of influence of boundary conditions

As discussed in paragraph 4.1.1. horizontal forces will be introduced in the specimen if the supports are not friction-free. To get an idea of the influence of friction in the supports, numerical simulations are firstly carried out using a finite element code (DIANA) with a smeared crack model, see Rots (1988). Frictional effects are studied by looking at some extreme situations. Three different types of boundary conditions are used in the numerical investigation, see also Schlangen & Van Mier (1990). Firstly, the behaviour of a four-point-shear beam is simulated where the loading points can move in the horizontal direction. In the second analysis the horizontal displacement of the loading points is restricted, whereas in the third simulation only the two middle loading points are fixed.
The finite element idealisation of the problem is shown in Figure 4.12. The situation of the old a-symmetric test set-up is modelled. One specimen size ($400 * 100 * 100\ mm^3$) is analysed. The fracture zone consists of eight-noded elements which are integrated using nine-point Gauss quadrature. A steel loading frame is included in the mesh to model the test rig. The nodes where the load is applied to the concrete beam are allowed to rotate and translate in all directions (simulation I). To prevent displacement of the loading points in the second analysis (simulation II), cross-diagonal steel trusses are used in the loading frame corresponding to the situation in the experiments, see Chapter 3. In the third simulation (III) the horizontal fixation of the middle loading points was realized by adding supports to the mesh for the horizontal direction at the nodes where the load is applied to the beam. The elastic concrete properties were

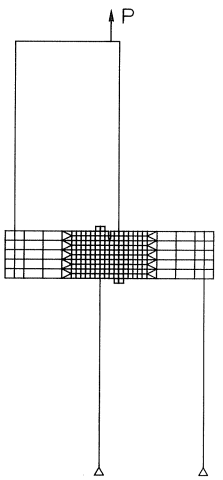

Fig. 4.12 Finite element mesh for simulation of four-point-shear test with smeared crack approach.

assumed to be: Young's modulus $E = 30$ GPa and Poisson's ratio $\nu = 0.2$, which corresponds to the normal weight concrete (con8) used in the experiments. The following parameters for the cohesive softening model (for more details about the model the reader is referred to Rots (1988)) have been taken: tensile strength $f_{ct} = 3.0$ MPa and fracture energy $G_f = 80$ J/m^2. The formulation for the tensile σ-w diagram as proposed by Reinhardt et al. (1986) is used. The crack band width is taken as $h = 10$ mm. The shear retention factor, for including the shear transfer in the crack plane, is $\beta = 0$ (in fact 0.001 to avoid numerical problems). To solve the non-linear equations, an incremental-iterative procedure under load control is required. To pass limit points of vertical tangent in the load-displacement space, the arc-length method introduced by Riks is used.

The results of the three simulations are summarised in Figures 4.13–4.15. Figure 4.13a, b shows the load P versus the deformation δ_1 and δ_2 respectively. The curves have been terminated at the stage where convergence of the iteration process could no longer be achieved. In Figure 4.14 the incremental displacements and the crack patterns for the beams at three stages in the load-displacement curve of simulation I are shown. The incremental displacement at a certain stage is the displacement which is added to the total displacement in the last loading step. An element is cracked in an integration point when the maximum tensile stress is exceeded. After this point stress can still be transferred according to the implemented softening curve. The incremental displacements for the three simulations at the peak of the load-displacement curve are compared in Figure 4.15.

A considerable difference in maximum load, crack propagation and deflection of the beam occurs between the three extremes. If the supports are fixed (simulation II) the load is almost 50% higher than in the case where they can rotate and move horizontally (simulation I). If the supports are fixed, horizontal forces will become active in the specimen. This counteracts the crack propagation in the beam. The crack trajectory in

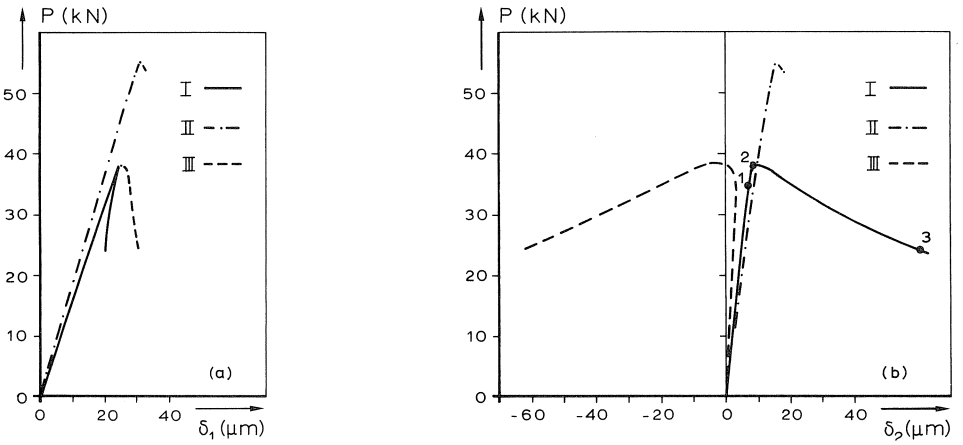

(a) (b)

Fig. 4.13 Total load P versus deformation δ_1 (a) and δ_2 (b).

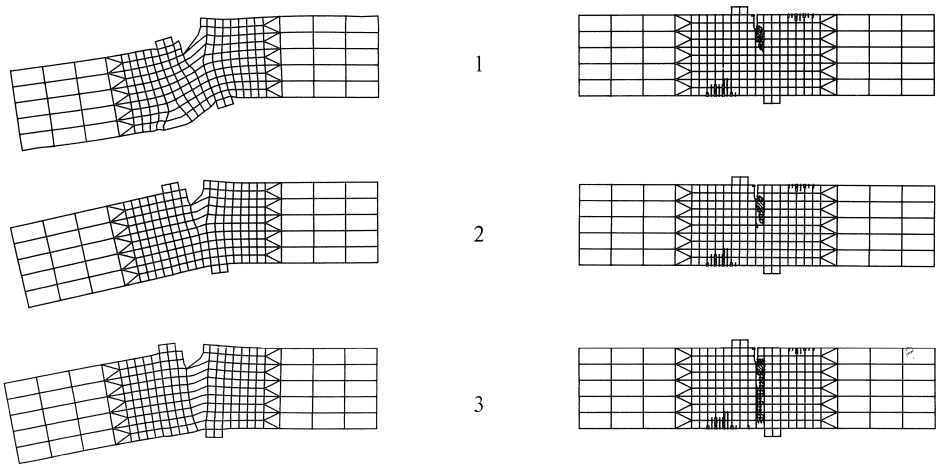

Fig. 4.14 Incremental displacements and crack patterns at three stages (see Fig. 4.13b) in the load displacement curve of simulation I.

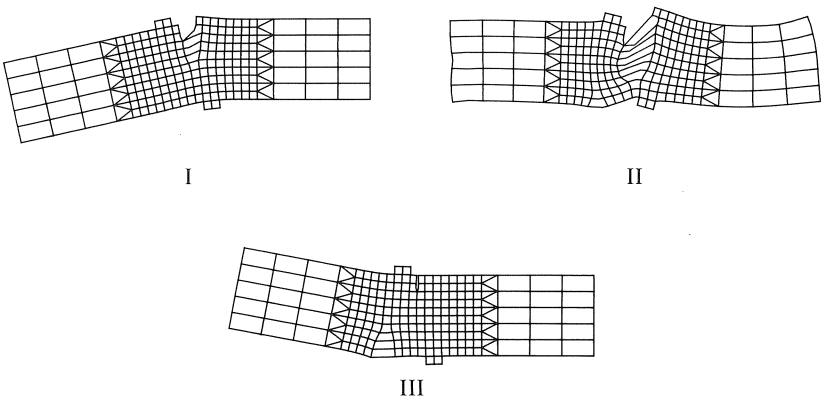

Fig. 4.15 Incremental displacements at peak load for the three simulations.

the numerical simulation with freely rotating supports (simulation I) is less curved if compared with the experimental crack patterns presented in paragraph 4.1.1. The cracks are confined to the edge of the elements. This seems to be the result of choosing a smeared crack approach as already explained in Chapter 2. If the horizontal displacement of the middle support is restricted (simulation III), the maximum load is almost the same as in simulation I, but the crack pattern differs. The flexural crack near the lower left middle support opens beyond peak, see Figure 4.15.
The extreme situations of the numerical simulations will never be reached in experiments. However, friction will always occur in the experiments. The simulations give an idea of what can happen in the experiments if horizontal forces are introduced at the supports as a result of frictional effects. In the next paragraph experimental results are presented of the effect of changing the boundary conditions.

4.1.4 Influence of boundary conditions: experimentally

The influence of the boundary conditions is studied experimentally by mounting diagonal bars to the loading frame as explained in Chapter 3. In both the old and new set-ups the boundary conditions are varied. Here only the results of experiments in the new symmetric set-up are presented. For the results obtained with the first set-up see Schlangen & Van Mier (1990, 1991a). The difference in load displacement curves is shown in Figure 4.16 for the small and the large beams. Here always the results of only

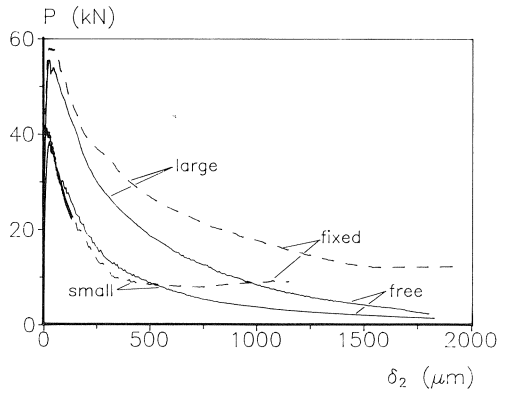

Fig. 4.16 Load displacement curves for beams of two different sizes with freely rotating and fixed supports.

one test are plotted. More results are included in Appendix A1. If the supports are fixed, the descending branch is higher and even increases again. At that stage the curved crack is arrested and for the small beams a second flexural crack develops in the specimen. This crack starts under the middle support at the unnotched side of the beam as shown in Figure 4.17. More crack patterns are included in Appendix A1. The difference in behaviour also becomes clear if the distribution of the loads in the pendulum bars is plotted versus the deformation δ_2 as done in Figure 4.18. This ratio of the loads deviates from the desired value. The ratio of the loads is constructed from the force in the pendulum bars and the vertical component of the force in the diagonal bars. The ratio of the reaction loads increases, which means that the load at the side of the beam (F_{2R}) decrea-

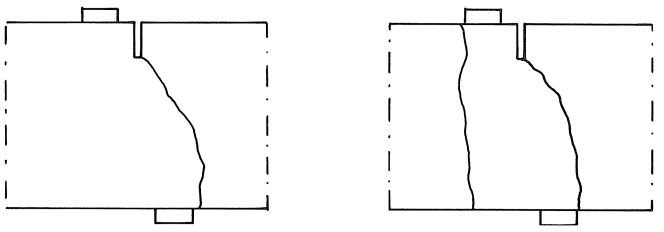

Fig. 4.17 Crack patterns in small beams with freely rotating (a) and fixed supports (b).

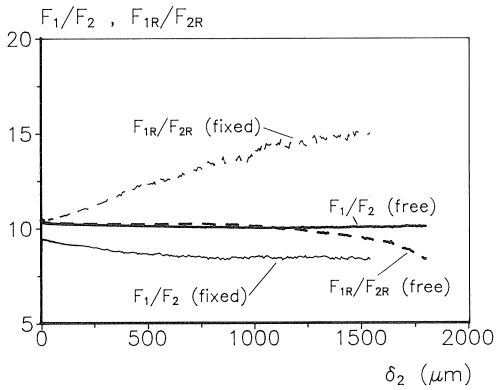

Fig. 4.18 Distribution of loads versus deformation δ_2 for two tests carried out in the new symmetric machine between freely rotating and fixed supports.

ses with respect to the middle load (F_{1R}). Actually the force in the pendulum bar at the side goes to compression, which means that the force in the diagonal bars is tensile. As a result, the horizontal component of the force in the diagonal bars gives a compressive load in the concrete beam. Due to this compressive load in the beam, the curved crack cannot open further. In the tests with fixed supports carried out in the old machine the deviation of the distribution of loads was larger than in the tests in the new machine, see Schlangen & Van Mier (1991a). This is caused by the differences in failure mechanism, as explained in paragraph 4.1.1.

4.2 *Four-point-shear; SEN beams other concretes*

4.2.1 Results of four-point-shear and uniaxial tensile test

In the new symmetric machine cracking in five different concretes is studied, viz. con8, lytag, hsc, fcon and hcp. In this paragraph the results of these experiments will be compared with observations in uniaxial tensile tests performed on specimens of the same material, see also Schlangen & Van Mier (1992h).
The differences in uniaxial tensile stress-deformation response for the various concretes, is shown in Figure 4.19. The load-displacement curves of the four-point-shear tests are plotted in Figures 4.20. Four experiments are performed for each of the materials and each of the two beam sizes. The curve of only one test is plotted. Results of more tests are presented in Appendix A2. In the tests on the large fibre concrete beams the maximum load capacity of the machine was reached. The test therefore had to be stopped. The cracks in the four-point-shear beams all have the same pattern for each of the different materials. The crack starts at the notch and continues to the opposite support as shown in Figure 4.21a. In the small fibre concrete beams a more distributed crack pattern was observed as shown in Figure 4.21b. The crack patterns of the other experiments are included in Appendix A2.

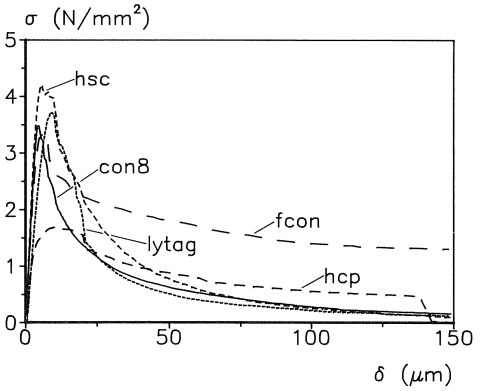

Fig. 4.19 Stress-deformation response of uniaxial tensile tests for different concretes.

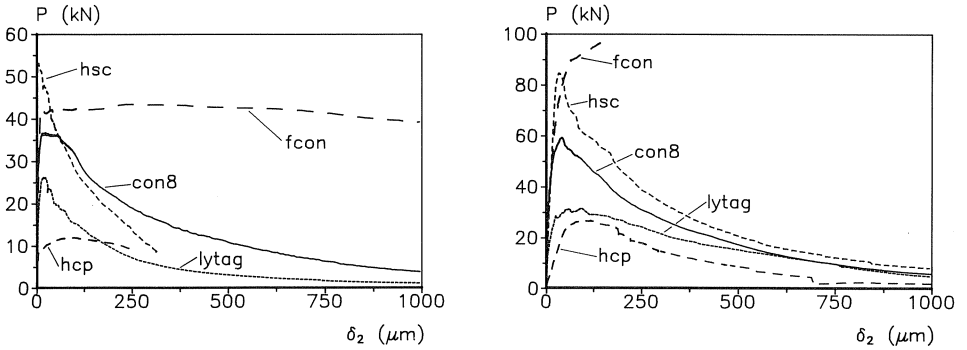

(a) (b)

Fig. 4.20 Load-displacement curves of four-point-shear tests on small (a) and large beams (b) made of different concretes.

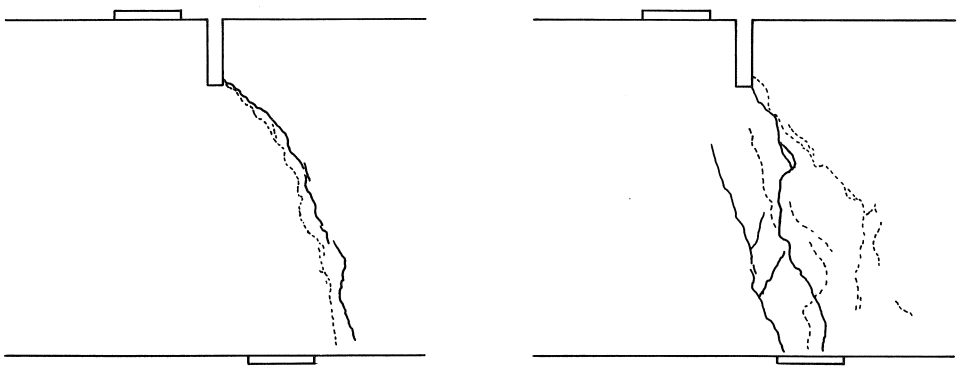

(a) (b)

Fig. 4.21 Crack patterns for con8 (a) and fcon (b).

4.2.2 Influences on fracture process

In the discussion below of the behaviour of the different materials under tension and shear, a comparison with the normal weight concrete (con8) will always be made.

Lytag

In the tensile tests the lytag gives a peak stress which is a few percent higher compared to the con8. However in the four-point-shear tests, the peak load is much lower for the lytag. For the small beams the difference is 30% and for the large beams even 45%. An explanation for this decrease in maximum load could be a difference in moisture content. To check this the specimens were dried in an oven after the test. After 30 days, when there was no further decrease in weight, it was found that the tensile specimens had lost 4% of their weight and the large beams 6.7%. Due to the larger thickness of the beam specimens, they contain more water at the time of testing. This probably leads to a stress gradient over the cross-section which enhances the probability of shrinkage cracking. Consequently the peak load will be smaller, as indicated earlier for normal weight concrete by Wittmann & Roelfstra (1987) and Van Mier & Schlangen (1989).

High strength concrete

Comparing the tensile strength of hsc with that of con8 shows that the increase is approximately 20%. In contrast, the compressive strength increases by 75%. One reason for this could be that the tensile specimens are all pulled parallel to the direction of casting, see also Hughes & Ash (1970). Due to bleeding under the aggregate particles this is probably the weakest direction.

In the four-point-shear tests, an increase of approximately 43% of the maximum load is observed for both beam sizes. Here the cracks start under an angle with the casting direction. At failure the direction of the crack is perpendicular to the casting direction. This supports the above-mentioned explanation for the relatively small increase in tensile strength compared to the increase of the compressive strength.

Fibre concrete

In the fcon the cracks are more distributed as compared to con8. Due to action of the fibres the stresses will be more redistributed, which leads to a wider crack band as shown in Figure 4.21b. The same tendency was found, among others, by Arslan et al. (1991) in shear tests on fibre concrete. From the stress-deformation curves of the tensile tests it can be seen that the maximum stress is almost equal for fcon and con8, but the descending branch is higher for fcon. Some crack opening is needed before the fibres start carrying load. In the beam test the crack starts opening on one side (at the notch). If the maximum load is reached in the small beams, the crack opening at the notch has already reached such a value that the fibres start transferring stress. Therefore almost no stress drop after the peak load occurs. In the large beams, before the peak load is reached, the crack opening at the notch is already so large that the fibres start transferring stress which increases the peak load. The capacity of the machine was not enough to break the large beams.

Hardened cement paste

In the hcp specimens, both in the prisms for the tensile tests and in the four-point-shear beams, a large number of shrinkage cracks could be observed before any loading was applied. During the hardening process the temperature in the material will increase, because of the large cement content. After demoulding the specimens are placed in a water basin. The temperature difference between the specimens and the water was probably too large which caused most of the shrinkage cracks. Alternatively the strength development of the hcp was not large enough at the time when the specimens were taken from the water to withstand the hygral stresses. Due to these cracks the maximum load measured in the tests was considerably lower than for con8.

It seems that cracks grow under mode I, even when the external loading is mixed-mode. The influence of the shear loading seems to be a rotation of the principal stress. To compare the fracture process in different concretes, it is important to include in the discussion influences due to differences in manufacturing, drying and hardening. Different fracture behaviour is often the result of the differences in microstructure, which is obvious in the case of fibre concrete, but lytag and high strength concrete also have a different fracture mechanism than normal weight concrete as shown by Van Mier (1991b).

4.3 *Four-point-shear; DEN beams*

The four-point-shear test on DEN beams are carried out for one material (con8) only. As explained in Chapter 3, two beam sizes are tested ($d = 150$ and 300 mm). The boundary conditions are varied in the same way as for the SEN beams. The tests are performed with freely rotating supports and with fixed supports, which is realized by mounting diagonal bars to the loading frame. At both notches and at the front and rear of the specimen, the CMSD and the CMOD was measured, see Chapter 3. The average signal of the two CMSD gauges and the two CMOD gauges at the front of the specimen was used as a feedback signal in the closed-loop servo control.

The crack patterns observed in the four different tests (two sizes and two different boundary conditions) are shown in Figure 4.22. More crack patterns can be found in Appendix A3. In Figure 4.23 the total load P is plotted versus the control signal in the experiment for four different tests. In Appendix A3 additional load-displacement curves are plotted. Figure 4.24 shows the total load P plotted versus the CMOD and the CMSD signal separately for an experiment on a small beam. Note that the CMOD is negative in the ascending branch, whereas the CMSD shows a steep drop beyond peak. In some tests even a snap-back behaviour was observed beyond peak. The average of both CMOD and CMSD, however, increases continuously, which is necessary for a stable test control. For the case with freely rotating supports, first two cracks start to grow at the two notches. After peak load only one crack propagates until complete failure of the beam. This can also be seen from Figure 4.25 where the total load P is plotted versus the CMOD at the top notch (average of front and rear) and the CMOD at

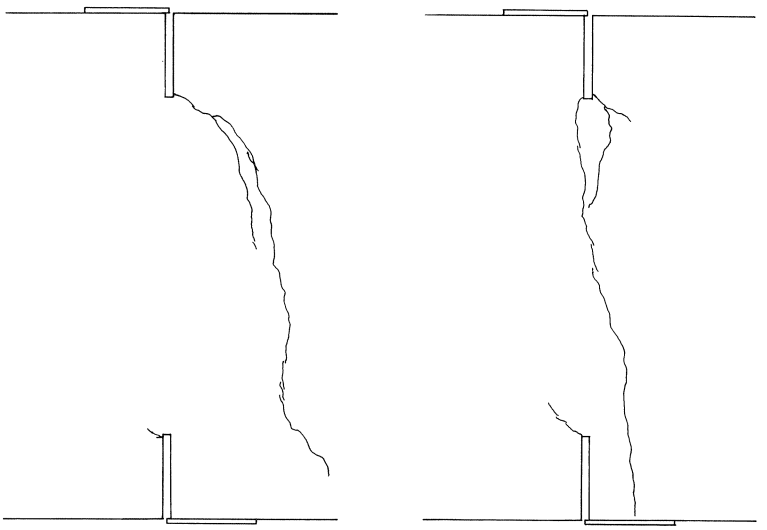

Fig. 4.22 Crack patterns in DEN beams of two sizes ($d = 150$ mm and $d = 300$ mm) loaded in four-point-shear with freely rotating and fixed supports.

the bottom notch (average of front and rear) for a small beam specimen. After the peak load only the opening displacement at the top notch increases, whereas the bottom notch closes again.

If the supports are fixed, two curved cracks again start to grow from the notches. These two cracks continue until they are arrested in the compressive zones in the beam. The cracks cannot open further, because of the restriction of horizontal movement of the outer supports. Final rupture of the beam occurs through the growth of a third splitting crack between the notches as shown in Figure 4.22. It was observed (with the naked eye) during the tests that this last crack starts in the middle of the beam. No difference in behaviour was observed for the small and the large DEN beams. In the load-displacement curves of Figure 4.23 it can be seen that the tail in the descending branch is higher for fixed supports and that at large deformations, the load even increases again.

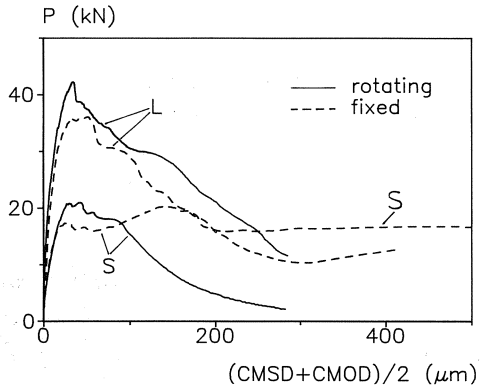

Fig. 4.23 Total load P versus control signal in tests for two small and two large beams loaded between freely rotating and fixed supports.

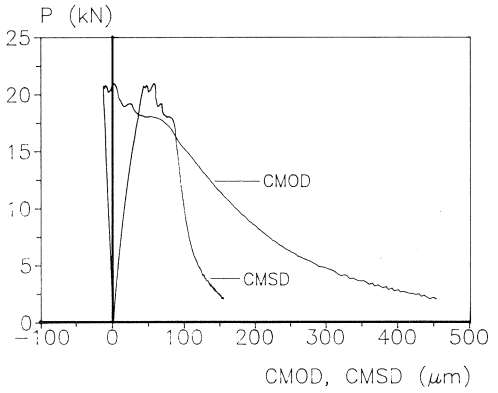

Fig. 4.24 Total load P versus CMOD and CMSD for a small beam tested between freely rotating supports.

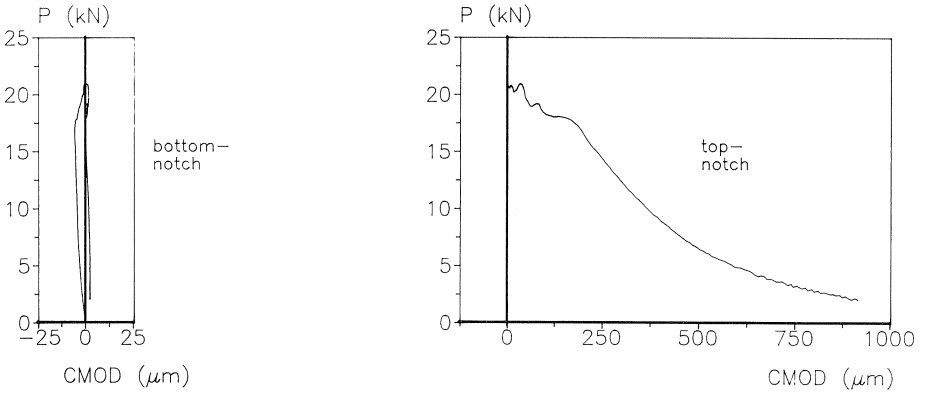

Fig. 4.25 Total load P versus CMOD at bottom (a) and top notch (b) for a small beam tested between freely rotating supports.

4.4 *Discussion of results*

From the experiments on single and double-edge-notched four point shear beams, it can be concluded that the fracture mechanism is mode I even if the global loading situation is a combination of mode I and mode II. The cracks open perpendicular to the maximum tensile stress in the beam. The influence of the shear load seems to be a rotation of the direction of this maximum tensile stress. No sliding over the crack faces is observed in the experiments.

The mechanism that takes place in the SEN beams loaded between freely rotating and fixed supports is sketched in Figure 4.26. When a beam is loaded between freely rotating supports, a crack will start to grow from the notch at an angle. The crack will subsequently propagate along a curved path as shown in Figure 4.26a. When on the other hand diagonal bars are mounted onto the loading frame, the free movement of the specimen is restricted. The curved crack (no 1 in Figure 4.26b) will not open completely due to horizontal confinement in the concrete beam. A flexural crack (no 2 in Figure 4.26b) will start at the unnotched side of the beam. Measurements of the distribution of the loads in the pendulum bars show that the ratio deviates if the supports are fixed. Friction in the supports, also indicated by a deviation of the ratio of load distribution, will lead to an introduction of horizontal forces in the specimen. Furthermore the cracked specimen will influence the load distribution as already explained in paragraph 4.1.1. The same mechanism is observed in the case where the machine is loaded in compression, see Ferrara (1991). It is likely that in the latter case the mechanism is exaggerated by friction effects as explained in paragraphs 4.1.3. and 4.1.4. However, in the symmetric machine used in this investigation the ratio of loads is forced to stay constant.

Although some undefined factors are involved in the calculation of fracture energy, it is concluded from the present investigation that no difference exists between fracture energy obtained from mode I and from mixed mode I and II tests. This in contradiction to the increase in fracture energy for mixed mode tests as reported by Carpinteri et al.

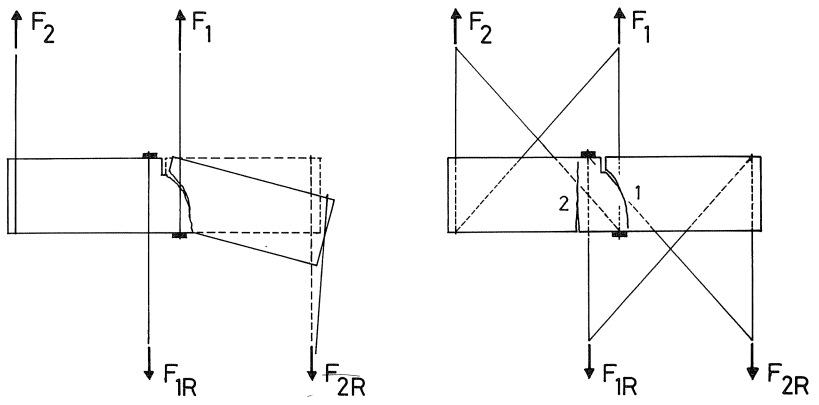

Fig. 4.26 Failure mechanisms for SEN beams loaded between rotating (a) and fixed supports (b).

(1989,1990). However, in that investigation the fracture energy was determined from the F_2-δ_2 curve, where F_2 was derived from the total load P in stead of measuring F_2. In this way the fracture energy is overestimated.
The results obtained from the shear tests on different concretes were not consistent. However, in several cases the variation in behaviour could be explained from the differences in microstructure, curing and hardening of the different concretes.
A comparison with the simulations already discussed in Chapter 2 shows that the prediction of crack patterns is in good agreement in cases where a discrete crack approach is adopted in the simulations, Arrea & Ingraffea (1982), Carpinteri et al. (1990) and Alfaiate et al. (1992). However in cases where a smeared crack approach was used, see for instance De Borst (1986) and paragraph 4.1.3. of this report, the obtained crack pattern is wrong. As a consequence shear softening has to be included to obtain correct load-displacement diagrams, but then the physics of the problem are highly debatable.
The mechanism that occurs in the DEN beams is sketched in Figure 4.27. When a specimen is loaded between rotating supports, initially two cracks start to grow from the two notches. However, after peak load only one crack will propagate until final failure, see Figure 4.27a. When on the other hand the specimen is loaded between fixed supports, two overlapping curved cracks (no. 1, 2 in Figure 4.27b) develop from the two notches. Both cracks are arrested due to horizontal forces in the specimen as already explained above for the SEN beams. Final rupture of the beam occurs due to the growth of a third splitting crack (no. 3 in Figure 4.27b) in between the two curved cracks.
The experiments of Bažant & Pfeiffer (1985) show a different mechanism. As discussed in Chapter 2, a straight crack between the supports led to failure of the beams. It was claimed that this was a real shear failure. Simulations of Ingraffea & Panthaki (1985) already pointed in the direction that splitting probably occurred. In the present investigation splitting failure was found in the case of fixed supports. Another explanation for the single straight crack found by Bažant & Pfeiffer (1985) could be that explosive

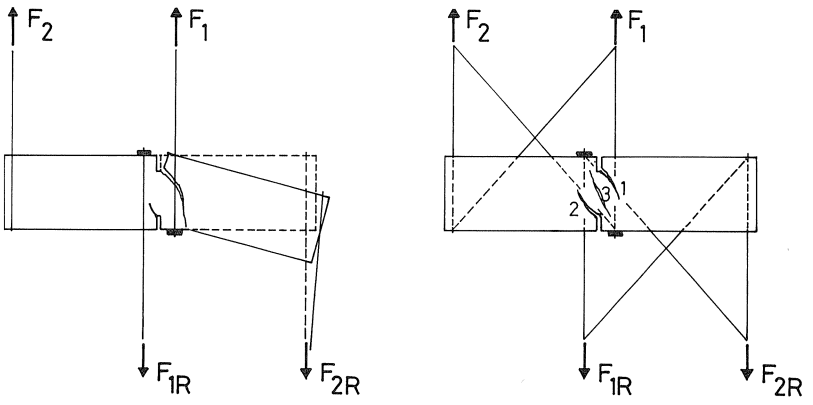

Fig. 4.27 Failure mechanisms for DEN beams loaded between rotating (a) and fixed supports (b).

failure probably occurred in the tests because the beams were loaded in stroke control. Using load control a single crack was observed in similar tests by Davies (1991). However in the latter tests the geometry of the specimens was slightly different. Test results obtained by Swartz & Taha (1987) showed a similar behaviour to the tests described in this report. Simulations of Rots et al. (1987) predicted a similar failure mechanism. However, the curvature of the cracks was not enough, which resulted in only one crack as final crack pattern. Further shear softening was necessary to obtain a correct load-displacement response.

5 Lattice model

This chapter deals with the concept of the numerical model used for the simulations of the fracture processes. The procedure for crack growth, three ways to implement heterogeneity and the determination of input parameters are discussed.

5.1 *Model concept*

5.1.1 Background of model

In the model a technique is used which has recently received much attention in theoretical physics, as already mentioned in Chapter 2. However, the basic idea is already older; in 1941 Hrennikoff (1941) proposed a model to describe a material on a macroscopic scale by means of a network of truss elements. In the present micromechanical model, the material is schematized as a lattice of small beam elements, see also Schlangen & Van Mier (1991a, b). A triangular shape for the lattice is chosen (Figure 5.1a), but other shapes are also possible, see for instance Herrmann et al. (1989). The beam elements have fixed connections in the nodes. They can transfer axial force, shear force and bending moments, see Figure 5.1b. To solve the elastic equations the finite element code DIANA is used. Networks with truss elements, where free rotations are possible in the nodes, are also used to investigate fracture in concrete (Burt & Dougill (1977), Schorn & Rode (1987), Bažant et al. (1990) and Berg & Svensson (1991)) or in other materials (Termonia et al. (1985) and Duxbury & Kim (1990)).

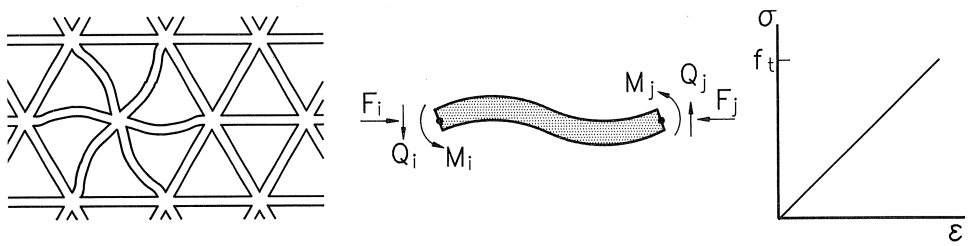

Fig. 5.1 Triangular lattice of beam elements (a); external forces on a single beam element (b); stress-strain relation of a single beam element (c).

In the previous chapters the fracture process in concrete is described. It is shown that first of all microcracks occur in the material. These microcracks grow further and start to localise in a main crack. However the main crack is not continuous; overlaps or crack face bridges develop, Van Mier (1990). These overlaps have different sizes, since they develop mostly around the aggregate particles in the concrete, see figures 2.5 and 2.6. The material between these overlapping cracks rotates as is shown in Figure 5.2a. Final failure of the material occurs by the bending of the bridges and continuation of one of the crack tips. Especially this last phenomenon in the fracture process, the rotation of the material that still connects the two crack faces, cannot be described with a network of truss elements. Since the formation of crack face bridges seems to be the main toughening mechanism for concrete, a numerical model for simulating concrete fracture on a microscale should be able to describe this mechanism.

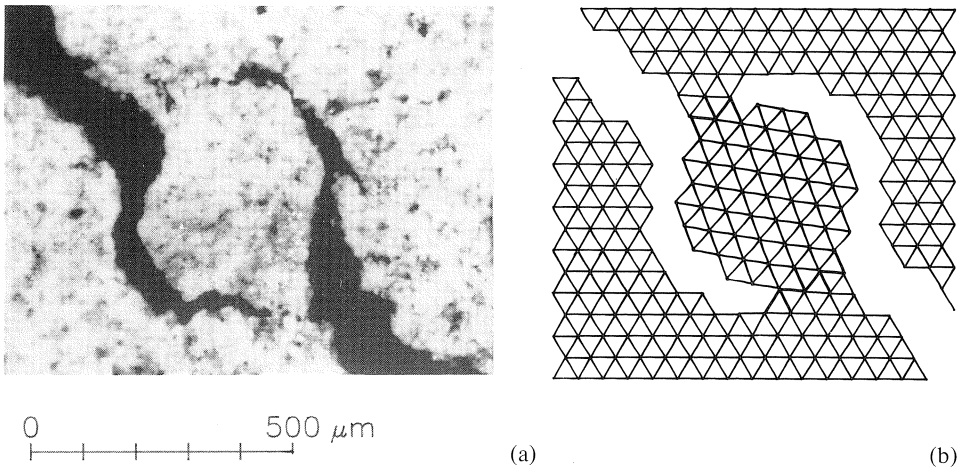

Fig. 5.2 Rotation of material in crack face bridge, experimental (a) and fictitious numerical example (b).

Fracture in the lattice of small beams is obtained by removing in every load-step the element, with the highest tensile stress relative to its tensile strength, from the lattice. This implies brittle fracture of a beam element. In Figure 5.1c the stress-strain relation of a single beam element is shown. The stress in each element is derived from a linear elastic analysis that is conducted using the finite element method (see 5.1.2. and 5.1.3.). This means that a crack grows through the material, following the direction which is governed by the combination of the maximum tensile strength and the weakest link in the material which is the result of the heterogeneity that is implemented, see paragraph 5.2. Following this very simple procedure, cracks as shown in Figure 5.2b can be obtained. (Figure 5.2b is not the result of a real simulation, but is a fictitious example of how fracture in a lattice can take place, only used to explain the mechanism). Because the beams are fixed in the nodes and bending can be transferred, local rotations of the material are possible, also if the material is connected by only a few beam elements to the crack faces.

If the fracture process in concrete is to be simulated on a micro-scale with a continuum model, this model should also be able to capture the rotation of the material as described above. A general continuum concept is not sufficient, because no bending terms are present (Figure 5.3a). The Cosserat equations for an elastic medium are therefore a better option to describe the process, because bending terms are included (Figure 5.3b). For simulating fracture such a continuum model is, for example, used by De Borst & Mühlhaus (1991) on a macroscopic scale. However the applications are limited to cases where compression and shear dominate and the determination of input parameters on this scale causes problems as described in Chapter 2. By coincidence the equations of a 2D-network of beam elements are a straightforward discretisation of the equations of a 2D-Cosserat elastic medium as shown for instance by Roux (1990).

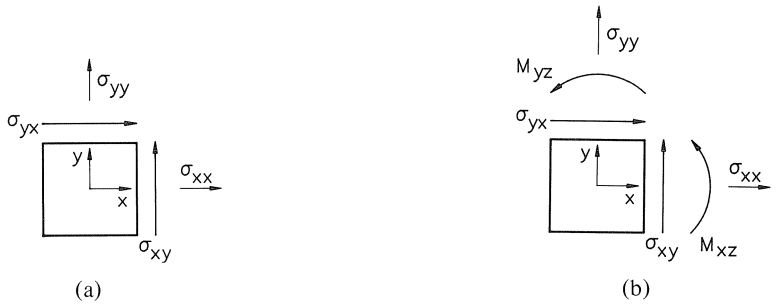

Fig. 5.3 Stress in a general continuum (a); stress and couple-stress in a Cosserat continuum (b).

5.1.2 Mesh construction and linear elastic analysis

For the determination of the stresses in the beam elements a linear elastic analysis using a finite element package is conducted. In the simulations presented here the package DIANA is used. As mentioned before the material is schematised as a lattice of small beam elements. In most of the simulations a regular triangular lattice is used in which all the beams have equal length. In paragraph 5.2.3. the construction of a random lattice in which all the beams have different lengths will be discussed. All the simulations are performed two-dimensional (plane stress), but for the construction of a three-dimensional mesh the same procedures can be followed. To reduce computer time only the part of the specimen where cracks are expected are modelled with the lattice. For the remainder of the specimen continuum elements (plane stress elements) are used. In the linear elastic analysis the specimen is loaded by giving nodal displacements or nodal loads. The outcome of the linear elastic analysis is the normal forces, shear forces and bending moments in the beams. In addition the displacements of the nodes of the mesh and reaction forces in the supports can be obtained.

5.1.3 Crack growth procedure

Crack growth is realised simply by removing an element from the mesh. For the removal procedure first the stress in the beam elements should be analysed. For the

stress the maximum tensile stress in a beam element due to normal force and bending moment is taken. The normal force F in each beam and bending moments M_i and M_j in the nodes i and j respectively are derived from the linear elastic analysis of the lattice with a prescribed external load P_{pre} or a prescribed nodal displacement u_{pre}. Next the maximum tensile stress σ_t in the beams is obtained from the following relation:

$$\sigma_t = (F/A + \alpha * (|M_i|, |M_j|)_{max}/W) \tag{5.1}$$

In this stress formula $A = b * h$, which represents the cross section of the beams and $W = b * h^2/6$. The parameter α is introduced to select a failure mode where bending plays either a dominant or a restricted role. The influence of the different parameters is discussed in paragraph 5.3.2.
Subsequently fracturing of the material takes place by removing the beam element with the highest stress σ_t relative to its tensile strength f_t. Thereafter the next loading step is undertaken followed by another removal until complete fracturing occurs. Following this procedure in each step an exact solution is obtained. If fracture in a heterogeneous material like concrete is to be simulated, a certain disorder has to be implemented in the properties that are taken as input for the lattice. The way heterogeneity can be implemented is discussed in paragraph 5.2.

5.1.4 Deriving the load-displacement response

The external load that can be carried by the lattice is in each loading step simply determined by multiplying P_{pre} by the factor $\beta * f_t/\sigma_t$ of the beam element that will be removed in that step. The parameter β is a scaling factor for the maximum global stress. The determination of β will be discussed in 5.3.2. The same procedure has to be followed to derive the total displacement in the case of a prescribed displacement u_{pre}, see also Schlangen & Van Mier (1992c, j).
The resulting load-displacement response of a simulation of a uniaxial tensile test is shown in Figure 5.4a. The sharp drops in the response can be explained by the fact that

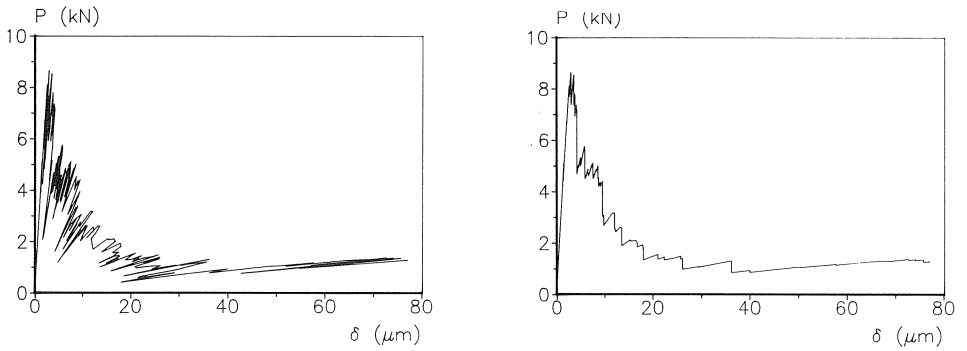

(a) (b)

Fig. 5.4 Load-displacement response: real output from simulation (a); result after smoothing (b).

after a beam element is removed, much less load is needed to break the next beam(s), after which again an increasing load is required to continue further. This can be compared with a small propagation of a crack in an experiment under constant load until the process becomes stable again. In most simulations presented in the following, the simulated curves have been smoothed out in the way shown in Figure 5.4b in order to make a comparison with the experimental curves more realistic. While adopting this procedure the assumption is made that, when a deformation controlled test is simulated, the monotonical increasing deformation that is used as feed back signal in the test also has a continuous increase in the simulation. However it should be mentioned that this procedure should used with great care because snap-backs in the load displacement curves cannot be captured with this procedure.

5.2 *Implementation of heterogeneity*

5.2.1 Statistical distribution of properties of beam elements

As mentioned above for simulating fracture processes in heterogenous materials disorder has to be implemented. A fairly straightforward way to do this is to assign different properties to all the beam elements in the lattice, see Schlangen & Van Mier (1991a, b). The most obvious parameter to distribute is the strength of the beam elements. In Chapter 6 some simulations will be shown where the strength values for the beams are randomly chosen from a normal distribution. In Figure 5.5 the resulting strengths are plotted that are used in the simulation of the four point shear test of paragraph 6.2.1. The average strength used is equal to 3 MPa and the standard deviation is 1 MPa. Both values are taken arbitrary. Of course other parameters too can be varied and other distribution functions can be used. In Herrmann et al. (1989), for instance, examples are shown with parameters randomly chosen from a Weibull distribution.

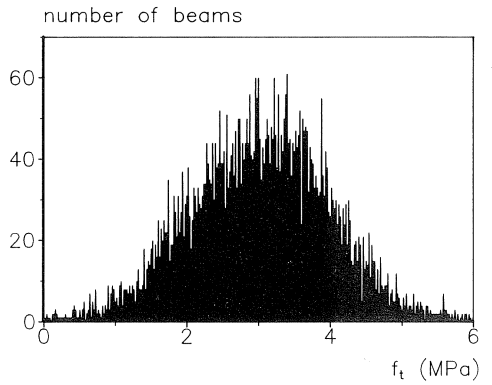

Fig. 5.5 Example of distribution of beam strengths.

5.2.2 Generation of grain structure

Concrete is a heterogeneous material in which the heterogeneity is clearly defined by its microstructure. Concrete can be considered as a two-phase material consisting of gravel aggregates embedded in a cement matrix. In this paragraph a method for implementing disorder is discussed that makes use of this existing heterogeneity.
First the grain structure of the material is generated. Since the simulations are two-dimensional, an assumption has to be made for the distribution of the diameters of the intersection circles (aggregate particles are assumed to be perfect spheres) in a cross section of a concrete body. For the distribution of the aggregate particles in the concrete mix a Fuller curve has been chosen. Equation 5.2 is the description of the Fuller curve in which p denotes the percentage by weight passing a sieve with aperture diameter D and D_{max} is the diameter of the largest aggregate particle. This curve represents a grading of aggregate particles which results in optimum density and strength.

$$p = 100\sqrt{(D/D_{max})} \tag{5.2}$$

Using a cumulative distribution function, for a certain concrete mix, the distribution of circle diameters in a certain cross-section can be generated. For this purpose equation 5.3, derived by Walraven (1980), is used. This function represents the probability P_c that an arbitrary point in the concrete body, lying in an intersection plane, is located in an intersection circle with a diameter $D < D_o$.

$$P_c(D < D_o) = P_k * (1.455 * D_o^{0.5} * D_{max}^{-0.5} - 0.50 * D_o^2 * D_{max}^{-2} + 0.036 * D_o^4 * D_{max}^{-4} + 0.006 * D_o^6 * D_{max}^{-6} + 0.002 * D_o^8 * D_{max}^{-8} + 0.001 * D_o^{10} * D_{max}^{-10}) \tag{5.3}$$

Using this function for a certain concrete mix the distribution of circle diameters in a certain cross-section can be generated, see Schlangen & Van Mier (1991b, i). For example in Figure 5.6a the generated grain structure is shown for a concrete cross-section of $125 * 125$ mm^2. The maximum aggregate size D_{max} in the mix is 16 mm. The ratio of the total volume of the aggregate to the concrete volume, P_k is taken 0.75. The distribution of circle diameters is shown in Table 5.1. The circles are randomly posi-

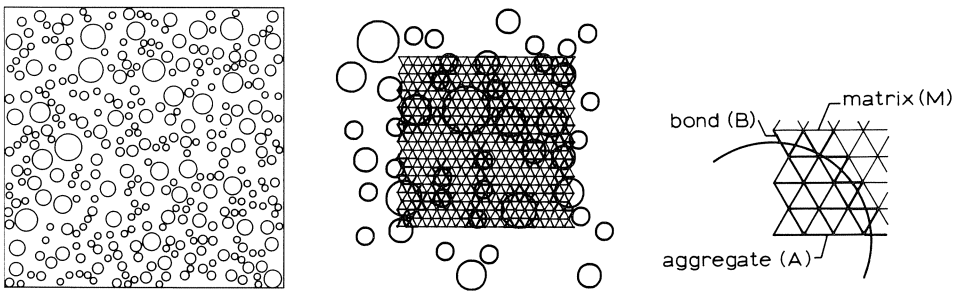

Fig. 5.6 Generated grain structure (a); projection of triangular lattice (b); definition of aggregate, bond and matrix beams (c).

tioned in the area starting with the largest circles, see Figure 5.6a. The minimum distance between the centres of two circles A and B is taken $1.1 * (D_A + D_B)/2$ according to Hsu (1963). Circles with small diameters are excluded from the generated grain structure, because the length of the beam elements should be at least two or three times smaller than the smallest circle diameter as will be discussed in paragraph 5.3.

Table 5.1 Particle distribution in grain structure

D (mm)	1*	2*	3	4	5	6	7	8	9	10	11	12	13	14	15	16
No.	771*	455*	155	71	37	21	13	8	5	3	2	1	0	0	0	0

* D=1 and D=2 mm are not placed in the grain structure of Figure 5.6a

It should be mentioned that by excluding small circles this does not mean that only small particles are excluded. In a 2D cross-section the diameter of larger particles can also be small.

For three-dimensional simulations the Fuller curve can directly be used to generate a three-dimensional grain structure as shown in Figure 5.7.

The triangular lattice is projected on top of the generated grain structure (Figure 5.6b), and different strengths and stiffnesses are assigned to the respective beam elements (Figure 5.6c). When a beam element is situated inside an aggregate particle, the failure strength of the aggregate will be assigned to this element; a beam element located on the boundary between aggregate and matrix will get a low bond strength when fracturing of normal weight concrete is simulated. Matrix strengths will be assigned to those beams projected on the cement matrix in the generated two-phase material.

5.2.3 Construction of random lattice

A disadvantage of the method for introducing disorder described above is the enor-

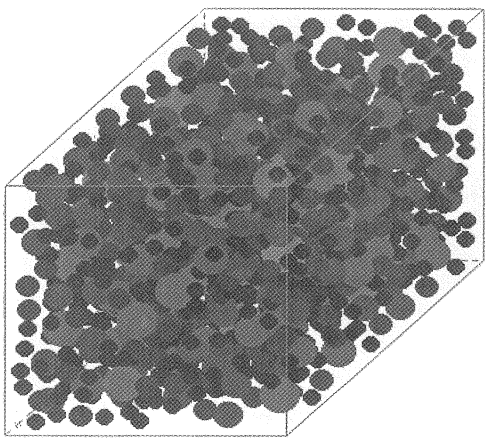

Fig. 5.7 3-Dimensional generated grain structure.

mous number of elements needed to describe the material correctly. Since the size of the aggregates in the concrete is defined, the maximum length of the beam elements in the latice is also fixed. To obtain realistic results at least a few elements are needed inside an aggregate particle. Another problem of the regular lattice is that the cracks tend to follow the direction given by the anisotropy in the mesh.

To overcome these problems random lattices can be used in which the disorder is introduced by selecting beams of different lengths, see Burt & Dougill (1977), Berg & Svensson (1991) and Bažant et al. (1990). In the approach adopted by Burt & Dougill and Berg & Svensson nodes are randomly placed in an area following which nodes are randomly connected with beam elements. This leads to crossing of the elements which makes the visualisation of the fracture process extremely difficult. Another disadvantage of these models is that to obtain correct results, strain softening is implemented as a material parameter, which means that iterative procedures have to be used.

In this investigation a special random lattice is adopted. It is a vectorizable lattice that has been developed by Moukarzel & Herrmann (1992). Disorder is implemented by a difference in beam length. Anisotropy is avoided without crossing of elements. The starting point for generating this random lattice is a regular square lattice. In each cell of the square lattice a point is selected at random with uniform distribution. Subsequently the random lattice is defined by connecting always the three points which are closest to each other using the Voronoi construction, see Figure 5.8a. The randomness can be varied by decreasing the size of the area in a square cell in which a point is chosen at random, see Figure 5.8b. In the limit case again the square lattice is the result. In the simulation presented in this report only lattices with the maximum randomness are used. The random lattice is used only in the part of the specimen where cracks are expected. The connections to plane stress elements are realized through dependency relations.

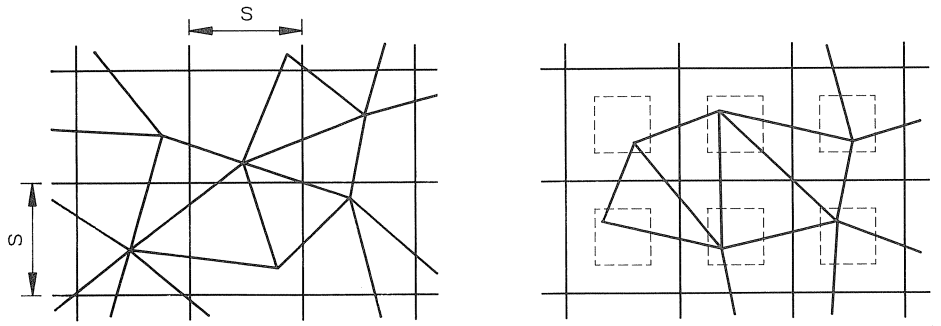

Fig. 5.8 Construction of random lattice (a); variation of randomness (b).

5.3 *Determination of input parameters*

5.3.1 Input parameters for lattice with aggregative structure and comparison with experiment

In this paragraph the determination of input parameters for the lattice model is discussed in the case the disorder is implemented by using the aggregative structure. The resulting parameters that are obtained from a parameter study are given. The results of a simulation of a uniaxial tensile test with these parameters are compared with the experiment. The influence of the individual parameters is discussed in the next paragraph. In 5.3.3. the input parameters for the random lattice are described. For the regular lattice with the distributed beam properties arbitrary parameters are taken as mentioned in 5.2.1. Only a limited number of simulations are carried out using this procedure, and no further study of the influence of the input parameters is undertaken.
To obtain the correct linear elastic behaviour for the lattice the following procedure is adopted. A lattice with beam elements is loaded in tension. The Young's modulus E of the beams is taken equal to the stiffness of the material. The thickness b of the beams is taken equal to the thickness of the material. These values are chosen so as to get an easy adjustment if fracture in materials with a different stiffness or specimens with a different thickness are to be simulated. The length l and the height h of the beams are chosen such that the overall Young's modulus of the lattice is equal to the material stiffness. This results in $h = 0.68 * l$ for the beam elements. The following remark has to be made: With the chosen input parameters (i.e. ratio of h and l), the beam theory is not valid any more. However it is chosen to persist to the concept of the beam theory. The length of the beams strongly depends on the smallest aggregate size in the grain structure as will be discussed further in the next paragraph. In the case of the aggregative structure the stiffness of beam elements in the respective parts of the two-phase material are given different values, as will be shown in the next paragraph. However this is done in such a way that the overall stiffness of the composite is not changed.
The Poisson's ratio for a regular triangular lattice with *hinges* in the nodes is equal to 1/3 as shown by Hrennikoff (1941). For a triangular lattice with *fixed* connections in the nodes, however, the Poisson's ratio can be adjusted by different parameters. The same conclusion was recently drawn from a study by Murat et al. (1992). With the input parameters mentioned above, i.e. the Young's modulus and the cross-section for the beams, a value for the Poisson's ratio of 0.16 is obtained. For concrete this value is accurate enough. By changing the stiffness of the respective beam elements in aggregates, matrix and bond zone, the Poisson's ratio can be changed. If the stiffness of the beams is varied the total stiffness of the composite should again be equal to the material stiffness. Also a variation of the cross-section values h and b leads to different values of the Poisson's ratio. However this also effects the overall stiffness, so that the beam stiffness has to be adjusted.
To determine the other input parameters a parameter study is undertaken. For this purpose the uniaxial tensile experiment described in paragraph 3.4 is simulated. In Table 5.2 the values of the input parameters giving the best fit with the experiment are

Table 5.2 Input parameters for simulations

beam elements:	l =5/3 mm	h =0.68 * l	b =specimen thickness
strengths:	$f_{t,A}$=10 MPa	$f_{t,M}$=5 MPa	$f_{t,B}$=1.25 MPa
stiffness:	E_A=70 GPa	E_M=25 GPa	E_B=25 GPa
	α =0.005	β =2.0	

listed. Figure 5.9 shows a comparison of the experiment and simulation. In the next paragraph the influence of the individual parameters on the load-displacement curve is discussed.

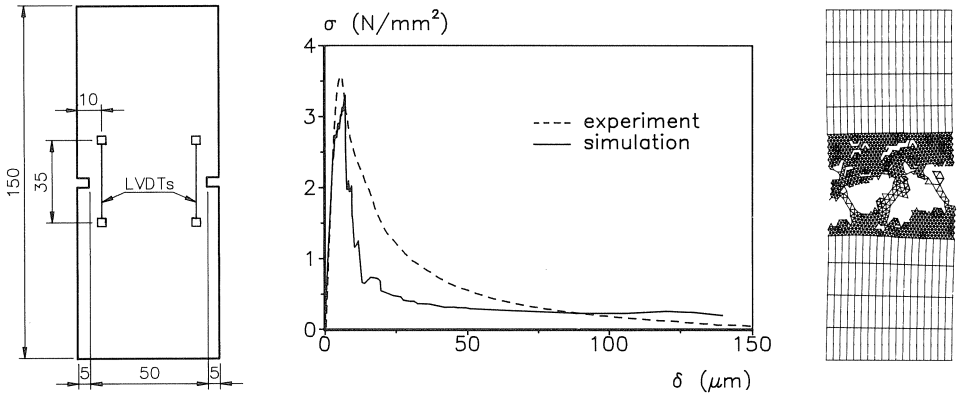

Fig. 5.9 Comparison of experiment and simulation of uniaxial tensile test on standard DEN specimen.

5.3.2 Influence of individual parameters

To study the influence of the individual parameters simulations of a uniaxial tensile test on double-edge-notched prisms are carried out, see Schlangen & Van Mier (1992c, j). The beam length, the fracture law parameter α and the strength of the beam elements in the bond zone are varied. One parameter is always varied, while the other parameters are kept constant. In the generated grain structure circles with diameters between 3 and 8 mm are included, because smaller circular diameters would imply too small an element length and thus too large a number of elements.

Length of beam elements

Three simulations with different lengths for the beam elements are carried out. For the beams, a length of 5/2, 5/3 and 5/5 mm is taken. The deformed and cracked meshes for the three simulations are shown in Figure 5.10. The stress-deformation curves are plotted in Figure 5.11. Only three different sizes are simulated. Nevertheless from the stress-deformation response it can be concluded that with a minimum aggregate size of 3 mm, a beam length of 5/3 mm seems accurate enough, because beam lengths of 5/3 and 5/5 mm give the same response.

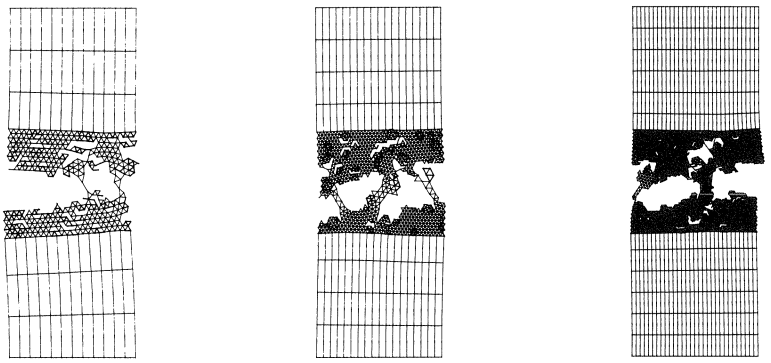

(a) (b) (c)

Fig. 5.10 Cracked and deformed meshes for three simulations with different beam lengths, $l = 5/2$ (a), $l = 5/3$ (b) and $l = 5/5$ mm (c).

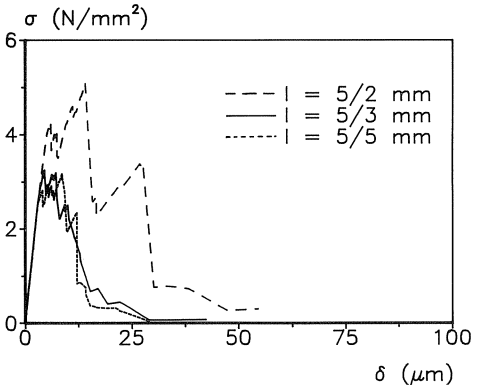

Fig. 5.11 Stress-deformation curves for three simulations with different beam lengths.

Parameter α in fracture law

The parameter α is used to control the fracture mode: bending can either play a dominant or a restricted role. Changing α affects the tail in the stress-deformation curve. However, the influence of changing α is small. In Figure 5.12 three curves for three different values for α are shown. The curves have been scaled in such a way that the peak loads are equal. A small α gives a long tail in the stress-deformation response, whereas a large α results in more brittle global behaviour. Nevertheless if α is taken too low, the fracture process that is predicted shows a peeling effect. This was obtained in simulations with a beam model, in which a rectangular lattice was used and where α was taken zero (Tzschichholz (1991)).

Strength and stiffness of beam elements

For a normal weight concrete the strength of the bond zone between aggregates and matrix is the weakest link. The aggregates are the strongest material in the composite

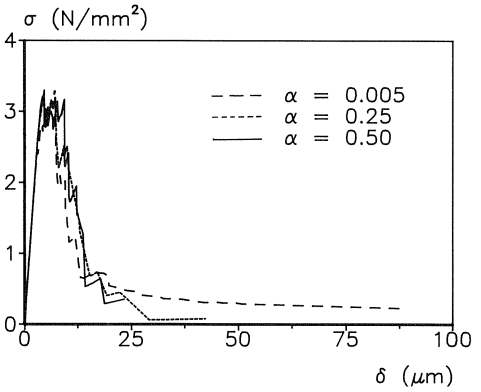

Fig. 5.12 Stress-deformation curves for three simulations with different values for α.

and therefore have the highest strength and stiffness in the simulations. In the simulations the strength of the bond zone is varied with respect to the strength of matrix and aggregates. Experimental values for the strength of the respective parts in the composite are given for instance by Rehm et al. (1977). In the simulations the stiffness is not varied, but taken equal to the values in Table 5.2.

In Figure 5.13 the load-displacement curves of four simulations (with bond strengths $f_{t,B}$ of 0.25, 0.50, 1.25 and 2.0 MPa) are shown. The curves have been scaled in such a way that the peak loads are equal. It can be seen that if the bond strength is decreased, the onset of cracking takes place earlier, i.e. the point in the ascending branch where the curve starts to deviate from linearly is earlier. Also the descending branch is less steep if the bond strength decreases: the fracture behaviour is less brittle. Figure 5.14 shows the final fracture patterns. Here it can be observed that with decreasing bond strength the amount of microcracks outside the main crack increases. The crack pattern is straighter if a higher bond strength is used.

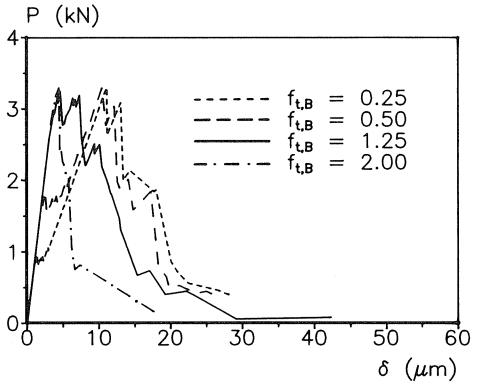

Fig. 5.13 Stress-deformation curves for four simulations with different bond strengths.

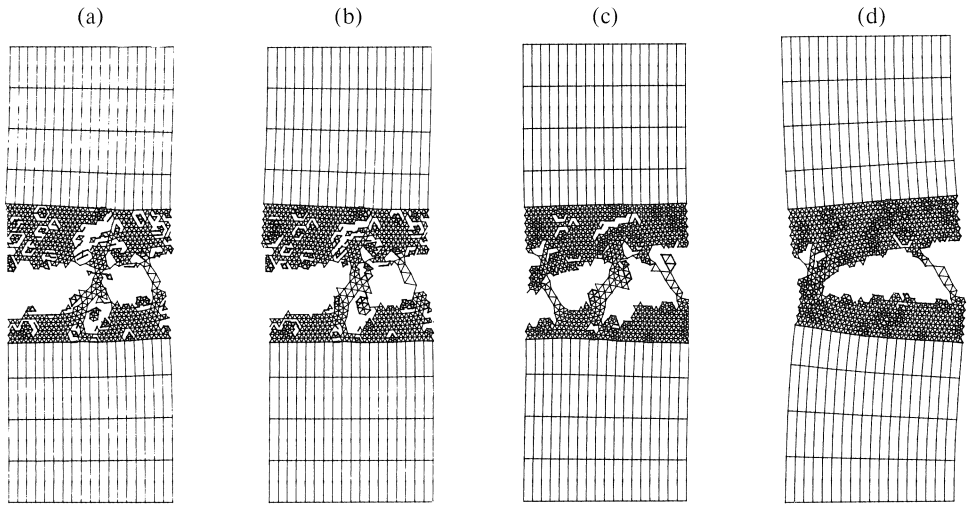

Fig. 5.14 Cracked and deformed meshes for four simulations with different bond strength: $f_{t,B}=0.25$ (a), 0.50 (b), 1.25 (c) and 2.00 MPa (d).

Parameter β

The parameter β (see paragraph 5.1.4.) is implemented for fitting the curve, after the simulation is carried out, such that the maximum load in the simulation is equal to the maximum load in the (uniaxial tensile) experiment. The load and deformations that are calculated in each linear elastic step are multiplied with this factor β as mentioned in paragraph 5.1.4 and as shown in Figure 5.15a. In Figure 5.15b the comparison of three experiments and three simulations, in which the input parameters of Table 5.2 are used, is shown from which the factor $\beta = 2.0$ for the regular lattice with generated grain structure is determined. Once the parameter β is determined this should not be changed if a simulation of an other experiment (for example a shear test) is carried out.

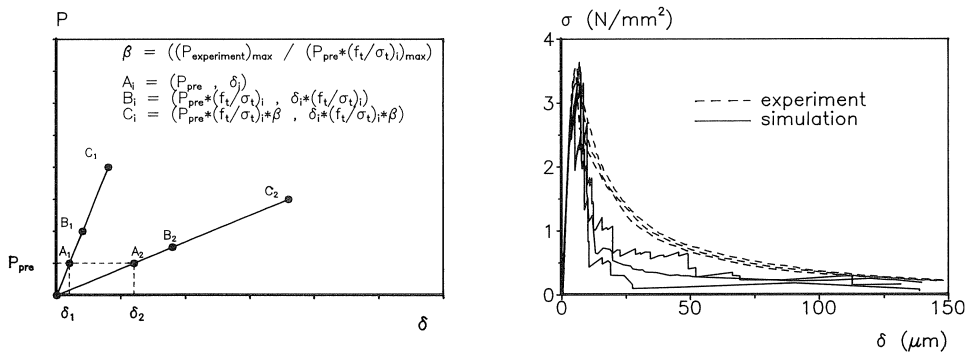

(a) (b)

Fig. 5.15 Procedure for the multiplication of the calculated load-displacement curve with factors f_t/σ_t and β for two steps ($i=1$ and $i=2$) in simulation (a); Comparison of three experiments and three simulations, with input parameters of Table 5.2, from which $\beta=2.0$ is determined (b).

Summarising, the procedure should be that first all the parameters have to be determined by simulating one particular experiment, for instance a tensile test. Thereafter simulations of other problems can be treated using the same input parameters.
It is obvious that not all possibilities have been studied. Only the influence on the load-displacement and the fracture pattern by varying the parameters is shown. To find the correct parameters it is also necessary to perform a large number of analyses and take average values, because of the heterogeneity of the material. It is therefore not claimed that the best parameters are chosen, but just a set of parameters that gives a good comparison with the experiment. Nevertheless it can be concluded that the simulations show a too brittle load-displacement response. An explanation for this could be the fact that a three-dimensional crack process is modelled in two dimensions. Alternatively, excluding small circular diameters from the generated grain structure can cause this effect. This problem will be discussed further in paragraph 6.5.2.

5.3.3 Input parameters for random lattice

For the determination of the Young's modulus of the random lattice the same procedure is followed as for the regular lattice, i.e. the stiffness of the individual beam elements should be equal to the stiffness of the overall material. It was decided to give all the beams the same cross-section. In this case the cross-section is not related to the length of the beams. Alternatively it could be decided to relate the cross-section again to the length of the beams. In the latter case this results in the relation $h = 0.68 * l$ for the beam height and length, which is simular to the regular lattice. If the random lattice should represent a homogeneous medium, the cross-section of the beams should be related to the area of the neighbouring Voronoi cells. However, since concrete is not homogeneous a certain disorder is necessary. The size of the square lattice that is taken as starting point to generate the random lattice must be chosen. In the simulations presented in this report an arbitrary size of 5 mm was chosen. It is not known how the disorder is affected if different sizes for the square lattice are used. With a size of the square lattice of 5 mm, a beam height of 4 mm gives the correct stiffness of the material. Using these input parameters a Poisson's ratio of 0.13 is calculated for this lattice. This value can be adjusted by varying the ratio between the height and depth of the beam elements. The Poisson's ratio can also be changed by changing the randomness of the lattice as described in 5.2.3. The effects of changing the parameter α in the fracture law, which determines the role of the bending moment, were not studied for the random lattice. The value is taken equal to 0.005 as for the regular lattice. The parameter β is determined by comparison with a tensile test on a single-edge-notched specimen. The experiment will be described in paragraph 6.1.1. The resulting value for β is 4.2 if the strengths for all the beams is taken equal to 1.0 MPa.

6 Numerical simulations

In this chapter an overview is given of the simulations carried out with the lattice model. First simulations of tensile tests on single-edge-notched specimens are shown.

The four-point-shear tests described in Chapters 3 and 4 are simulated. Further simulations of mixed mode tests on double-edge-notched plates are shown. The last example is the problem of pull-out of anchor bolts, whereafter a discussion of the numerical simulations is given.

6.1 *Tensile test on SEN specimen*

6.1.1 Summary of experimental results

Experiments of single-edge-notched plates loaded in uniaxial tension between non-rotating end platens were conducted by Van Mier (1990, 1991a). Some of the main results of the experiments will be presented here; for a complete overview see Van Mier (1990, 1991a). In the experiments a vacuum impregnation technique was adopted for determining the extent of internal cracking. The specimen dimensions are shown in Figure 6.2a. After a specimen was loaded to a prescribed axial deformation, it was unloaded to zero load. At this moment the specimen was taken out of the machine and vacuum impregnated with a low viscosity fluorescenting epoxy. After hardening of the epoxy the specimen was cut into slices. The internal surfaces were photographed under ultra-violet light.

In Figure 6.1a the load-displacement diagrams for normal weight concrete and mortar loaded up to different crack openings are shown. From the photos of the internal surfaces, see Van Mier (1990, 1991a), it can be concluded that up till a crack opening of about 50 μm the crack is propagating through the specimen's cross-section. At larger opening, the crack has traversed the specimen completely but is not continuous: overlaps with intact ligaments in between, called crack face bridges, can be observed (Figure

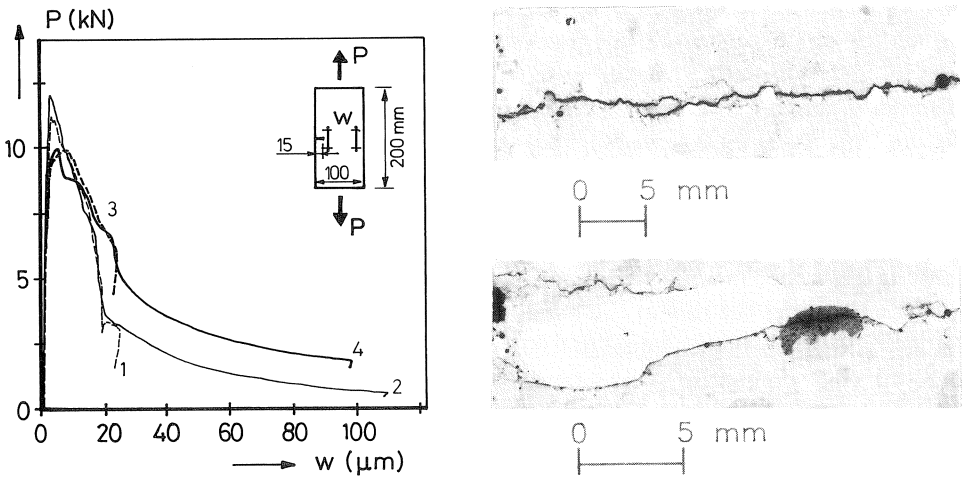

(a) (b)

Fig. 6.1 Load-displacement curves for normal weight concrete (3, 4) and mortar (1, 2) loaded up to a prescribed deformation of 25 and 100 μm (a); crack face bridges in concrete and mortar (b), Van Mier (1990).

6.1b). This implies that load can still be transferred between the crack faces. The long tail in the softening diagram can probably be explained by a large deformation between the crack faces through bending of the bridges.

6.1.2 Crack development in simulation

The experiments described in the previous paragraph have been simulated with the lattice model. For implementing disorder the model with the generated grain structure was used. However, in this simulation the grain structure is generated manually using the real material. Because this simulation was carried out before the parameter study of the previous chapter was carried out, the input parameters used in this simulation differ from the parameters used in all the other simulations. Nevertheless this simulation is included, because smaller beam lengths and smaller particles in the grain structure are used. This produces more details in the fracture process.

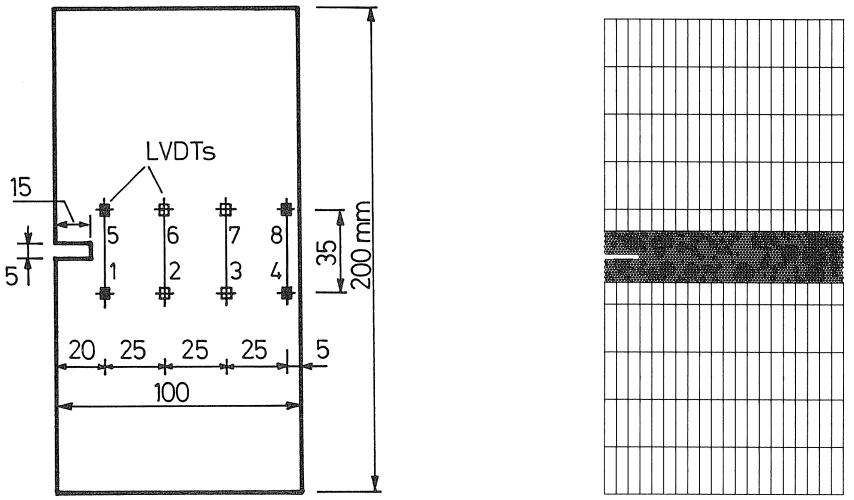

(a) (b)

Fig. 6.2 Single-edge-notched specimen used for uniaxial tensile tests (a); element mesh with generated grain skeleton (b).

The mesh used in this simulation is given in Figure 6.2b. Table 6.1 gives the input parameters for this simulation. The bottom edge of the specimen is supported in the vertical direction. The specimen is loaded by giving the upper edge a vertical displacement. The crack history for this simulation is given in Figure 6.3. The load-displacement curve is plotted in Figure 6.4. In the curve the places are marked where the pictures of the crack history are made. It can be concluded that microcracking in the entire cross-section already starts before the maximum load is reached (Figure 6.3a). After peak load the crack starts to localize in one main crack (Figure 6.3b). Notice that the main crack starts at the unnotched side of the specimen. This phenomenon is also observed in some of the experiments, see Van Mier (1990, 1991a). A combination of

Table 6.1 Input parameters for simulation

grain structure:	particles between 2 and 8 mm						
beam elements:	l	=1.25 mm	h	=125 mm		b	=350 mm
strength:	$f_{t,A}$	=10 MPA	$f_{t,M}$	=5 MPa		$f_{t,B}$	=0.5 MPa
stiffness:	E_A	=5.355 GPa	E_M	=1.912 GPa		E_B	=1.912 GPa
	$\Rightarrow E_{concrete}$	=30 GPa	E_A/E_M	=70/25		E_A/E_B	=70/25
	α	=1/3	β	=2.4			

bending moments, which occur due to the fixed end platen, and eccentricities in specimen structure (in the simulated mesh there are more large aggregate particles located at the unnotched side) probably causes this effect. At the beginning of the long tail in the descending branch, the cross-section is almost completely cracked (Figure 6.3c). Small intact material pieces bridging the crack faces are the reason for the long tail in the load-displacement curve (Figure 6.3d).

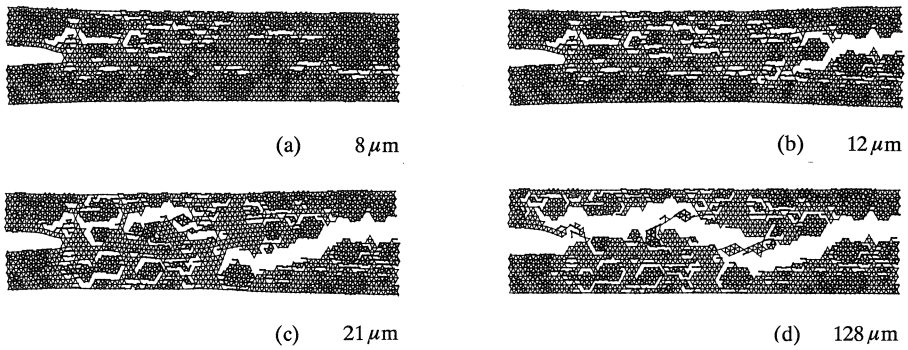

Fig. 6.3 Crack history of simulation of uniaxial tensile test.

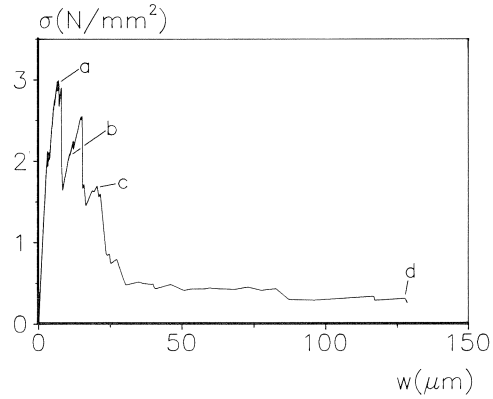

Fig. 6.4 Load-displacement curve of simulation of uniaxial tensile test on SEN specimen; the crack patterns are plotted at four stages (a), (b), (c) and (d) and shown in Fig. 6.3.

As already shown in Chapter 5, if the strength of the beam elements in the bond zone is increased with respect to the matrix and aggregate strength, the number of microcracks outside the main crack will decrease and the load-displacement response will be more brittle, see Schlangen & Van Mier (1991b, 1992c, g).

6.1.3 Influence of boundary conditions

In the experiments the specimens are loaded between fixed end platens. The difference in behaviour of tensile specimens loaded between fixed and rotating end platens is studied experimentally by Daerga (1992). Here simulations of the experiments between fixed end platens discussed in paragraph 6.1.1. are compared with simulations between rotating end platen. The input parameters found in the parameter study described in paragraph 5.3. are used. For both cases simulations with three different grain structures (generated following the procedure explained in paragraph 5.2.2) but with equal distribution of particles are carried out to get some idea about the scatter in the results. Figure 6.5 shows the load-displacement curves of a simulation with fixed and freely rotating boundaries. In this Figure the average values of the deformations at the left and right side of the specimen (at the same place as LVDTs 1 and 4 in the test) are plotted. In Table 6.2 the maximum loads are given for the six simulations. The scatter in the results is small. In Figure 6.6 the deformation on the left and right and the average deformation are plotted separately for one simulation with fixed (6.6a) boundaries and one with freely rotating (6.6b) boundaries. The simulations of specimens between rotating platens have a lower maximum load, a smaller deformation at peak and a more brittle post peak response. This can be explained from the crack histories (places marked in Figure 6.5) of simulations with the different boundary conditions, Figure 6.7. It can be seen that in the case the boundaries are fixed, at peak load the crack has crossed a larger part of the cross-section. More microcracking outside the main crack, especially on the unnotched side of the specimen, can be observed if the boundaries are fixed. The reason for this are the bending moments as mentioned in 6.1.2. In Figure 6.6b it can be

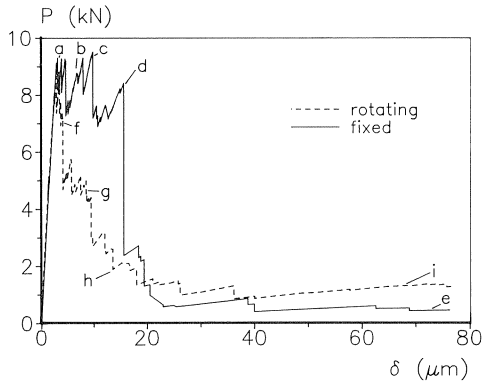

Fig. 6.5 Load-displacement curves for simulations of uniaxial tensile tests with fixed and freely rotating boundaries.

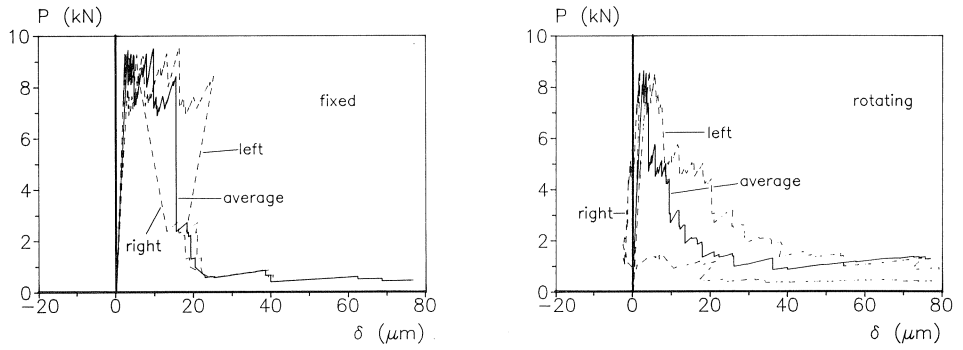

(a) (b)

Fig. 6.6 Load-displacement curves (average, left and right of specimen) for simulations of uniaxial tensile tests with fixed (a) and freely rotating (b) boundaries.

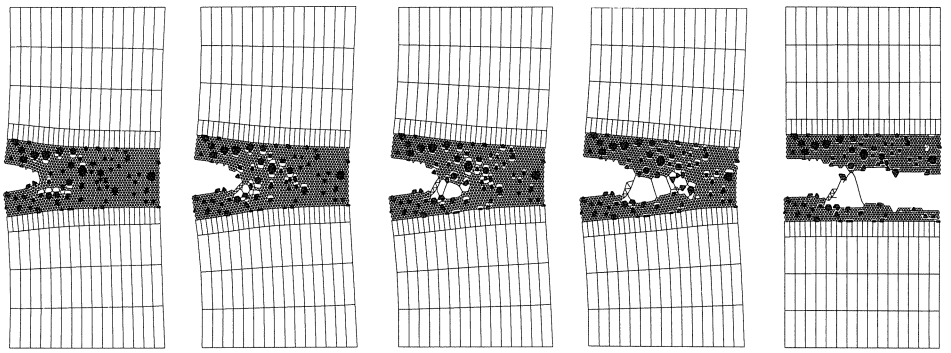

(a, b, c, d, e) fixed boundaries

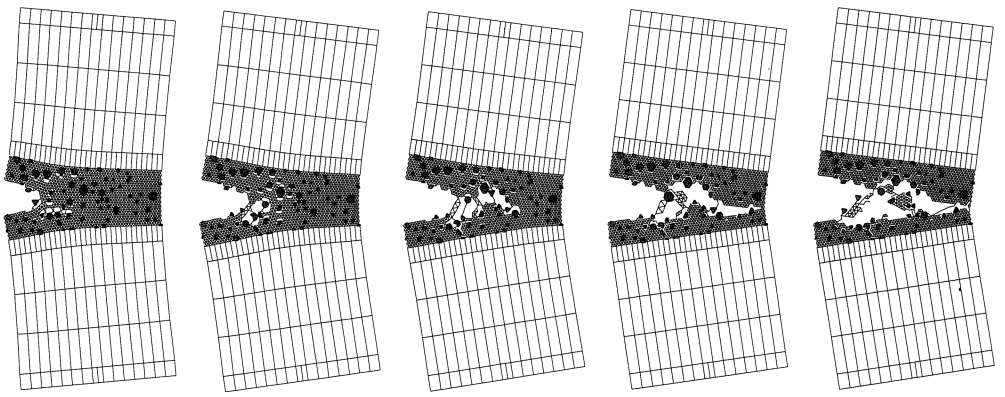

(f, g, h, i, j) freely rotating boundaries

Fig. 6.7 Crack histories for simulations with fixed and freely rotating boundaries.

seen that if the boundaries are free the unnotched side goes to compression. If the boundaries are fixed the difference between the deformations on the left and right are smaller. The fast load drop beyond peak in the case with fixed boundaries can be explained by the fact that the crack has traversed the entire cross-section at that moment. Beyond this point the two crack faces are only connected by means of crack face bridges (Figure 6.7e). A further discussion of the simulations is presented in paragraph 6.5.1.

Table 6.2 Peak loads in kN for six simulations

fixed boundaries	freely rotating boundaries
9.51	8.66
10.85	8.95
10.67	9.01

6.2 *Four-point-shear beams*

6.2.1 Single-edge-notched beams

The four-point-shear experiments described in Chapter 4 are simulated with the lattice model. In this paragraph simulations of the single-edge-notched beams with freely rotating boundary conditions are discussed, see also Schlangen & Van Mier (1991a, 1992h). In the next paragraph simulations of the experiments on double-edge-notched beams with different boundary conditions are shown, see also Schlangen & Van Mier (1992a, b, e, f).

First the single-edge-notched beam is simulated with the lattice model by using the method of implementing disorder explained in paragraph 5.2.1. Arbitrarily chosen input parameters are used. A beam length of 2.5 mm and beam strengths randomly chosen from a normal distribution with an average value of 3 MPa and a standard deviation of 1 MPa are taken. The final crack pattern is plotted in Figure 6.8. The crack starts at the notch and grows as a curved crack to the support at the opposite side of the specimen. The number of microcracks is small and almost no crack face bridges are observed. This implies that a smaller beam size and/or another distribution of strengths is needed to obtain a correct description of the fracture process.

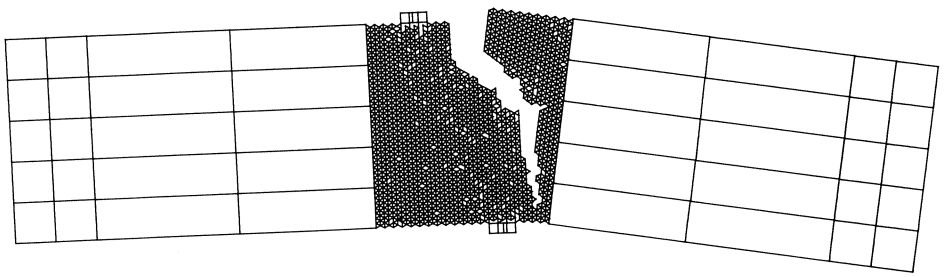

Fig. 6.8 Cracked and deformed four-point-shear beam, simulated with regular lattice with distribution of beam strengths.

The four-point-shear beams are also simulated using the second option for implementing disorder as discussed in paragraph 5.2.2. For the input parameters the values listed in paragraph 5.3 are used. However the properties of the individual components in the grain structure of the concrete are varied. Simulations are carried out for three different sets of input parameters representing normal weight, lytag and high strength concrete. The final crack patterns for the three simulations are plotted in Figure 6.9. In Figure 6.10a the load-displacement curves of the simulation and the experiment of the normal weight concrete are compared. Figure 6.10b shows the comparison of load-displacement responses of the three simulations. It is shown that if the bond strength is increased (III) the crack pattern is straighter and there is less crack branching and bridging compared with the simulation for normal weight concrete (I). In the simulation of the lytag concrete (II) the first cracks appear inside the aggregates. Thereafter, the matrix elements reach their maximum stress. If the calculated load-displacement curves are compared with the experimental results it can be seen that the response is again too brittle. Possible explanations for this were discussed in Chapter 5. If the bond strength is doubled (III) the maximum load of the specimen is only increased with 10%. This means that the maximum load is mainly governed by the strength of the matrix. The same tendency is observed in a large survey of experiments by Mindess (1989). It should

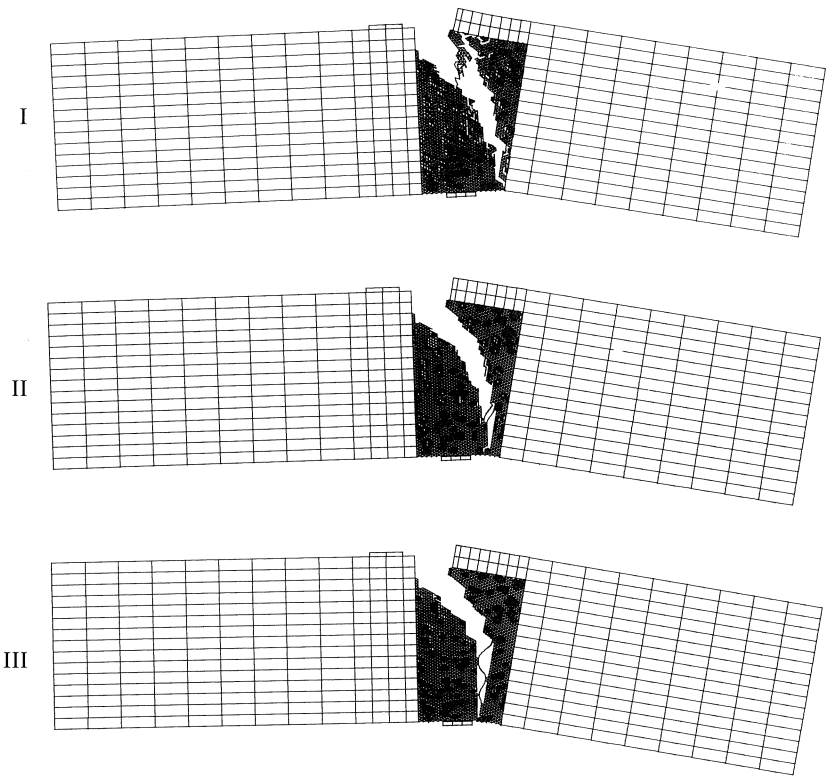

Fig. 6.9 Simulated crack patterns in normal weight (I), lytag (II) and high strength concrete (III).

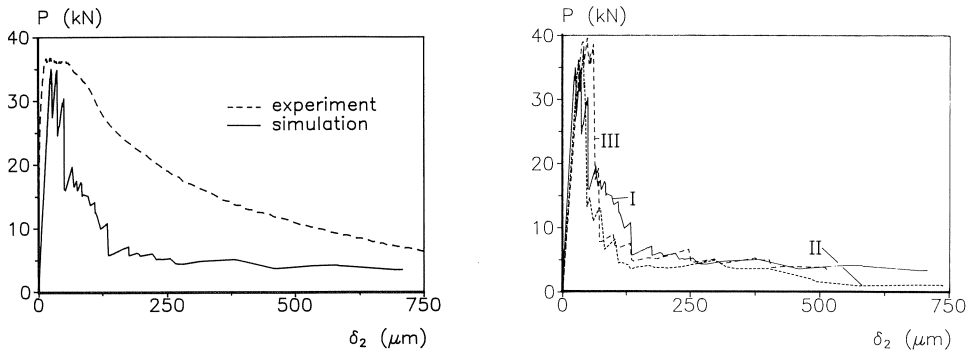

Fig. 6.10 Load displacement curves: experiment and simulation of single-edge-notched four-point-shear beams of normal weight concrete (a); simulations I, II and III (b).

be mentioned that for simulating the high strength concrete (III) only the bond strength is increased. In the real concrete the matrix strength is also increased, resulting in higher maximum loads.

6.2.2 Double-edge-notched beams

The experiments of the double-edge-notched beams are simulated with the lattice model using two ways of implementing disorder, namely as described in paragraphs 5.2.2. and 5.2.3. Variations in the simulation are specimen size, boundary conditions and bond strength. Furthermore the mesh depency is studied for the random lattice.

Specimen size and boundary conditions

For the case where the disorder is implemented through the generation of an aggregative structure, simulations with different specimen sizes, different boundary conditions and different strength of the bond zone are carried out. Specimens of three

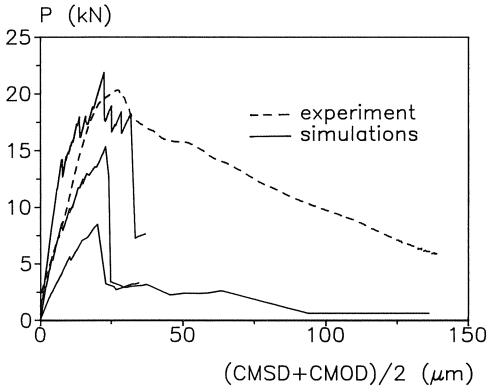

Fig. 6.11 Load-displacement curves for three simulated beam sizes; Experimental curve of larger beam size.

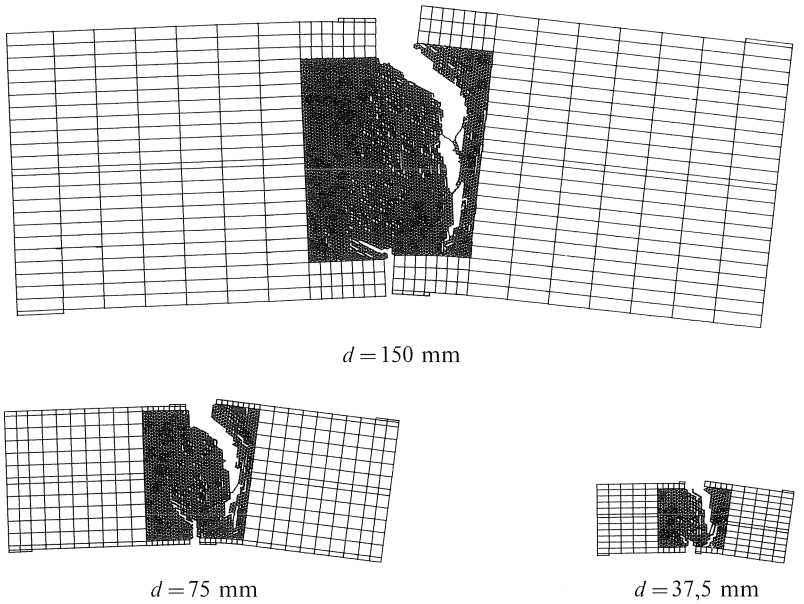

Fig. 6.12 Three sizes of simulated double-edge-notched beams simulated using the regular lattice with the generated grain structure.

different sizes are simulated, viz. $d = 150$, 75 and 37.5 mm. Figure 6.12 shows the final crack patterns for the three sizes with freely rotating supports. The input parameters of Table 5.2 are used. Before peak load crack growth is observed at both notches. After peak load one crack becomes dominant and opens. It is a curved crack which grows outside the shear zone and ends at the outer side of the middle support. The corresponding load-displacement curves are plotted in Figure 6.11. The result of the simulation of the largest beam is compared with the experimental outcome: again the simulated curve is too brittle.

If the supports are fixed the two cracks both continue to grow until they are arrested in the compression zone. Then the cracks are prevented from opening further because the support-nodes cannot move horizontally. As a result a splitting crack in the middle occurs, as shown in Figure 6.13. In Figure 6.14 the simulated curve is compared with the experimental load-displacement response. Now the simulated response is too stiff. The model will probably have to be improved if compression dominates, which happens if the two curved cracks stop and the splitting crack starts. This will be discussed further in 6.5.2.

Bond strength

The problem of the four-point-shear test on double-edge-notched beams is used to study the influence of changing the bond strength on the specimen behaviour, see also Schlangen & Van Mier (1992f). All the input parameters are kept equal to the param-

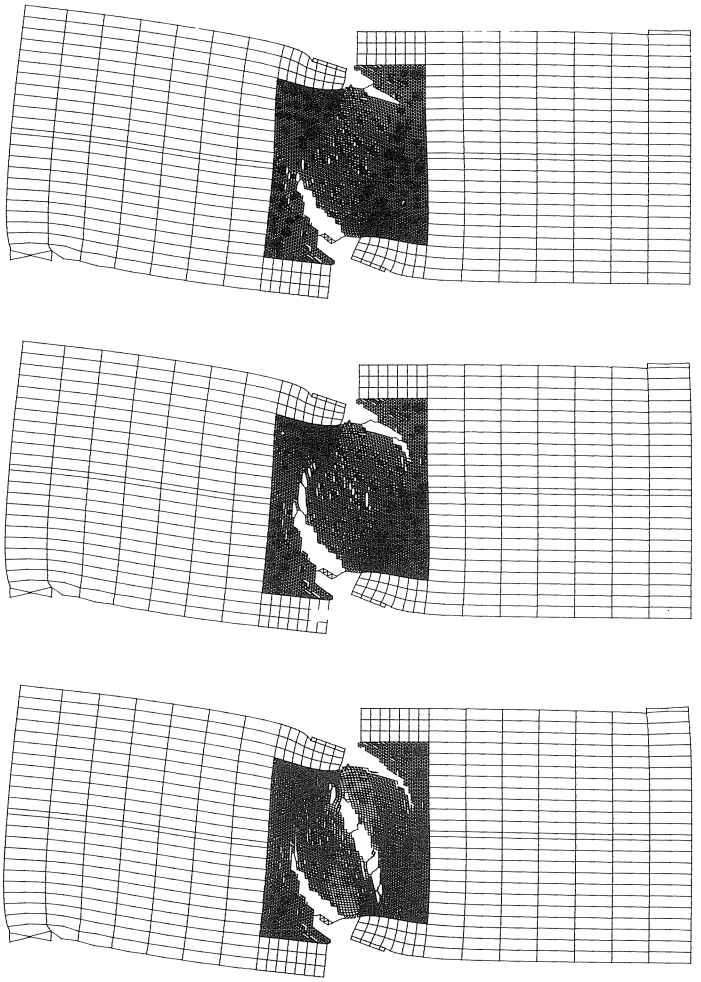

Fig. 6.13 Two stages of cracking of the simulation with fixed supports.

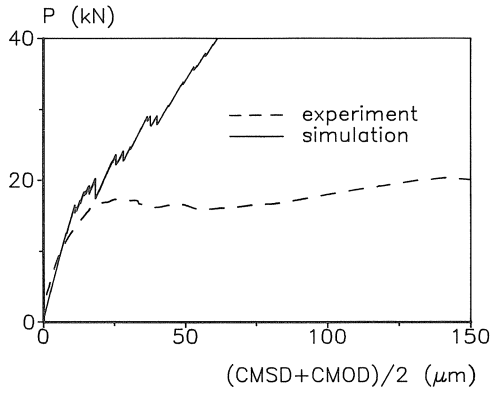

Fig. 6.14 Load-displacement curves of simulation and experiment with fixed supports.

eters found in paragraph 5.3. (Table 5.2), except the bond strength. Nine different values for the strength of the beam elements in the bond zone are taken, see Table 6.3. In Figure 6.15 the crack patterns of three beams with different bond strengths are shown. Table 6.3 gives the maximum load values for the nine simulations. It can be concluded that if the bond strength is increased the number of microcracks outside the main crack is reduced. The result agrees with the simulations of the uniaxial tensile tests presented in paragraph 5.3.2. There is less crack branching for increasing strength of the bond elements. The load that can be carried by the specimen is only slightly affected by the bond strength. In Figure 6.15 it can be seen that the crack starts either at the top or at the bottom notch. This depends on the bond strength and the position of the aggregate particles.

Table 6.3 Bond strength and peak loads for the nine simulations

Analysis No.	1	2	3	4	5	6	7	8	9
$f_{t,B}$ [MPa]	1.25	0.5	0.75	1.0	1.5	1.75	2.0	3.0	5.0
P_{max} [kN]	14.3	14.6	14.7	12.6	14.3	15.6	16.4	17.8	19.4

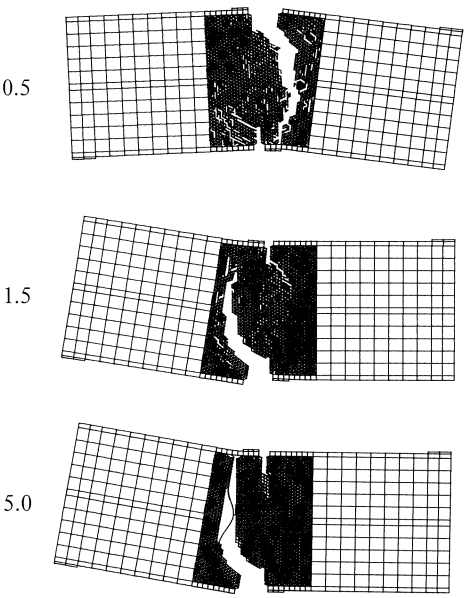

Fig. 6.15 Crack patterns in four-point-shear beams with different values for the bond strength (0.5, 1.5 and 5.0 MPa).

Boundary conditions and mesh dependency; random lattice

The beams with both boundary conditions, freely rotating and fixed, are also simulated with the random lattice, see also Schlangen & Van Mier (1992a). In Figure 6.16a and 6.16b the final crack patterns of simulations with a random lattice of 30 * 30 nodes are

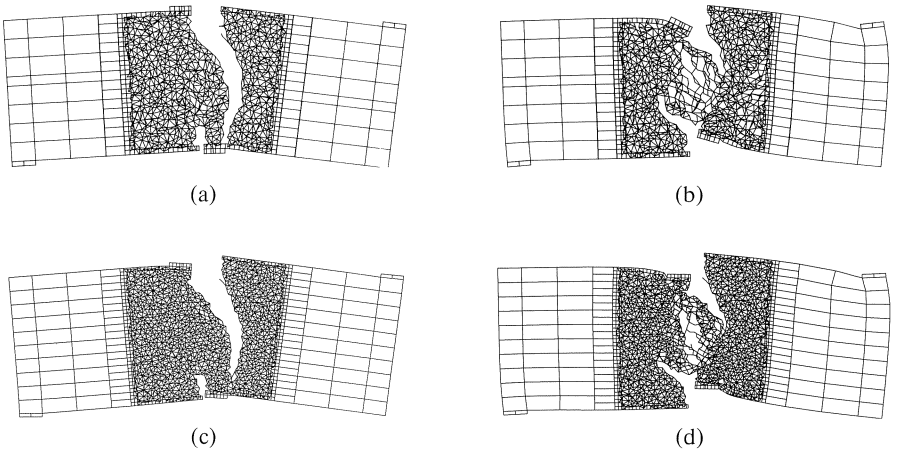

Fig. 6.16 Four-point-shear beams simulated with the random lattice; freely rotating (a) and fixed supports (b) with lattice of 30 * 30 nodes and freely rotating (c) and fixed supports (d) with lattice of 40 * 40 nodes.

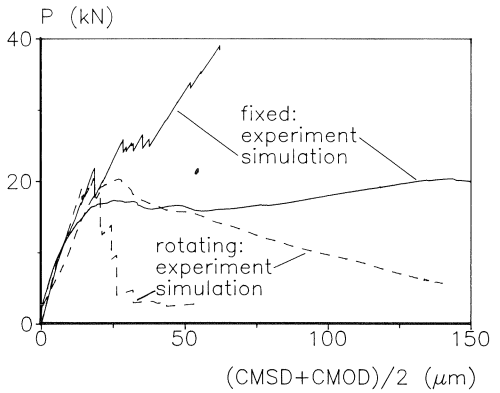

Fig. 6.17 Experimental and simulated load-displacement curves.

shown. Figure 6.16c and 6.16d show simulations with a random lattice of 40 * 40 nodes. The crack patterns obtained with both lattices are identical. In Figure 6.17 the curves of the simulations with the random lattice of 30 * 30 nodes are compared with the experimental curves. The peak loads are again predicted correctly, but the post peak response is too brittle in the case of freely rotating and too stiff in the case of fixed supports. Figure 6.16a is a simulation with the random lattice of the four-point-shear experiment on a beam with height $d = 150$ mm. The random lattice contains of 2530 beam elements and 90 beams had to be broken to fracture the beam. The computer time needed was 8 hours on a Sun Sparc 2 workstation. For the simulation of the same experiment with the regular lattice with generated grain structure (figure 6.12 ($d = 150$ mm)) significantly more computer time was needed, i.e. 14 days on the same workstation. The

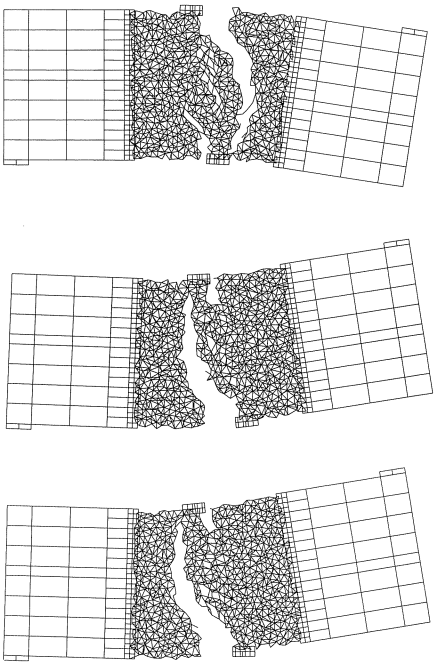

Fig. 6.18 Final crack pattern in three simulations with different configuration of random lattice.

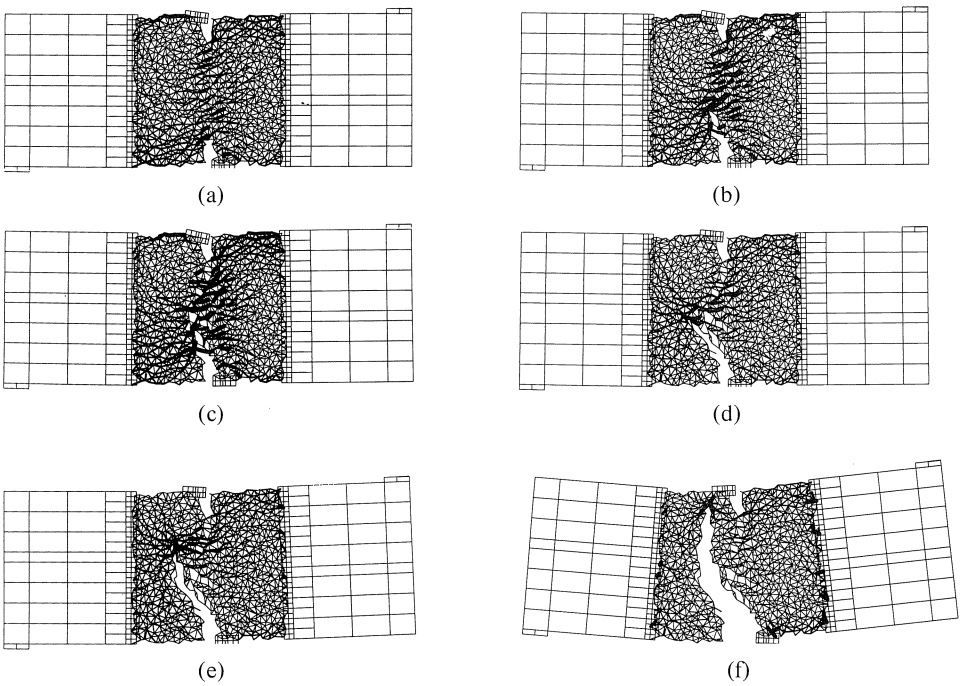

Fig. 6.19 Crack history of simulation with random lattice of four-point-shear beam. the stresses are indicated with differences in line thickness.

regular lattice contained of 11900 beam elements and 800 beams had to be broken to fracture the beam.
Three simulations with different meshes are performed to study if the shape of the curved crack is independent of the generated configuration of the random lattice. In Figure 6.18 the final crack patterns of these three simulations are shown. The three crack patterns are identical. However the crack at the bottom or the top notch opens depending on which side is most critical.
In Figure 6.19 the crack history of a simulation with the random lattice of the four-point-shear beam tested between freely rotating supports is shown. In the Figures the line thickness of the beam elements is varied to indicate the development of the stress. Thicker lines represent beams with higher tensile stress. Plot 6.19b is taken just before and plot 6.19c just after the peak load. Around peak load the highest stresses in the specimen are located between the two notches. Though the final crack pattern shows a curved crack if the analysis is continued by removing only one element in every load step and analysing always the new stress distribution. This represents an experiment performed in displacement control.
From Figure 6.19 it can be seen that a test carried under load control will lead to a different fracture mechanism. In that case the load is increased further at the stage where the maximum load is reached in a deformation controlled test, viz. figure 6.19c. This obviously leads to a straight crack between the two notches. The simulations are further discussed in paragraph 6.5.

6.3 *Mixed mode tests on DEN plates*

6.3.1 Explanation of tests

Nucleation and growth of cracks under combined tension and shear were studied by Nooru-Mohamed (1992) using the biaxial machine at the Stevin Laboratory. The machine consists of two independent loading frames, with two independent control systems to perform deformation controlled tests. Double-edge-notched plate specimens (Figure 6.20) were tested following seven different load-paths. Here two load-paths are simulated, viz. load-paths 4 and 6.
In load-path 4 first a compressive shear load P_s is first applied to the specimen in displacement control until $P_s = -5$ kN (loadpath 4a) or $P_s = -10$ kN (loadpath 4b) or $P_s =$ maximum compressive shear (loadpath 4c). During this first shearing regime, a zero axial load $(P = 0)$ is maintained while the vertical deformation is kept free. Subsequently, the lateral test control is changed to load control and an axial tensile load is applied in displacement control until failure.
In load-path 6 an axial tensile and a lateral compressive load were applied to the specimen such that the ratio of axial (δ) to lateral deformation (δ_s) remained constant throughout the test. The δ/δ_s ratios for load-path 6a, 6b and 6c were 1.0, 2.0 and 3.0 respectively.
In both load-paths three different specimen sizes were tested, i.e. $200 * 200$, $100 * 100$ and $50 * 50$ mm^2 (the thickness was always 50 mm). The results of the experiments are presented and compared with the simulations in 6.3.3.

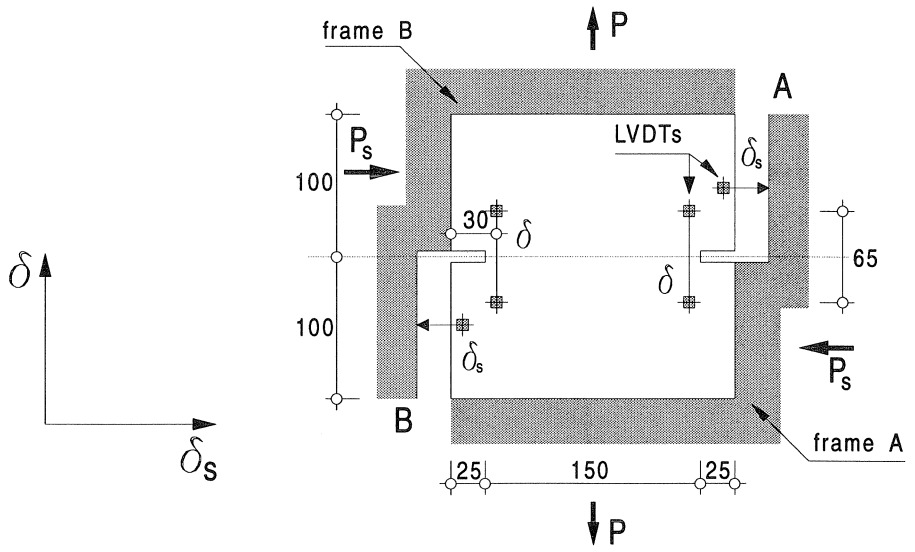

Fig. 6.20 Double-edge-notched plate specimen.

6.3.2 Description of loading procedure in the case of two independent loading systems

In the problems simulated above, only one loading system is used. In the experiments described in 6.3.1. the specimens are tested using two independent systems. This has also consequences for the loading procedure in the simulations. Infact, in each step of the simulation, two loading situations must be analysed. However because of the fact that each loading step is linear elastic, the resulting stresses in the beams of two analysis with different load-vectors can simply be added. The two load-vectors are the tensile load and the compressive shear load. For each load-path the adding procedure is different. Suppose the tensile stress in the beams due to the tensile load (load-vector 1) is $\sigma_{t,1}$ and due to the shear load (load-vector 2) is $\sigma_{t,2}$. The corresponding deformations (Figure 6.20) are δ_1 and $\delta_{s,1}$ for load-vector 1 and δ_2 and $\delta_{s,2}$ for load-vector 2.
In the case of load-path 4 in each step a check is first made to see whether a beam element exceeds its tensile strength under the shear loading (load-vector 2) only. If this is the case, the element is removed and a new load step is started. If not, the beam with the highest value for relation 6.1 is removed.

$$\text{load-path 4: } \beta * \sigma_{t,1}/(\beta * f_t - \sigma_{t,2}) \tag{6.1}$$

in which $\sigma_{t,2}$ is the stress in a beam due to the applied shear force ($P_s = -5$ kN, -10 kN or maximum) on the specimen. The stress $\sigma_{t,1}$ is obtained from the analysis with load-vector 1 equal to a prescribed tensile load P_{pre}, f_t is the tensile strength of the beam and β is of course equal to the value obtained from the simulations of the uniaxial tensile tests discussed in 5.3.2. The value for the stresses are determined with equation 5.1

with the restriction that not the maximum of the absolute values of the moments M_i and M_j is taken. Now the relation 6.1 must be checked for all four possibilities, i.e. M_i, $-M_i$, M_j and $-M_j$.
For load-path 6 the highest value for relation 6.2 defines the beam that is removed.

$$\text{load-path 6: } (\sigma_{t,1} + \gamma * \sigma_{t,2})/f_t \tag{6.2}$$

and γ is determined from:

$$(\delta_1 + \gamma * \delta_2)/(\delta_{s,1} + \gamma * \delta_{s,2}) = 1 \text{ (, 2 or 3)}$$
$$\text{for load path 6a (, b or c respectively)} \tag{6.3}$$

in which the stresses and deformations are obtained for both load-vectors to a prescribed load of 1 kN. To determine the total load that can be carried by the lattice and the total displacements, the procedure described in 5.1.4 must again be followed.

6.3.3 Numerical results

The load-path 4 experiments are simulated with the random lattice. Only one specimen size is analysed, i.e. $200 * 200$ mm^2. In Figure 6.21 the crack patterns of the simulations and the experiments are shown for the three cases, i.e. $P_s = -5$ kN, -10 kN and maximum shear load. For the maximum shear case in the simulation, only one load vector is applied, because it is expected that this gives the same result. The crack pattern is the result of the shear loading only. What can be seen is that there is a relation between the lateral shear load and the area of the compressive strut. In both the simulations and the experiments the specimen with the maximum shear load shows the largest strut area, whereas the specimen with the lowest shear gives the smallest strut size. If a higher shear force is applied, cracks start to grow at the lower left and the upper right corner, see Figure 6.21b2 where the shear load is equal to 10 kN. Therefore in this case a row of plane stress elements (with concrete stiffness) is connected at those edges (Figure 6.21b3). This leads to a higher stiffness at the edges, which increases the load needed to start crack growth. Also load-path 4a with 5 kN shear is repeated with those elements at the edge. The size of the compressive strut increases, see Figure 6.21a3. Nevertheless in the case of maximum shear some cracks near the steel plates still occur (Figure 6.21c3), which leads to cracking inside the compressive strut. For the case with maximum shear a simulation is also conducted with additional steel plates at those edges (Figure 6.21c4). The set-up is in that case similar to a shear-box test. Then no cracks at the edges are observed. During the experiments in some cases when higher shear loads were applied, cracking at the steel plates was also observed. To prevent this, sidegrooves were sawn in the specimens to enlarge the glue area. In some later tension shear tests on SIFCON an additional steel plate was glued to the free sides of the specimen corresponding to the situation of Figure 6.21c4, in order to prevent cracking at the glue plates (Van Mier & Timmers (1992)).
Figure 6.22 shows the load displacement curves for the experiments and the simulations. For the simulations the curves corresponding to the crack patterns in Figure 6.21a2, 6.21b3 and 6.21c3 are plotted.

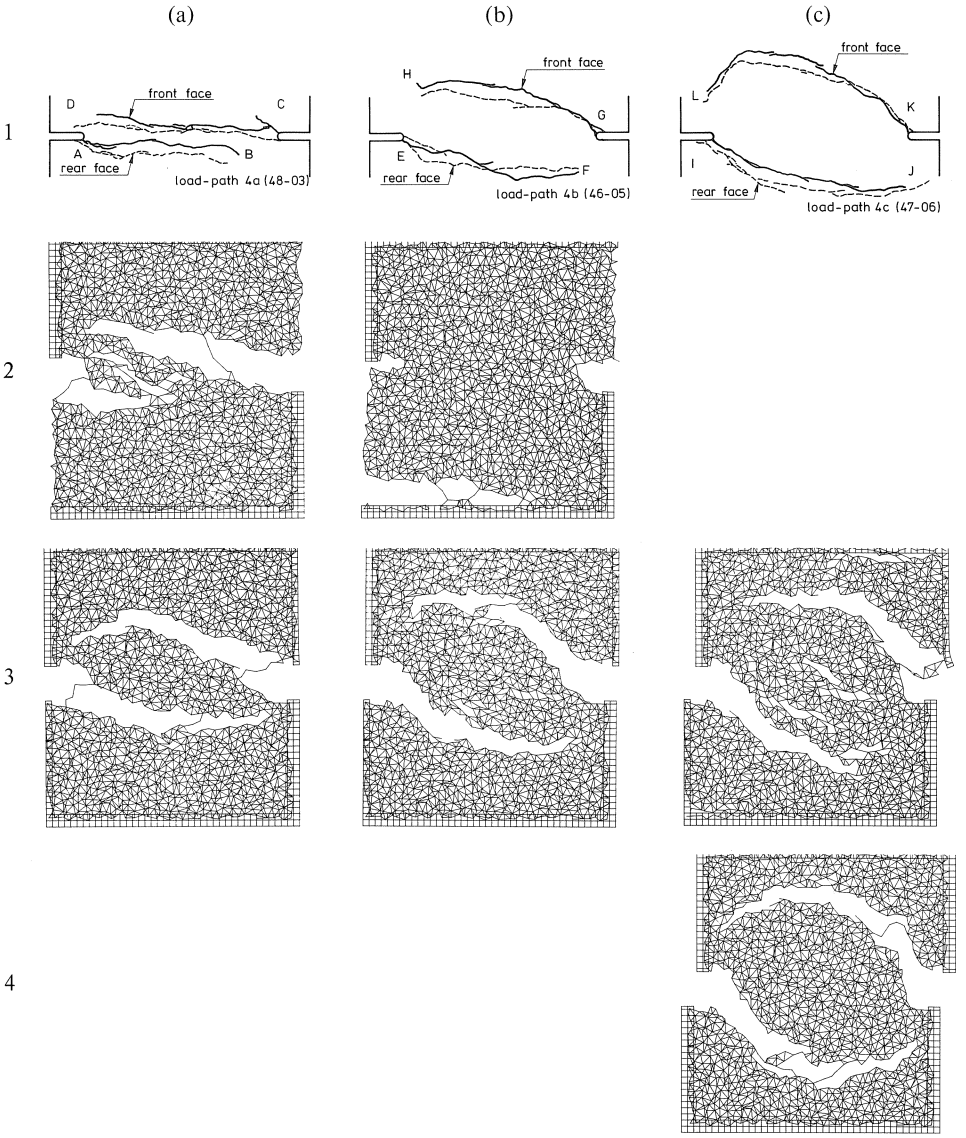

Fig. 6.21 Experimental and numerical crack patterns for load-path 4; (a) $P_s = -5$ kN; (b) $P_s = -10$ kN; (c) $P_s =$ maximum shear.

For load-path 6 three different sizes are simulated. The sizes $200 * 200$ and $100 * 100$ are analysed with the random lattice and the sizes $100 * 100$ and $50 * 50$ are analysed using the regular lattice with the generation of a grain structure. With those four meshes three simulations are always carried out. The ratio between the axial (δ) and shear (δ_s) deformation is 1, 2 and 3 respectively. The deformations are analysed at the same positions as in the experiment. From the crack patterns, Figure 6.23, it can be seen

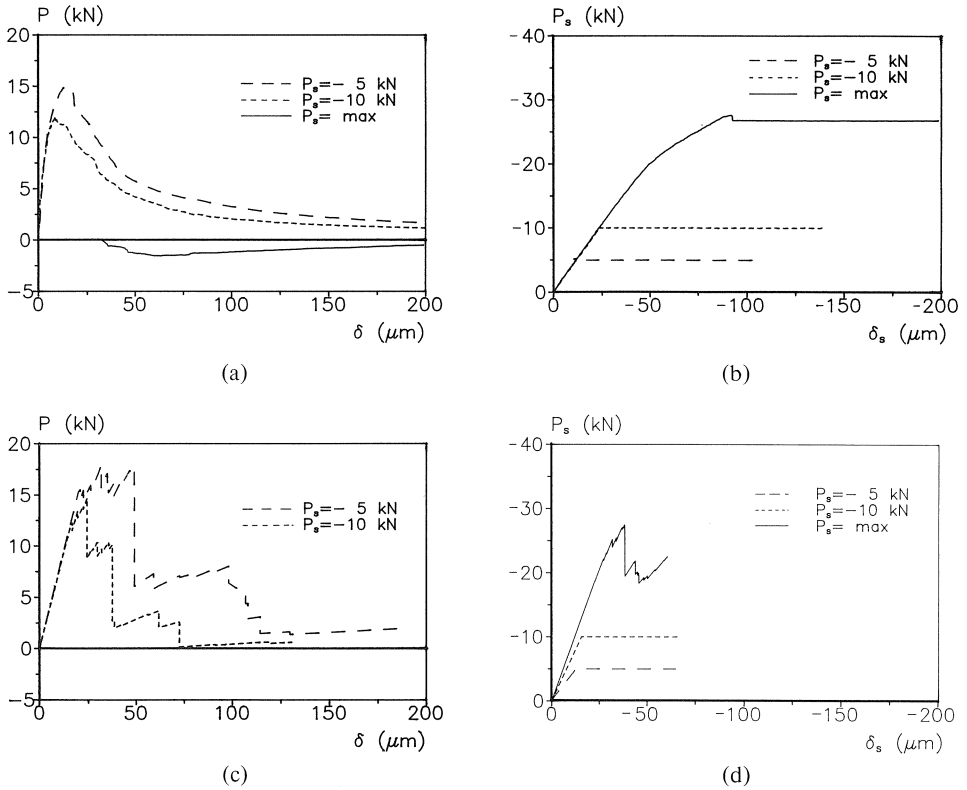

Fig. 6.22 Load-displacement curves for load-path 4; Experiments (a) P-d, (b) P_s-d_s; Simulations (c) P-d, (d) P_s-d_s.

that when the ratio δ/δ_s increases the area of the compressive strut decreases. For the ratio $\delta/\delta_s = 3$ the two curved cracks grow together to one straight crack. In the same figure the experimental crack patterns are shown for the middle-sized specimen. The crack patterns in the other sizes are identical, see Nooru-Mohamed (1992).
The load-displacement curves are plotted in Figure 6.24. If the ratio δ/δ_s increases the slope of the P_s-δ_s curve decreases. In the P-δ diagrams it can be seen that the tensile load changes into a compressive load if the cracks open. For a smaller ratio δ/δ_s the compression is larger.

6.4 *Pull-out of anchor bolts*

6.4.1 Round Robin proposal of RILEM

The last example that is simulated with the model is the pull-out of a steel anchor embedded in concrete. The pull-out failure of rigid anchors embedded in brittle materials is difficult to analyse using conventional methods. A steel anchor is often used as connection in concrete structures, roof bolts in rock tunnels and tie backs in rocks,

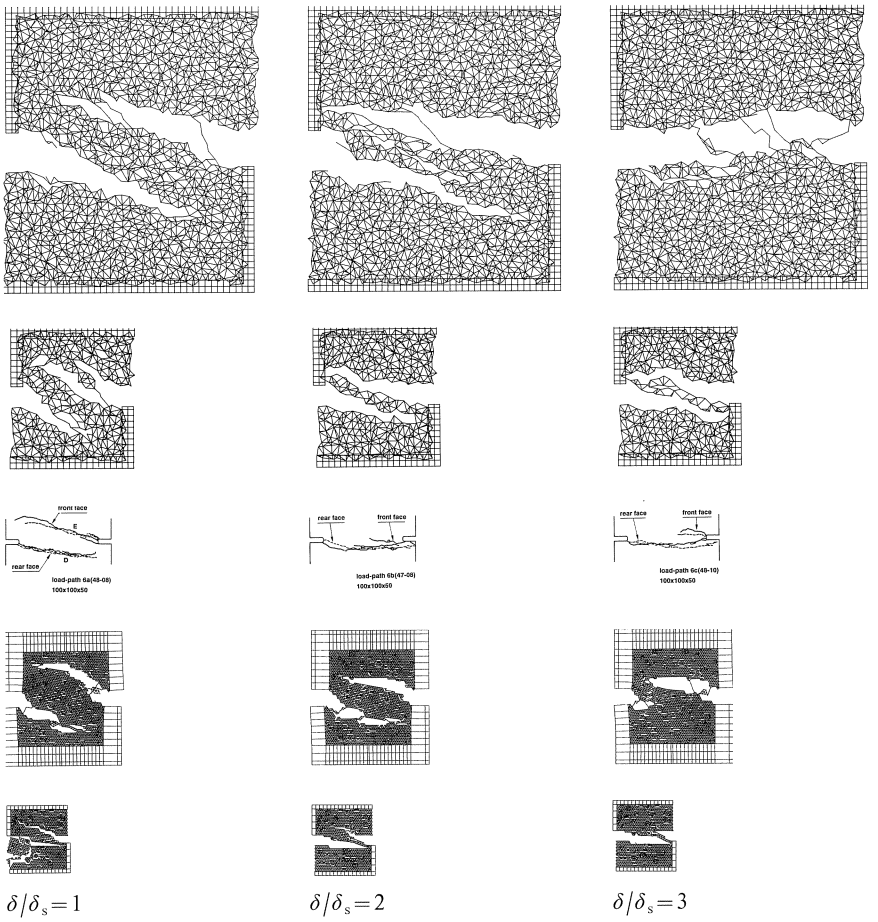

Fig. 6.23 Simulated and experimental crack patterns for load-path 6.

Ballarini et al. (1986). The crack patterns found in laboratory experiments on this type of construction contradict each other, because the direction of crack propagation depends mainly on the boundary conditions. RILEM committee TC-90 FMA (Fracture Mechanics Applications) organised a round robin analysis to study the failure of this type of structure, Elfgren (1991). The objective was to calculate the load-deformation curve and predict the failure mechanism for a plane stress (2D) and an axial symmetric (3D) situation. This example was selected for demonstrating the potential of fracture mechanics based approaches in (reinforced) concrete design.

The 2D-geometry used in the round robin is shown in Figure 6.25a. The results of the contributions to the first invitation showed a large scatter. The main reason for this was the fact that no material was present to which the analysis could be fitted. In most of the simulations it was assumed that the cracks started at the anchor bolt and propagated in a straight line to the supports. Later experiments, Helbling et al. (1991), Fathy et al.

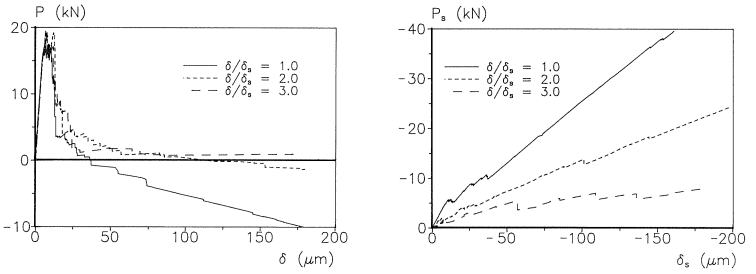

(a) 200 * 200 mm^2 random lattice

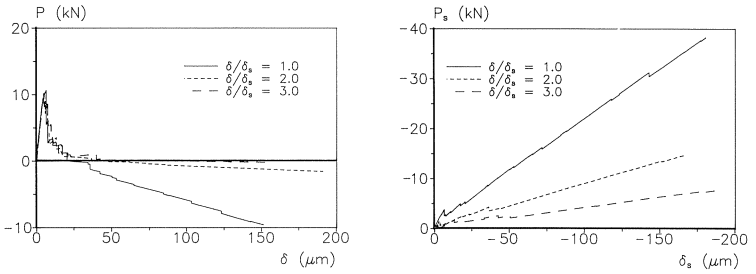

(b) 100 * 100 mm^2 random lattice

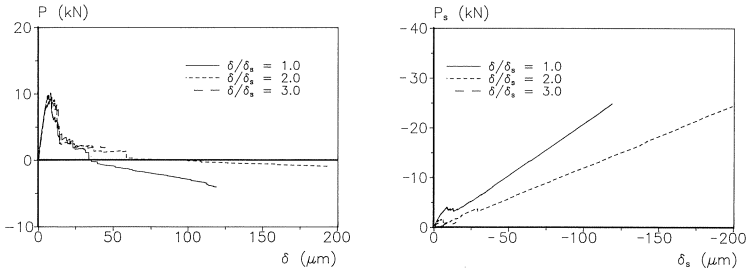

(c) 100 * 100 mm^2 regular lattice
(the simulation with ratio $\delta/\delta_s = 3.0$ had to be stopped earlier, because one crack reached the opposite edge)

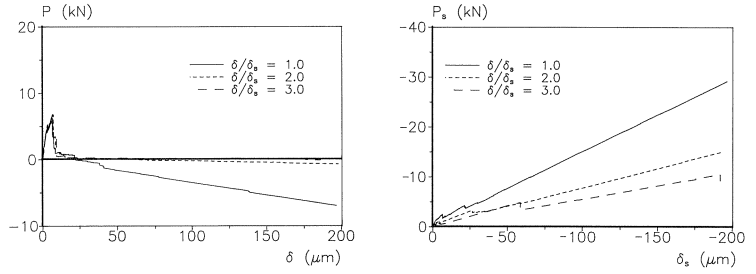

(d) 50 * 50 mm^2 regular lattice

Fig. 6.24 Load-displacement curves for load-path 6.

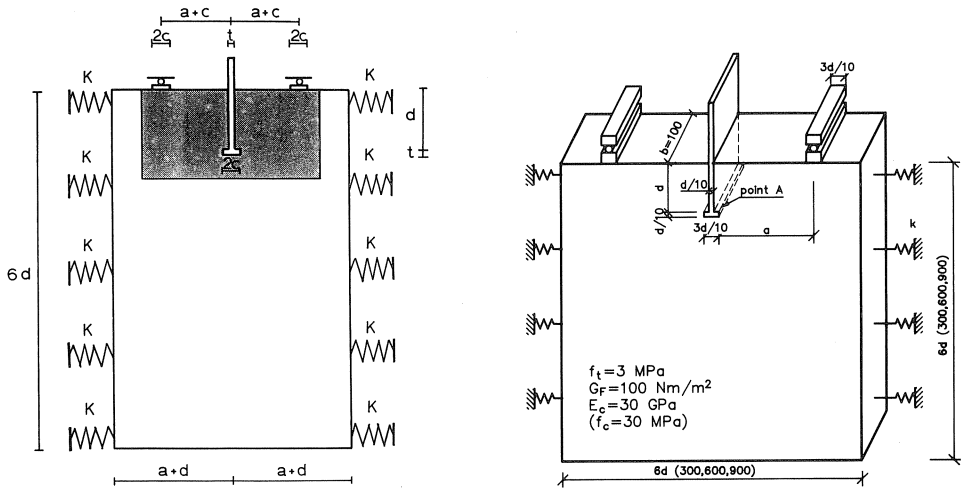

(a) (b)

Fig. 6.25 First (a) and second (b) geometry for pull-out of anchor bolts.

(1992) and Vervuurt et al. (1992), proved this assumption to be wrong. In paragraph 6.4.2. the contribution, performed with the lattice model, to the first invitation is presented.
Because of the large scatter in the results the RILEM-committee decided to continue the round robin and invite more researchers to contribute. Numerical and experimental results were requested. The geometry was slightly changed as shown in Figure 6.25b. The results of the contributions to the second round were more consistent if the peak load is considered. However a large scatter in crack patterns was still obtained. In paragraph 6.4.3. the second contribution of the Stevin Laboratory is presented.

6.4.2 Simulations with regular lattice

The first proposed geometry of the concrete plate with the embedded anchor is shown in Figure 6.25a. Two situations should be considered, i.e. a plane stress and an axial symmetric situation. In addition the lateral constraint should be varied.
With the lattice model only the plane stress situation is simulated. Two simulations with free ($k = 0$) and completely fixed ($k = \infty$) boundaries are carried out, see also Schlangen & Van Mier (1991b). Disorder is implemented using the method described in 5.2.1., i.e. assigning strengths at random to the beam elements. For the input parameters arbitrary values as mentioned in 5.2.1 are taken. The two resulting crack patterns are shown in Figure 6.26. In the case of free boundaries ($k = 0$) a horizontal crack is observed. If the boundaries are fixed ($k = \infty$) the cracks tend to grow more to the supports.

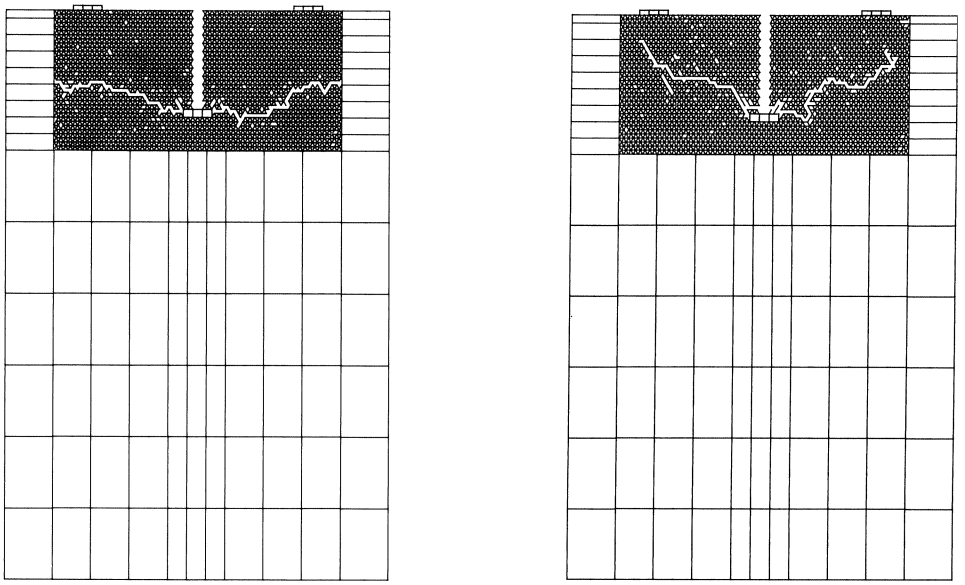

(a) (b)

Fig. 6.26 Simulated crack pattern with regular lattice; $k=0$ (a) and $k=\infty$ (b).

6.4.3 Simulations with random lattice compared with experiments

It was decided to contribute also to the second invitation. However, now experiments and simulations are carried out. A complete overview of the testing procedure and experimental and numerical results is given in Vervuurt et al. (1992, 1993). Here a few results are presented to show the mechanism. In Figure 6.25b the geometry for the plane stress situation is shown. Figure 6.27 gives the experimental crack pattern and the

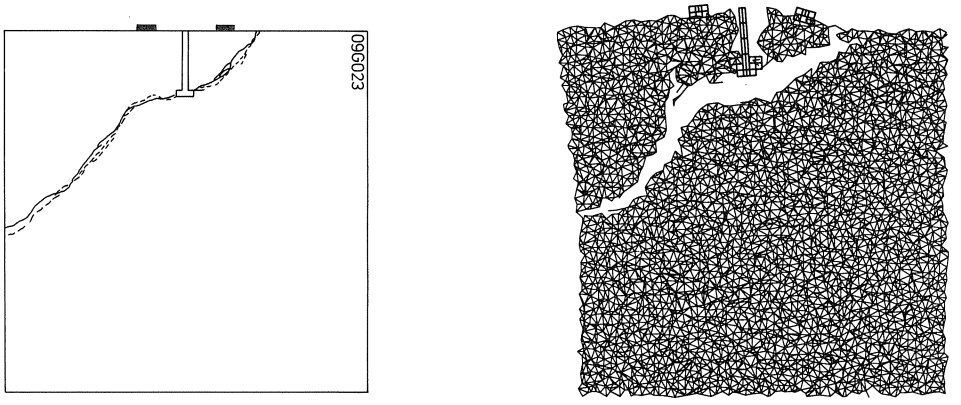

(a) (b)

Fig. 6.27 Experimental crack pattern (a) and simulation with random lattice (b).

simulated result with the random lattice. The support distance is equal to 0.5 times the embedded depth and the boundaries are kept free. It can be seen that a straight crack develops in the specimen. The crack starts at both sides of the anchor bolt, but propagates upwards to the support on one side and downwards on the other side. If the distance between the supports is increased the same crack pattern is observed, only the angle with the horizontal axis is smaller. The simulated descending branch in the load-displacement curves is again too brittle. The simulated peak loads are too low for the anchor bolts compared to the experiments. This can probably be explained by the fact that the load is introduced into the lattice by means of a small number of elements. This leads locally to high stresses which results in a lower peak load. In all the other simulations presented in the previous chapters the load was introduced into the lattice through more elements.

6.5 *Discussion*

6.5.1 Comparison of numerical and experimental results

In general it can be concluded that the lattice model is able to *predict* the crack patterns in all the simulations that are presented in this chapter correctly. However, in order to obtain the correct load-displacement response some further study is needed. Ways to improve the model in this respect will be discussed in the next paragraph. In the following, a comparison is made with simulations and experiments published in literature and in the preceeding chapters of this report.

Uniaxial tensile tests on SEN specimens
In paragraph 6.1.2. is shown that the lattice model is capable of simulating the fracture process in concrete correctly. The simulated results are in good agreement with the outcome of the experiments by Van Mier (1990,1991a). First microcracking occurs in the material which starts around the aggregates. Beyond peak load the crack starts to localise. At the end of the steep drop in the descending branch the crack has traversed the cross-section completely. The long tail can be explained by crack face bridging. In the model, local brittle failure of the elements is implemented. However the global behaviour of the specimen is "ductile". The ductility of the concrete is a result of the fracture mechanism, which is simulated correctly with the lattice model. No complicated iteration procedures, which are required when softening is implemented as a material property, have to be used in the lattice model.
In paragraph 6.1.3 the difference between freely rotating and fixed boundaries is studied for a tensile test. A difference in failure is found. If the boundaries are free to rotate a smooth curve is found. The crack starts at the notched side and gradually grows to the other side. The opening is far from uniform, the unnotched side of the specimen is even compressed when the crack opens at the notch. Fixed boundary conditions also lead to non-uniform opening, but the mechanism is different. The crack starts to open at the notched side but later the unnotched side also opens, which is indicated by a

bump in the load-displacement curve. The same failure mechanisms were recently observed in tensile tests on cylindrical specimens carried out by Daerga (1992). The peak loads obtained with the lattice model are different for different boundary conditions. A higher peak load is found with fixed boundaries. The same conclusions were drawn from an analytical study by Zhou (1988). In simulations carried out by Rots & De Borst (1989) with a smeared crack model (thus implementing softening as a material property) no difference in peak loads and post-peak behaviour is found if the boundary conditions are varied.

Four-point-shear tests
The fracture mechanism in the simulations of the four-point-shear tests on single- and double-edge-notched beams is in good agreement with the mechanism found in the experiments described in Chapter 4. It is shown that the boundary conditions are very important, because they affect the fracture mechanism.
The simulation of the four-point-shear beam ($d = 150$ mm) with the random lattice also produces the correct crack patterns with a considerable reduction in the number of elements (factor 4.7) and thus of computer time (factor 42) compared to the simulations with the regular lattice with the generated grain structure. Because of the increased size of the elements the amount of detail in the crack pattern (crack face bridges) is reduced.

Mixed mode tests on DEN plates
The complicated mixed mode experiments carried out by Nooru-Mohamed (1992) are simulated quite easily with the lattice model, see also Nooru-Mohamed et al. (1993). It is essential is that the specimen is always analysed using boundary conditions in accordance with the experiment. The curvatures of the overlapping cracks are the result of the (ever-changing) stress state in the specimen. Also in this case the cracks grow perpendicular to the direction of maximum tensile stress.
In the load-path 6 simulations the uniaxial tensile load becomes a compressive load to ensure the desired ratio of displacements. The same phenomenon is observed in the experiments by Nooru-Mohamed (1992) as well as in similar experiments carried out by Hassanzadeh (1992).

Pull-out of anchor bolts
The example of the pull-out of anchor bolts demonstrates that symmetry in geometry and loading does not automatically lead to symmetric crack patterns. However, in performing simulations this is often assumed, resulting in useless answers, see the contributions to the round robin (Elfgren (1991)). Concrete should be considered as a heterogeneous material to obtain correct crack patterns, see also Rossi (1991).

6.5.2 Improvements and extension of the model

One of the improvements that has to be realised is that the simulated load-displacement response should be less brittle. There are several options to improve this. One of them is

the small particle effect, which will be discussed here. In the analyses only particles of 3 mm and larger were included in the generated grain structure. This means that the amount of crack face bridging is not sufficient, and probably gives a too brittle load-displacement response. Recently Van Mier (1991b) found that a strong correlation exists between aggregate size, size of crack face bridges and the amount of stress that can be transferred in the tail of the softening diagram in tension. For including small particles in the generated grain structure, the beam length has to be reduced. It is obvious that, when all small particles are included, the computational effort in the analysis will be tremendous, and clearly with the present status of computer technology no analysis can be performed on a mesh containing all the small particles in a given concrete. To study the effect of including the small particles on the tail of the load-displacement curve, several analyses were carried out on a lattice containing one large particle, and on the same lattice containing the same large particle surrounded by numerous small particles, see Schlangen & Van Mier (1992d). The diameter of the large particle was five times the diameter of the small particles. Figure 6.28 shows the resulting crack patterns and load-displacement curves. As can be seen a more complicated crack pattern develops when the small particles are included in the grain structure. Considerable branching and bridging is observed. The result is a more ductile post-peak response, see Figure 6.28b.

The random lattice gives correct results with fewer elements and without forcing the crack to follow the direction given by the mesh. This problem probably occurs in the regular lattice. However, the regular lattice with the generated grain structure represents better the heterogeneity in the concrete material. A combination of both ap-

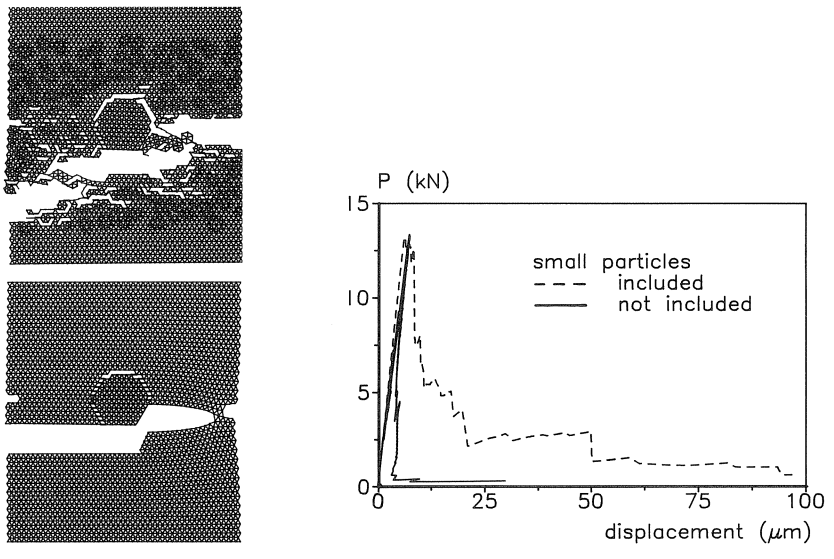

(a) (b)

Fig. 6.28 Effect of small particles on crack patterns (a) and on load-displacement diagram (b).

proaches, using a random lattice with small beam lengths and implementing disorder with a grain structure, could lead to an even better representation of the fracture process. Obviously this results in an increase of the computational effort.
A further improvement should be made in cases where compression plays an important role or dominates. An example of such a case is the four-point-shear beams loaded between fixed supports. If the two curved cracks are arrested in the compression zone, the splitting crack in the middle, between the supports, starts to grow. This leads to an enormous increase in load, much higher than found in the experiments. When the crack in the middle starts, the two curved cracks close again. Yet, closure of the cracks would imply transfer of compressive load again. This is not possible, because of the removal of the beam elements. To overcome this, a check could be implemented in which the distance between two nodes which were connected by a beam is calculated. If in a certain loading step this distance becomes smaller than the original beam length, the element must be placed back, and the loading step repeated. In order to get a permanent deformation after unloading, which occurs in real situations due to loose mate-

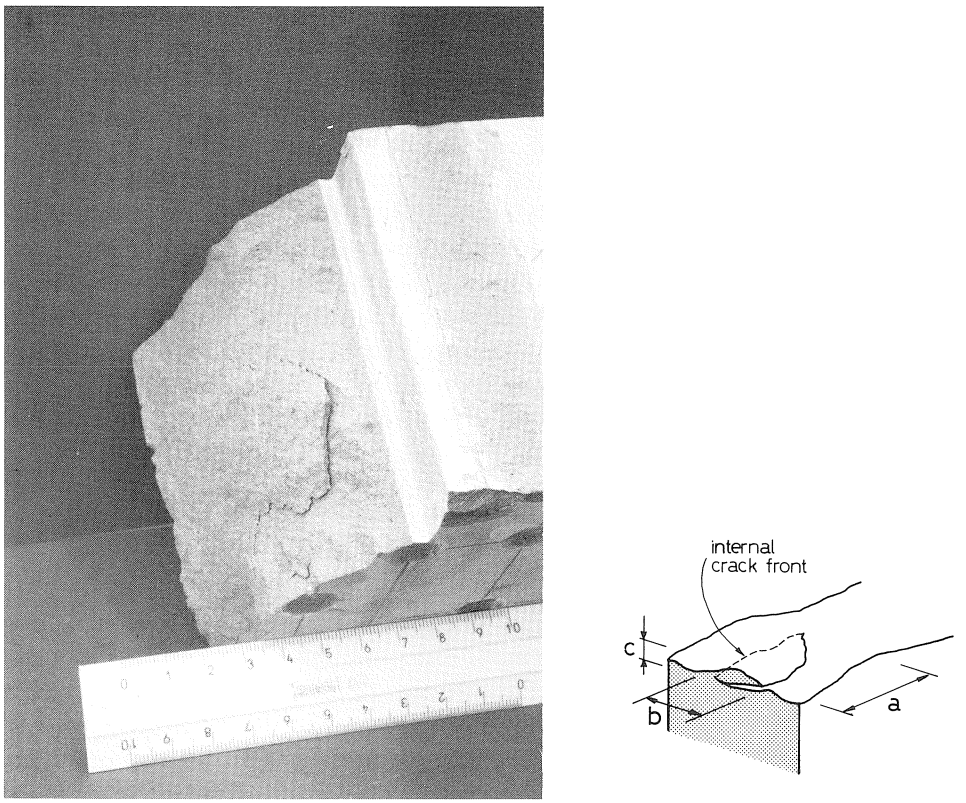

(a) (b)

Fig. 6.29 Photograph of three-dimensional crack face bridge in four-point-shear beam of hardened cement paste (a); Schematical 3D crack face bridge according to Van Mier (1991b),

rial between the crack faces, the distance between two connected nodes could be made a little larger.
The fracture process in concrete is a three-dimensional process. Crack face bridging is not a two-dimensional phenomenon, see Figure 6.29. In order to obtain more reliable results the simulations have to be performed in three dimensions. This probably will also lead to a less brittle load-displacement response. Just as with the above-mentioned improvements, this results in an increase in computer time.
A faster solving procedure for the linear elastic analysis could speed up the process. In addition relaxation techniques, as used by Herrmann (1988, 1991), could be implemented. Then the load in the beam that is to be removed in a load step can be hand over to the neighbouring elements, and it is no longer necessary to solve the whole set of equations, see Chaoxi & Suaris (1992) and Krenk et al. (1992). To give an idea about the reduction in computer time that can be obtained, a comparison is made between the lattice model and the beam model developed by Herrmann et al. (1989). With both models a simulation was carried out on a Cray-YMP (at HLRZ-KFA Germany) in which 10 beams were broken in a square lattice of $40 * 40$ nodes. From a comparison of CPU-time needed, it turned out that the beam model was a factor 75 faster than the lattice model. However an advantage of the lattice model is that it is coupled to a finite element program (DIANA), which makes it easier to change the lattice type (i.e. square, triangular, random) and to simulate real experiments with complicated specimen geometries.
A further possible extension is to make the model suitable for simulating real structures. One way to realise this could be to first model a structure only with continuum elements. As soon as in part of the structure a certain maximum stress level is reached, the continuum element(s) in that part must be substituted by a block of beam elements. Subsequently fracturing takes place in that block of beams. If in the meantime another continuum element reaches the maximum stress, this element should also be replaced by beam elements. If a block of beams is completely cracked it can be removed again and two half continuum elements can be replaced. In such a way fracturing in real structures on a material level could be studied without waiting for supercomputers of "the far distant future".

7 Discussion of results and conclusions

In the preceeding chapters an investigation of fracture processes in concrete is described. Experimentally an attempt is made to enlarge the knowledge of cracking of concrete subjected to a combination of tension and shear loading. A test set-up is used, which has already been adopted in many investigations to study the effect of shear on the fracture behaviour, i.e. beams loaded in four-point-shear. Two different beam geometries are tested, i.e. single and double edge notched beams. The difference in the machine developed in this research and similar machines used by others (e.g. Bažant & Pfeiffer (1985), Swartz & Taha (1987) & Carpinteri et al. (1989)) is the way the loads are introduced in the specimen. Here it is tried to give the specimen the freedom to move, deform, translate and rotate, while keeping the applied loading situation constant. This

is achieved by introducing the loads into the specimen by means of pendulum bars. Furthermore the distribution of the loads is measured, which gives an indication of the eccentricities in the test set-up and the amount of friction in the supports. Such an approach is necessary to give explanations for the fracture process. If the test set-up is complicated the stress situation in the specimen will not be straightforward and no conclusions can be drawn regarding the failure mechanism of the specimen. With the machine described in Chapter 3 it is possible to perform stable tests in which the loading situation remains constant and is known.

The conclusions obtained from the experiments are the result of combining different measurements and observations. Measurements of load-distribution, crack mouth displacements and local deformations on the specimen surface combined with the monitoring of the crack development in the specimen using a long distance microscope have led to an increased insight in the mixed mode fracture process. The main conclusion is that fracture in concrete under combined tensile and shear loading is a mode I process only. In the experiments on the beam specimens, the affect of the mode II (shear) loading seems to be a rotation of the principle stresses in the specimen only. The direction of crack growth, however, is perpendicular to the maximum tensile stress, thus perpendicular to the mode I stress. The opening of the crack is a mode I opening only; there is no shear displacement over the crack faces. Furthermore the phenomenon of crack face bridging observed in uniaxial tension by Van Mier (1990), occurs also in the curved cracks in the four-point-shear beams. The foregoing situation occurs when the supports are free to rotate and translate.

A different fracture mechanism takes place when the free movement and deformability of the specimen are restricted. This is done by mounting diagonal bars to the loading frame, as explained in Chapter 3. Now horizontal loads are introduced in the specimen and the vertical loading distribution in the four-point-shear test starts to deviate. This also results in a more complicated fracture mechanism. After opening of the first cracks and deformation of the specimen, the stress situation changes and additional cracking occurs. If the additional horizontal loadings are neglected in the analysis of the experiments, doubtful conclusions can be drawn. For example the higher fracture energy (compared to mode I fracture energy) found in mixed mode tests by Carpinteri et al. (1989,1990) and the existence of real shear fracture found by Bažant & Pfeiffer (1985) can be mentioned.

The question whether shear fracture exists in real structures can be answered if the above is understood and assumed to be correct. Cracks in a concrete material (structure) will follow the direction which is governed by a combination of the maximum tensile stress and the weakest link in the material. Of course it is not possible to separate both factors, because the heterogeneity of the material will affect the stress situation in the material. However, in order to predict crack growth in a material the heterogeneity and the stress distribution should be known. In real structures the stress distribution is never straightforward and an ideal situation as in laboratory scale tests can never be obtained. However, even in experiments on small specimens, differences in behaviour are found due to variations in manufacturing, curing and drying as shown in paragraph

4.2. For large structures the differences in behaviour of the material over the cross-section of the structure becomes larger too. Further the stress situation becomes more complex due to reinforcement in the structure and due to a combination of different loading types (mechanical and physical loading) on the structures. In addition the fracture mechanism in fibre concrete can be mentioned. Here crack patterns which seem to be shear cracks are observed, see Arslan et al. (1991) and Van Mier & Timmers (1992). However, by including fibres in the concrete the microstructure is changed enormously, and with that the stress distribution. It is the author's opinion that also in those cases locally only mode I failure takes place. The history of loading plays an important role too, as cracks in a material lead to a redistribution of stress, or in other words to an increased heterogeneity.

As discussed in Chapter 2, two main approaches can be distinguished for developing programs to simulate and predict fracture in concrete:

In the first approach, concrete is treated as a homogeneous material. The behaviour of the homogeneous medium has to be extracted from experiments. To include all the influences discussed above in a general material behaviour, complicated tests are required. There should always be a relation between the homogeneous medium and the degree of heterogeneity of the concrete. Since the degree of heterogeneity changes in time (micro-cracking due to loading, moisture content, stresses due to creep and shrinkage) the general homogeneous material behaviour must necessarily be very complicated. Perhaps the derivation of such a macroscopic law is simply impossible.

In the second approach, as adopted in this investigation, the heterogeneity of the material is modelled directly. Implementing disorder automatically leads to a stress distribution in the material which is not uniform. Simple experiments are sufficient to study the effects of different loading types on the fracture behaviour. All effects can be observed in a change in the microstructure (heterogeneity) of the material.

With respect to the above, the level of observation is often considered very important. From an engineering point of view, the exact fracture mechanism is of less interest. In many practical cases concrete can be treated as a homogeneous material. As long as cracking is distributed through the structure, the behaviour can be simulated with a homogeneous model. However, if the crack width in a particular part of a structure becomes important or if for instance the collapse of a structure is the result of the propagation of one single crack, the heterogeneity of the material must be taken into account. Fracture is a local phenomenon, which acts on the scale of the individual aggregates in the concrete, even if the structure made of concrete is many times larger than the single aggregates.

In the present study a lattice model is developed in which the heterogeneity of the material can be implemented using several procedures. The model is extremely simple since it only makes use of a linear elastic analysis. The material is represented as a network of small beam elements. For the single elements there are only two possibilities: either stress can be transferred, or it cannot. Local fracture of the elements is brittle. However by implementing the heterogeneity, a global ductile behaviour is obtained. From a parameter study, for which simulations of a uniaxial tensile experiment are

used, a set of input parameters for the model are determined. All the parameters are single valued. It is not stated that the best or the only possible set of parameters is obtained. However, after studying the effect of changing the various parameters, a parameter set is chosen showing good results in crack patterns and maximum load, but a too brittle post-peak behaviour in the load-displacement response. Besides these somehow arbitrary chosen input parameters other assumptions are made for the development of the model, i.e. local fracture is brittle and plasticity, healing, friction between crack faces and cohesive forces are neglected. However, simulations of different experiments have shown that the lattice model is very powerful in the prediction of fracture in concrete. The phenomenon of crack face bridging as well as curved crack growth are predicted in good agreement with experimental observations. Of course many improvements and extensions of the model are possible, as discussed in paragraph 6.5.2. Nevertheless a model is developed which has many applications:

- To improve materials, a study can be undertaken with the lattice model to gain knowledge about the weakest parts in the material. Moreover such analyses may indicate which changes in the material structure lead to better fracture behaviour.
- Simulations with the model provide more insight into how specimens behave in experiments for determining material properties. In this way better experimental setups can be designed.
- The outcome of simulations with a micro-mechanical model (lattice model) can probably be used to determine the input parameters for a macro-mechanical model.

In summary the following conclusions are drawn from the present investigation:

- Fracture in concrete, a material with a low tensile strength, seems to be a mode I mechanism. A shear loading on a specimen results in a rotation of the principle stresses. Fracture, however, will take place perpendicular to the maximum tensile stress.
- Boundary conditions in experiments are very important, because they affect the stress distribution in the specimen. If the real situation does not correspond with the assumptions, wrong conclusions can be drawn from the experimental observations.
- The observations made in the experiments and the results obtained with the developed lattice model indicate that fracture in concrete is brittle and that the measured ductile behaviour in a test is the result of the heterogeneity. Cracks will follow the weakest parts in the material, which means that in a normal weight concrete the cracks will grow around aggregate particles. The conclusion that the formation of crack face bridges, Van Mier (1990), are an explanation for the ductile behaviour of concrete, is supported by the results of this investigation.
- For simulating and predicting fracture in concrete correctly, including the above-mentioned mechanism of crack face bridging, the heterogeneity of the material must be implemented in numerical models. For the implementation of heterogeneity various procedures can be followed.
- The lattice model as presented in this report is capable of predicting fracture patterns in concrete and provides insight into how a heterogeneous material behaves.

References

ALFAIATE, J., PIRES, E. B. and MARTINS, J. A. C. (1992), A finite element model for the study of crack propagation in concrete, Localized Damage II Vol I: Fatigue and Fracture Mechanics (eds. M. H. Aliabadi, D. J. Cartwright & H. Nisitani), Computational Mechanics Publications, Southampton/Boston, pp. 261–280.

ARBABI, S. and SAHIMI, M. (1989), Test of universality for three-dimensional models of mechanical breakdown in disordered solids, Physical Review B, 41(1), pp. 772–775.

ARREA, M. and INGRAFFEA, A. R. (1982), Mixed mode crack propagation in mortar and concrete, Report No. 81-13, Department of Structural Engineering, School of Civil and Environmental Engineering, Cornell University.

ARSLAN, A., HUGHES, T. G. and BARR, B. I. G. (1991), Mixed mode fracture – including torsion in a new compact test specimen geometry, in Fracture Processes in Concrete, Rock and Ceramics (eds. J. G. M. Van Mier, J. G. Rots & A. Bakker), Chapman & Hall/E & FN Spon, London, pp. 737–746.

BALLARINI, R., SHAH, S. P. and KEER, L. M. (1986), Failure characteristics of short anchor bolts embedded in a brittle material, Proc. R. Soc. London. A404, pp. 35–54.

BALLATORE, E., CARPINTERI, A., FERRARA, G. and MELCHIORRI, G. (1988), Mixed mode fracture energy of concrete, Engineering Fracture Mechanics, 35(1/2/3), 1990, pp. 145–157.

BAŽANT, Z. P. and OH, B. H. (1983), Crack band theory for fracture of concrete, Materials and Structures (RILEM), 16(93), pp. 155–177.

BAŽANT, Z. P. and PFEIFFER, P. A. (1985), Tests of shear fracture and strain-softening in concrete, Proceedings of the 2nd Symposium on the Interaction of Non-Nuclear Munitions with Structures, April 15–19, Panama City Beach, Florida.

BAŽANT, Z. P. and PFEIFFER, P. A. (1986), Shear fracture test of concrete, Materials and Structures (RILEM), 110(19), pp. 111–121.

BAŽANT, Z. P., TABBARA, M. R., KAZEMI, M. T. and PIJAUDIER-CABOT, G. (1990), Random particle model for fracture of aggregate or fiber composites, Journal of Engineering Mechanics, ASCE, 116(8), pp. 1686–1705.

BERG, A. and SVENSSON, U. (1991), Datorsimulering och analys av brottförlopp i en heterogen materialstruktur, Report No. TVSM-5050, Lund Institute of Technology, Division of Structural Mechanics, Lund, Sweden.

BREMAECKER DE, J. CL. and SWENSON, D. V. (1990), Origin of overlapping spreading centers: a finite element model, Tectonics, 9(3), pp. 505–519.

BROEK, D. (1984), Elementary Engineering Fracture Mechanics, Martinus Nijhoff Publishers, The Hague.

BRÜHWILER, E. (1988), Fracture mechanics of dam concrete subjected to quasi-static and seismic loading conditions, Thesis, No. 739, (LMC) Swiss Federal Institute of Technology, Lausanne.

BURT, N. J. and DOUGILL, J. W. (1977), Progressive failure in a model heterogeneous medium, Journal of the Engineering Mechanics Division, ASCE, 103(3), pp. 365–376.

CARMELIET, J. and HENS, H. (1992), Fracture of a fabric reinforced mortar based on a stochastic approach to initial damage, Localized Damage II Vol I: Fatigue and Fracture Mechanics (eds. M. H. Aliabadi, D. J. Cartwright & H. Nisitani), Computational Mechanics Publications, Southampton/Boston, pp. 283–298.

CARPINTERI, A., FERRARA, G. and MELCHIORRI, G. (1989), Single edge notched specimen subjected to four point shear: an experimental investigation, in Fracture of Concrete and Rock – Recent Developments (eds. S. P. Shah, S. E. Swartz & B. Barr), Elsevier Applied Science Publishers, London/New York, pp. 605–614.

CARPINTERI, A., FERRARA, G., MELCHIORRI, G. and VALENTE, S. (1990), The four point shear test on single notched specimens: an experimental and numerical analysis, in Fracture Behaviour and Design of Materials and Structures (ed D. Firrao), EMAS Publishers, Warley, pp. 667–675.

CARPINTERI, A. and FERRO, G. (1992), Apparent tensile strength and fictitious fracture energy of concrete: a fractal geometry approach to related size effects, International Conference on Fracture and Damage of Concrete and Rock, FDCR-2, November 9–13, Vienna, Austria, Chapman & Hall, London, (in press).

CARPINTERI, A., VALENTE, S., FERRARA, G. and IMPERATO, L. (1992), Experimental and numerical fracture modelling of a gravity dam, in Proceedings FraMCoS I (ed. Z. P. Bažant), Elsevier Publishers, London/New York, pp. 351–360.

CARPINTERI, A., VALENTE, S., FERRARA, G. and MELCHIORRI, G. (1991), Is mode-II fracture toughness a real material property? Proceedings of the International Conference on Mixed-Mode Fracture and Fatigue, July 15–17, Vienna, Austria.

CHAOXI, L. and SUARIS, W. (1992), Generalized analysis of changing structures, Personal Communication.

CUNDALL, P. A. and STRACK, O. D. L. (1979), A discrete numerical model for granular assemblies, Journal of Géotechnique, 29(1), pp. 47–65.

DAERGA, P. A. (1992), Some Experimental Fracture Mechanics Studies in Mode I of Concrete and Wood, Licenciate Thesis, Luleå University of Technology, Sweden.

DAVIES, J. (1991), Numerical and experimental study of development of fracture path under mixed mode loading, in Fracture Processes in Concrete, Rock and Ceramics (eds. J. G. M. Van Mier, J. G. Rots & A. Bakker), Chapman & Hall/E & FN Spon, London, pp. 717–726.

DE BORST, R. (1986), Constitutive models for continua and numerical techniques for analysis of granular materials, PhD-thesis, Delft University of Technology, Delft, The Netherlands.

DE BORST, R. and MÜHLHAUS, H.-B. (1991), Continuum models for discontinuous media, in Fracture Processes in Concrete, Rock and Ceramics (eds. J. G. M. Van Mier, J. G. Rots & A. Bakker), Chapman & Hall, London/New York, pp. 601–618.

DUDA, H. (1991), Grain model for the determination of the stress-crack-width-relation, in Analysis of Concrete Structures by Fracture Mechanics (eds. L. Elfgren & S. P. Shah), Chapman & Hall, London, pp. 88–96.

DUXBURY, P. M. and KIM, S. G. (1990), Scaling theory of elasticity and fracture in disordered networks, in Mechanical Properties of Porous and Cellular Materials (eds. K. Sieradzki, D. J. Green & L. J. Gibson), Materials Research Society, Pittsburgh, Pennsylvania, pp. 179–195.

ELFGREN, L. (1991), Round-robin analysis of anchor bolts, RILEM TC 90-FMA, Division of Structual Engineering, Luleå, Sweden.

ELICES, M., GUINEA, G.V. and PLANAS, J. (1992), Measurement of the fracture energy using three point bend tests: part 3-influence of cutting the P-δ tail, Materials and Structures (RILEM), 25, pp. 327–334.

FATHY, A., PLANAS, J., ELICES, M. and GUINEA, G. V. (1992), Fracture of anchors in rock, Anales de Mechanica de la Fractura, 9, pp. 69–74.

FERRARA, G. (1991), On the accuracy of the mixed mode tests performed at the enel-cris laboratories, Report No. 4275 GeF/av, Enel-Cris, Milan, Italy.

GJØRV, O. E., SØRENSEN, S. I. and ARNESEN, A. (1977), Notch sensitivity and fracture toughness of concrete, Cement and Concrete Research, 7(3), pp. 333–344.

GOLDBERG, D. E. (1989), Genetic Algorithms in Search, Optimization and Machine Learning, Addison-Wesley, Reading, Massachusetts.

GRIFFITH, A. A. (1920), The phenomena of rupture and flow in solids, Philosofical Transactions, Royal Society of London, A 22, pp. 163–198.

GUINEA, G. V., PLANAS, J. and ELICES, M. (1992), Measurement of the fracture energy using three point bend tests: part 1 – influence of experimental procedures, Materials and Structures (RILEM), 25, pp. 212–218.

HASSANZADEH, M. (1992), Behaviour of fracture process zones in concrete influenced by simultaniously applied normal and shear displacements, PhD-thesis, Lund Institute of Technology, Division of Building Materials, Lund, Sweden.

HELBLING, A., ALVAREDO, A. M. and WITTMAN, F. H. (1991), Round-robin analysis of anchor bolts, RILEM TC-90 FMA, preliminary report, second edition.

HERRMANN, H. J. (1988), The hunt for universality in fracture, Universalities in Condensed Matter, Springer Verlag, Proceedings in Physics 32, March 15–24, Les Houches, France, pp. 132–135.

HERRMANN, H. J. (1991), Patterns and scaling in fracture, in Fracture Processes in Concrete, Rock and Ceramics (eds. J. G. M. Van Mier, J. G. Rots & A. Bakker), Chapman & Hall/E & FN Spon, London, pp. 195–211.

HERRMANN, H. J., HANSEN, H. and ROUX, S. (1989), Fracture of disordered, elastic lattices in two dimensions, Physical Review B, 39(1), pp. 637–648.
HILLERBORG, A. (1985), Results of three comparative test series for determining the fracture energy G_f of concrete, Materials and Structures (RILEM), 18(107), pp. 33–39.
HILLERBORG, A., MODÉER, M. and PETERSSON, P.-E. (1976), Analysis of crack formation and crack growth in concrete by means of fracture mechanics and finite elements, Cement and Concrete Research, 6(6), pp. 773–782.
HORDIJK, D. A. (1989), Deformation-controlled unaxial tensile tests on concrete, Report 25.5-89-15/VFA, D.U.T., Faculty of Civil Engineering, Stevin Laboratory, The Netherlands.
HORDIJK, D. A. (1991), Local approach to fatigue of concrete, PhD-thesis, Delft University of Technology, Delft, The Netherlands.
HRENNIKOFF, A. (1941), Solution of problems of elasticity by the framework method, Journal of Applied Mechanics, 12, pp. 169-175.
HSU, T. T. C. (1963), Mathematical analysis of shrinkage stresses in a model of hardened concrete, Journal of the American Concrete Institute, 3, pp. 371–390.
HSU, T. T. C., SLATE, F. O., STURMAN, G. M. and WINTER, G. (1963), Microcracking of plain concrete and the shape of the stress-strain curve. Journal of the American Concrete Institute, 2, pp. 209–224.
HUGHES, B. P. and ASH, J. E. (1970), Anisotropy and failure criteria for concrete, Materials and Structures (RILEM), 3(18), pp. 371–374.
INGRAFFEA, A. R. and PANTHAKI, M. J. (1985), Analysis of shear fracture tests of concrete beams, Finite Element Analysis of Reinforced Concrete Structures, ASCE, Tokyo, pp. 151–173.
INGRAFFEA, A. R. and SAOUMA, V. (1985), Numerical modeling of discrete crack propagation in reinforced and plain concrete, in Fracture Mechanics of Concrete (eds. G. C. Sih & A. DiTommaso), EAFM series, Martinus Nijhoff publishers, Dordrecht, pp. 171–222.
IOSIPESCU, N. (1967), New accurate procedure for single shear testing of metals, Journal of Materials, 2(3), pp. 537–566.
JENQ, Y. S. and SHAH, S. P. (1988), Mixed-mode fracture of concrete, International Journal of Fracture, 38, pp. 123–142.
KEUSER, W. (1989), Bruchmechanisches Verhalten von Beton unter Mixed-Mode Beanspruchung, Dissertation, Technischen Hochschule Darmstadt, Fachbereich Konstruktiver Ingenieurbau, Darmstadt, Germany.
KRENK, S., VISSING, S. and VISSING-JØRGENSEN (1992), A finite step updating method for elasto-plastic analysis of frames, Personal Communication.
KUMOSA, M. and HULL, D. (1987), Mixed-mode fracture of composites using iosipescu shear test, International Journal of Fracture 35, pp. 83–102.
MAZARS, J. (1984), Description of multiaxial behaviour of concrete with an elastic damaging model, in Proceedings of RILEM-CEB Symposium on Concrete under Multiaxial Conditions, INSA, session 6, 1, Toulouse, pp. 190–200.
MEAKIN, P., LI, G., SANDER, L. M., LOUIS, E. and GUINEA, F. (1989), A simple two-dimensional model for crack propagation, Journal of Physics, A: Math. Gen. 22, pp. 1393–1403.
MELIN, S. (1989), Why are crack paths in concrete and mortar different from those in PMMA? Materials and Structures (RILEM), 22, pp. 23–27.
MINDESS, S. (1989), Interfaces in Concrete, in Materials Science of Concrete I (ed. J. P. Skalny), The American Ceramic Society, Inc., Westervill (OH), pp. 163–180.
MINDESS, S. (1991), Fracture process zone detection, in Fracture Mechanics Test Methods for Concrete (eds. S. P. Shah & A. Carpinteri), Chapman & Hall, London/New York, pp. 231–261.
MOUKARZEL, C. and HERRMANN, H. J. (1992), A vectorizable random lattice, Preprint HLRZ 1/92, HLRZ KFA Jülich.
MURAT, M., ANHOLT, M. and WAGNER, H. D. (1992), Fracture behaviour of short-fiber reinforced materials, Journal Material Research, 7(11), pp. 3121–3131.
NOORU-MOHAMED, M. B. (1992), Mixed mode fracture of concrete: an experimental approach, PhD-thesis, Delft University of Technology, Delft, The Netherlands.

NOORU-MOHAMED, M. B., SCHLANGEN, E. and VAN MIER, J. G. M. (1993), An experimental and numerical study on the behaviour of concrete subjected to biaxial tension and shear, Advanced Cement Based Materials, accepted for publication.

PETERSSON, P.-E. (1981), Crack growth and development of fracture zones in plain concrete and similar materials, Report TVBM-1006, Lund Inst. of Technology, Sweden.

PLANAS, J., ELICES, M. and GUINEA, G. V. (1992), Measurement of the fracture energy using three point bend tests: part 2-influence of bulk energy dissipation, Materials and Structures (RILEM), 25, pp. 305-312.

REHM, G., DIEM, P. and ZIMBELMANN, R. (1977), Technische Möglichkeiten zur Erhöhung der Zugfestigkeit von Beton, Deutscher Ausschuss für Stahlbeton, 283, pp. 1-76.

REINHARDT, H. W., CORNELISSEN, H. A. W. and HORDIJK, D. A. (1986), Tensile tests and failure analysis of concrete, Journal of Structural Engineering, ASCE, 112(11), pp. 2462-2477.

REINHARDT, H. W., CORNELISSEN, H. A. W. and HORDIJK, D. A. (1987), Mixed mode fracture tests on concrete, International Conference on Fracture of Concrete and Rock, June 17-19, Houston, Texas, pp. 324-337.

RILEM TC-50 FMC (1985), Determination of the fracture energy of mortar and concrete by means of three-point bending tests on notched beams, Materials and Structures (RILEM), 18(106), pp. 287-290.

ROCHA, M. M. and RIERA, J. D. (1991), On size effects and rupture of nonhomogeneous materials, in Fracture Processes in Concrete, Rock and Ceramics (eds. J. G. M. Van Mier, J. G. Rots & A. Bakker), Chapman & Hall/E & FN Spon, London, pp. 451-460.

ROELFSTRA, P. E., SADOUKI, H. and WITTMANN, F. H. (1985), Le béton numérique, Materials and structures (RILEM), 18(107), pp. 327-335.

ROSSI, P. (1991), Round-robin analysis of anchor bolts, RILEM TC-90 FMA, in Elfgren (1991).

ROSSI, P. and RICHER, S. (1987), Numerical modeling of concrete cracking based on a stochastic approach, Materials and Structures (RILEM), 20, pp. 334-337.

ROTS, J. G. (1988), Computational modeling of concrete fracture, PhD-thesis, Delft University of Technology, Delft, The Netherlands.

ROTS, J. G. (1992), Removal of finite elements in strain-softening analysis of tensile fracture, in Proceedings FraMCoS I (ed. Z.P. Bažant), Elsevier Publishers, London/New York, pp. 330-338.

ROTS, J. G. and DE BORST, R. (1989), Analysis of concrete fracture in "direct" tension, International Journal of Solids and Structures, 25(12), pp. 1381-1394.

ROTS, J. G., KUSTERS, G. M. A. and BLAAUWENDRAAD, J. (1987), Strain-softening simulations of mixed-mode concrete fracture, in Proceedings SEM/RILEM International Conference on Fracture of Concrete and Rock (eds. S P. Shah & S. E. Swartz), Springer Verlag, New York, pp. 175-189.

ROUX, S. (1990), Continuum and discrete description of elasticity and other rheological behaviour, in Statistical Models for the Fracture of Disordered Media (eds. H. J. Herrmann & S. Roux), North-Holland, pp. 87-114.

SCHLANGEN, E. and VAN MIER, J. G. M. (1990), A fe-supported investigation of mixed mode fracture in concrete, in Proceedings 9th International Conference on Experimental Mechanics, August 20-24, Copenhagen, Denmark, pp. 1403-1412.

SCHLANGEN, E. and VAN MIER, J. G. M. (1991a), Boundary effects in mixed mode I and II fracture of concrete, in Fracture Processes in Concrete, Rock and Ceramics (eds. J. G. M. Van Mier, J. G. Rots & A. Bakker), Chapman & Hall/E & FN Spon, London, pp. 705-716.

SCHLANGEN, E. and VAN MIER, J. G. M. (1991b), Lattice model for numerical similation of concrete fracture, in Proceedings International EPRI Conference on Dam Fracture (eds. V. E. Saouma, R. Dungar & D. Morris), EPRI, Palo Alto, pp. 511-527.

SCHLANGEN, E. and VAN MIER, J. G. M. (1992a), Fracture modelling of granular materials, in Computational Methods in Materials Science (eds. J. E. Mark, M. E. Glicksman & S. P. Marsh), MRS Symposium Proceedings Vol. 278, Pittsburgh, pp. 153-158.

SCHLANGEN, E. and VAN MIER, J. G. M. (1992b), Shear fracture in cementitious composites part II: numerical simulations, in Proceedings FraMCoS I (ed. Z. P. Bažant), Elsevier Publishers, London/New York, pp. 659-670.

SCHLANGEN, E. and VAN MIER, J. G. M. (1992c), A new lattice model for predicting localized fracture in concrete, in Localized Damage II Vol I: Fatigue and Fracture Mechanics (eds. M. H. Aliabadi, D. J. Cartwright & H. Nisitani), Computational Mechanics Publications, Southampton/Boston, pp. 425–438.
SCHLANGEN, E. and VAN MIER, J. G. M. (1992d), Lattice model for simulating fracture of concrete, in Proceedings 1st Bolomey-Workshop, July 16–17, ETH-Zürich, Zürich, Balkema, Rotterdam, (in press).
SCHLANGEN, E. and VAN MIER, J. G. M. (1992e), Numerieke micromechanica van beton: gereedschap voor het ontwikkelen van nieuwe materialen, Cement, 6, pp. 20–28.
SCHLANGEN, E. and VAN MIER, J. G. M. (1992f), Numerical study of the influence of interfacial properties on the mechanical behaviour of cementbased composites, in Interfaces in Cementitious Composites (ed. J. C. Maso), Chapman & Hall/E & FN Spon, London, pp. 237–246.
SCHLANGEN, E. and VAN MIER, J. G. M. (1992g), Experimental and numerical analysis of micromechanisms of fracture of cement-based composites, Cement & Concrete Composites, 14, pp. 105–118.
SCHLANGEN, E. and VAN MIER, J. G. M. (1992h), Mixed mode fracture propagation: a combined numerical and experimental study, International Conference on Fracture and Damage of Concrete and Rock, FDCR-2, November 9–13, Vienna, Austria, Chapman & Hall, London, (in press).
SCHLANGEN, E. and VAN MIER, J. G. M. (1992i), Simple lattice model for numerical simulations of fracture of concrete materials and structures, Materials & Structures (RILEM), 25, pp. 534–542.
SCHLANGEN, E. and VAN MIER, J. G. M. (1992j), Micromechanical analysis of fracture of concrete, International Journal of Damage Mechanics, 1, pp. 435–454.
SCHORN, H. and BERGER-BÖCKER, T. (1989), Test method for determining process zone position and fracture energy of concrete, Experimental Techniques, 6, pp. 29–33.
SCHORN, H. and RODE, U. (1987), 3-D-modeling of process zone in concrete by numerical simulation, in Proceedings SEM/RILEM International Conference on Fracture of Concrete and Rock (eds. S. P. Shah & S. E. Swartz), Springer Verlag, New York, pp. 220–228.
SLUYS, L. J. (1992), Wave Propagation, Localisation and Dispersion in Softening Solids, PhD-thesis, Delft University of Technology, Delft, The Netherlands.
SWARTZ, S. E., LU, L. W. and TANG, L. D. (1988), Mixed-mode fracture toughness testing of concrete beams in three-point bending, Materials and Structures (RILEM), 21, pp. 33–40.
SWARTZ, S. E. and TAHA, N. M. (1987), Preliminary investigation of the suitability of the iosipescu test specimen for determining mixed mode fracture properties of concrete, Report #191, Kansas State University, College of Engineering, Manhattan, Kansas.
TERMONIA, Y., MEAKIN, P. and SMITH, P. (1985), Theoretical study of the influence of the molecular weight on the maximum tensile strength of polymer fibres, Macromolecules, 18, pp. 2246–2252.
TZSCHICHHOLZ, F. (1991), Peeling instability in cosserat like media, Preprint HLRZ 68/91, HLRZ KFA Jülich.
VAN MIER, J. G. M. (1984), Strain softening of concrete under multiaxial loading conditions, PhD-thesis, Eindhoven University of Technology, Eindhoven, The Netherlands.
VAN MIER, J. G. M. (1986), Fracture of concrete under complex stress, Heron, 31(3), pp. 1–90.
VAN MIER, J. G. M. (1990), Internal crack detection in single edge notched concrete plates subjected to uniform boundary displacement, in Proceedings International Conference on Micromechanics of Failure of Quasi-Brittle Materials (eds. S. P. Shah, S. E. Swartz & M. L. Wang), Elsevier Applied Science Publishers, London/New York, pp. 33–42.
VAN MIER, J. G. M. (1991a), Mode I fracture of concrete: discontinuous crack growth and crack interface grain bridging, Cement and Concrete Research, 21, pp. 1–15.
VAN MIER, J. G. M. (1991b), Crack face bridging in normal, high strength and lytag concrete, in Fracture Processes in Concrete, Rock and Ceramics (eds. J. G. M. Van Mier, J. G. Rots & A. Bakker), Chapman & Hall/E & FN Spon, London, pp. 27–40.
VAN MIER, J. G. M. (1992), Assessment of strain softening curves for concrete, Lecture Notes, COMETT course on "Fracture of Concrete", November 25–27, Madrid.

VAN MIER, J. G. M., ROTS, J. G. and BAKKER, A. (eds.) (1991), Fracture Processes in Concrete, Rock and Ceramics, Chapman & Hall/E & FN Spon, London.

VAN MIER, J. G. M. and SCHLANGEN, E. (1989), On the stability of softening systems, in Fracture of Concrete and Rock-Recent Developments (ed. S. P. Shah, S. E. Swartz & B. Barr), Elsevier Applied Science Publishers, London/New York, pp. 387–396.

VAN MIER, J. G. M., SCHLANGEN, E. and NOORU-MOHAMED, M. B. (1992), Shear fracture in cementitious composites part I: experimental observations, in Proceedings FraMCoS I (ed. Z. P. Bažant), Elsevier Publishers, London/New York, pp. 659–670.

VAN MIER, J. G. M. and TIMMERS, G. (1991), Shear fracture in slurry infiltrated fibre concrete (SIFCON), in Proceedings RILEM/ACI Workshop on High Performance Fiber Reinforced Cement Composites (eds. H. W. Reinhardt & A. E. Naaman), Chapman & Hall, London, pp. 348–360.

VAN MIER, J. G. M., VERVUURT, A. and SCHLANGEN, E. (1993), Effect of specimen boundary rotations on tensile crack propagation in concrete and rock, in Proceedings 4th International Symposium on Plasticity, Baltimore, July 19–23, (in press).

VERVUURT, A. H. J. M., SCHLANGEN, E. and VAN MIER, J. G. M. (1992), Pull-out of steel anchors embedded in concrete, Special Seminar on Anchorage Engineering, november 13, Vienna, Austria, Chapman & Hall, London, (in press).

VERVUURT, A., SCHLANGEN, E. and VAN MIER, J. G. M. (1993), A Numerical and Experimental Analysis of the Pull-out Behaviour of Steel Anchors Embedded in Concrete, Report 25.5-93-1/VFI, Delft University of Technology, The Netherlands.

VONK, R. A. (1992), Softening of concrete loaded in compression, PhD-thesis, Eindhoven University of Technology, Eindhoven, The Netherlands.

VONK, R. A., RUTTEN, H.S., VAN MIER, J. G. M. and FIJNEMAN, H. J. (1991), Micromechanical simulation of concrete softening, in Fracture Processes in Concrete, Rock and Ceramics (eds. J. G. M. Van Mier, J. G. Rots & A. Bakker), Chapman & Hall/E & FN Spon, London, pp. 129–138.

WALRAVEN, J. C. (1980), Aggregate interlock: a thmeoretical and experimental analysis, PhD-thesis, Delft University of Technology, Delft, The Netherlands.

WANG, J., NAVI, P. and HUET, C. (1992a), Finite element analysis of anchor bolts pull-out based on fracture mechanics, Special Seminar on Anchorage Engineering, November 13, Vienna, Austria, Chapman & Hall, London, (in press).

WANG, J., NAVI, P. and HUET, C. (1992b), Numerical study of granule influences on the crack propagation in concrete, in Proceedings FraMCoS I (ed. Z. P. Bažant), Elsevier Publishers, London/New York, pp. 373–378.

WITTMANN, F. H. (1983), Structure of concrete with respect to crack formation, in Fracture Mechanics of Concrete (ed. F. H. Wittmann), Elsevier, Amsterdam, pp. 43–74.

WITTMANN, F. H. and ROELFSTRA, P. E. (1987), Constitutive relations for transient conditions, in Proceedings IABSE Colloquium Delft, IABSE, Zürich, pp. 239–259.

YACOUB-TOKATLY, Z., BARR, B. and NORRIS, P. (1989), Mode-III fracture – a tentative test geometry, in Fracture of Concrete and Rock, Recent Developments (eds. S. P. Shah, S. E. Schwartz & B. Barr), Elsevier Applied Science Publishers, London/New York, pp. 596–604.

ZHOU, F. (1988), Some aspects of tensile fracture behaviour and structural response of cementitious materials, Report TVBM 1008, Lund Institute of Technology, Division of Building Materials, Lund, Sweden.

APPENDIX A1:

Additional experimental results of SEN beams loaded between fixed supports

Appendix A1 shows additional experimental results of SEN beams loaded between fixed supports. The load-displacement curves of three small beams and three large beams are shown in figure A1.1. The total load P is plotted versus the deformation δ_2. Crack patterns of three small beams tested between fixed supports are given in figure A1.2. The crack patterns of the large beams tested between fixed supports are identical to the crack patterns in large beams tested between freely rotating supports. For large beams only the curved cracks develop in the specimen.

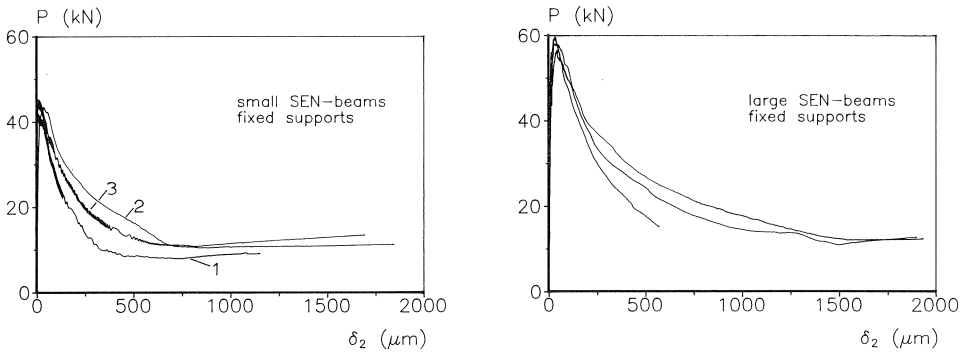

Fig. A1.1 Total load P versus deformation δ_2 in three small SEN beams (a) and three large SEN beams (b) tested between fixed supports.

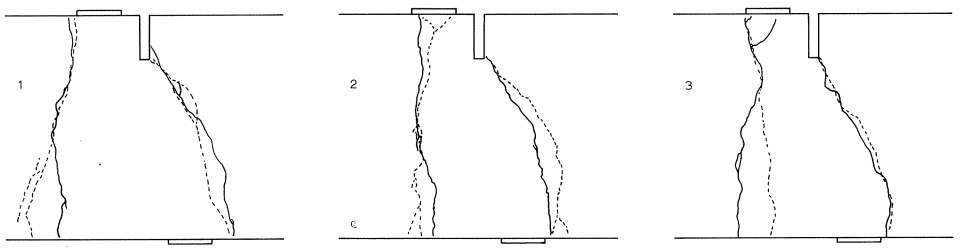

Fig. A1.2 Crack patterns in three small SEN beams tested between fixed supports.

APPENDIX A2:

Additional experimental results of SEN beams made of different concretes

In appendix A2 load-displacement curves of SEN beams made of different concretes are presented. The total load P is plotted versus δ_2. The crack patterns in the different concretes were identical to the tests on the normal weight concrete (con8) beams, except for the fcon specimens. For lytag three curves for both the small and the large beams are shown in figure A2.1. For hsc two curves for the large beams are plotted in figure A2.2. Only one test on a small hsc beam was succesful. For fcon three curves of the small beams are shown in figure A2.3. The carrying capacity of the testing machine was not enough to break the large fcon beams. Three crack patterns for the small fcon beams are shown in figure A2.4. For hcp three curves of small beams and two curves of large beams are plotted in figure A2.5. Only two tests on large beams hcp were successful.

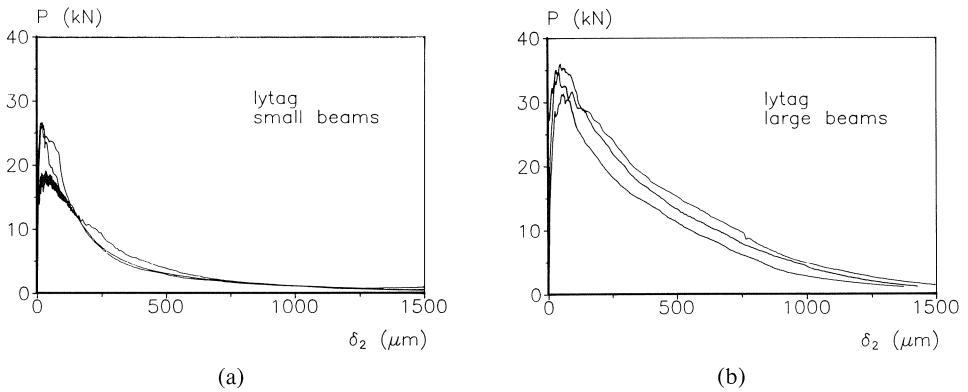

Fig. A2.1 Total load P versus δ_2 for small (a) and large (b) lytag beams.

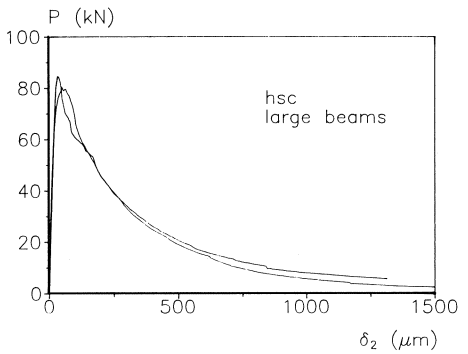

Fig. A2.2 Total load P versus δ_2 for large hsc beams.

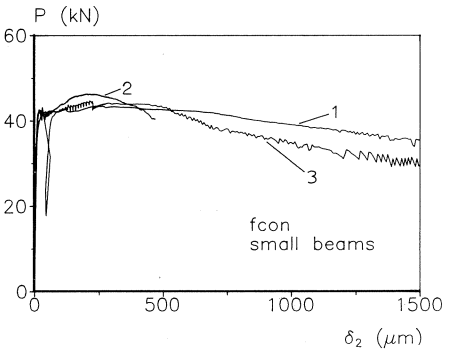

Fig. A2.3 Total load P versus δ_2 for small fcon beams.

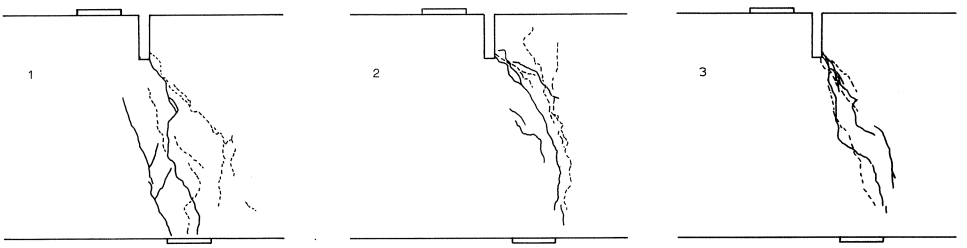

Fig. A2.4 Crack patterns in small fcon beams.

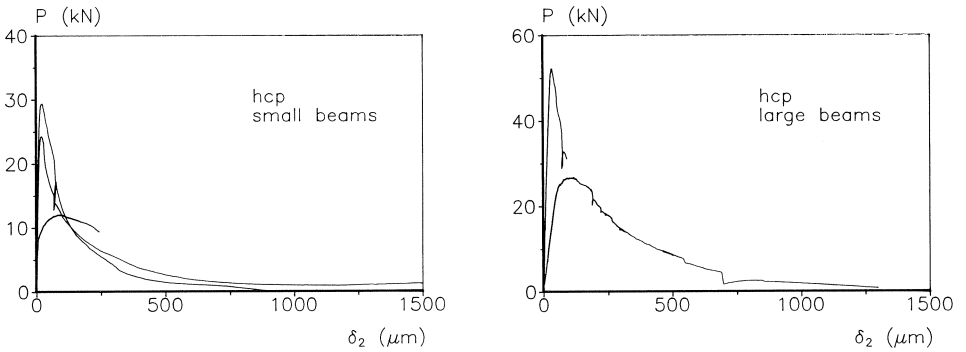

(a) (b)

Fig. A2.5 Total load P versus δ_2 for small (a) and large (b) hcp beams.

Appendix A3:

Additional experimental results of DEN beams

In appendix A3 load-displacement curves and crack patterns are presented of the DEN beams of two sizes tested between freely rotating and fixed supports. In the load-displacement curves the total load P is plotted versus the average of CMSD and CMOD measured at the two notches at the front side of the specimen. The results for the small beams are shown in figure A3.1. The crack patterns are shown in figure A3.2. In one small beam tested between fixed supports, the final splitting crack did not occur. This crack patterns belongs to the load-displacement curve with the most brittle post peak response in figure A3.1b. The load-displacement curves of the tests on the large beams are plotted in figure A3.3. The crack patterns for the large beams are shown in figure A3.4. Also for the large beams one specimen shows a different crack pattern for the tests with fixed supports. Probably the fixation of the supports was not sufficient.

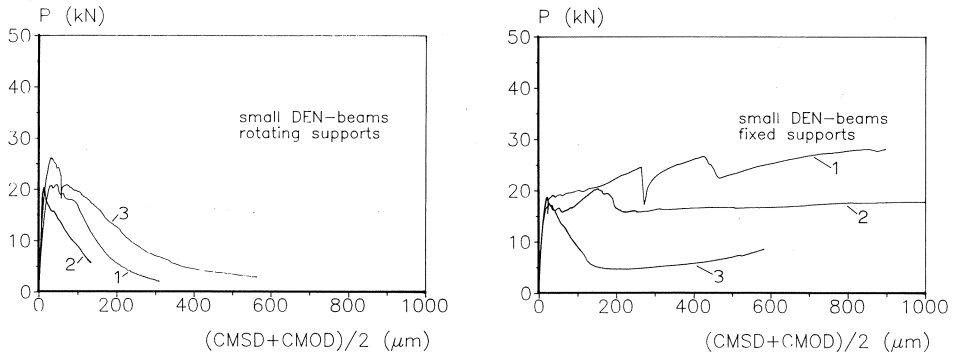

Fig. A3.1 Load-displacement curves of small DEN beams tested between freely rotating (a) and fixed (b) supports.

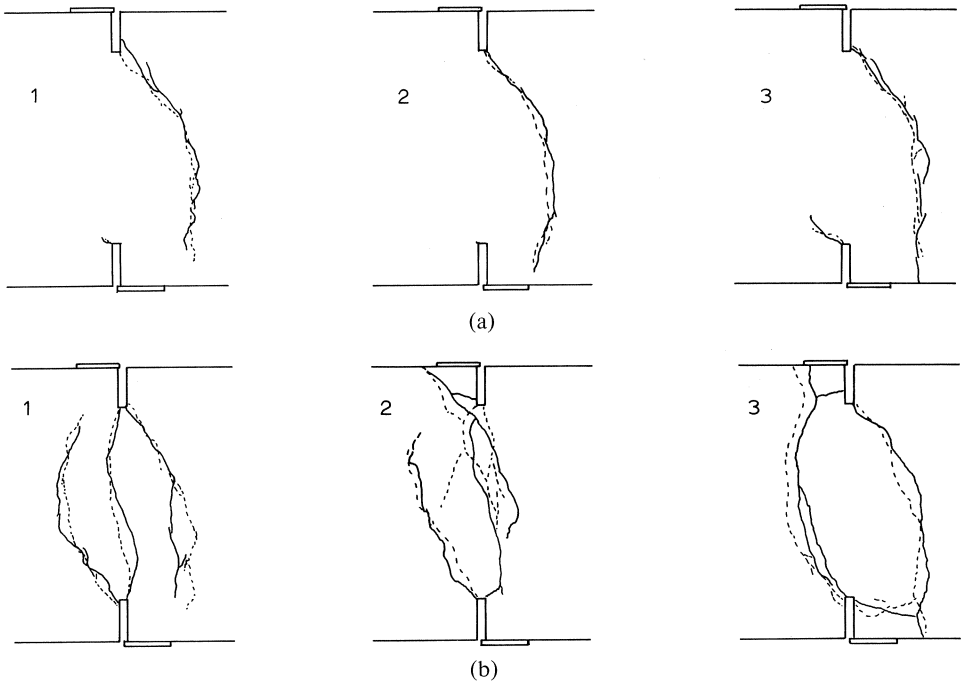

Fig. A3.2 Crack patterns of small DEN beams tested between freely rotating (a) and fixed (b) supports.

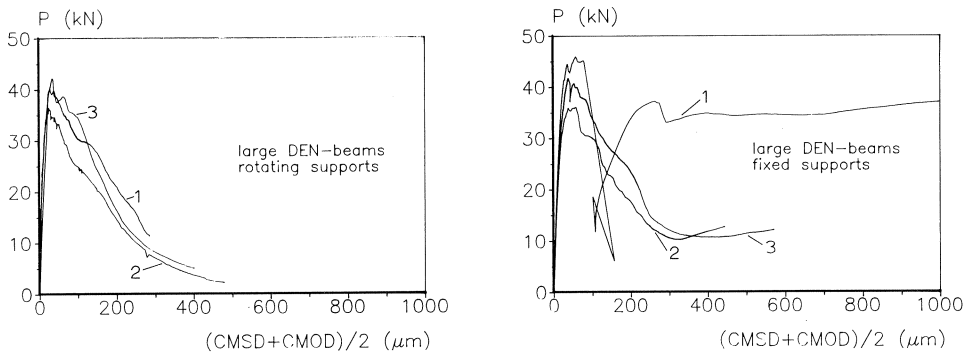

Fig. A3.3 Load-displacement curves of large DEN beams tested between freely rotating (a) and fixed (b) supports.

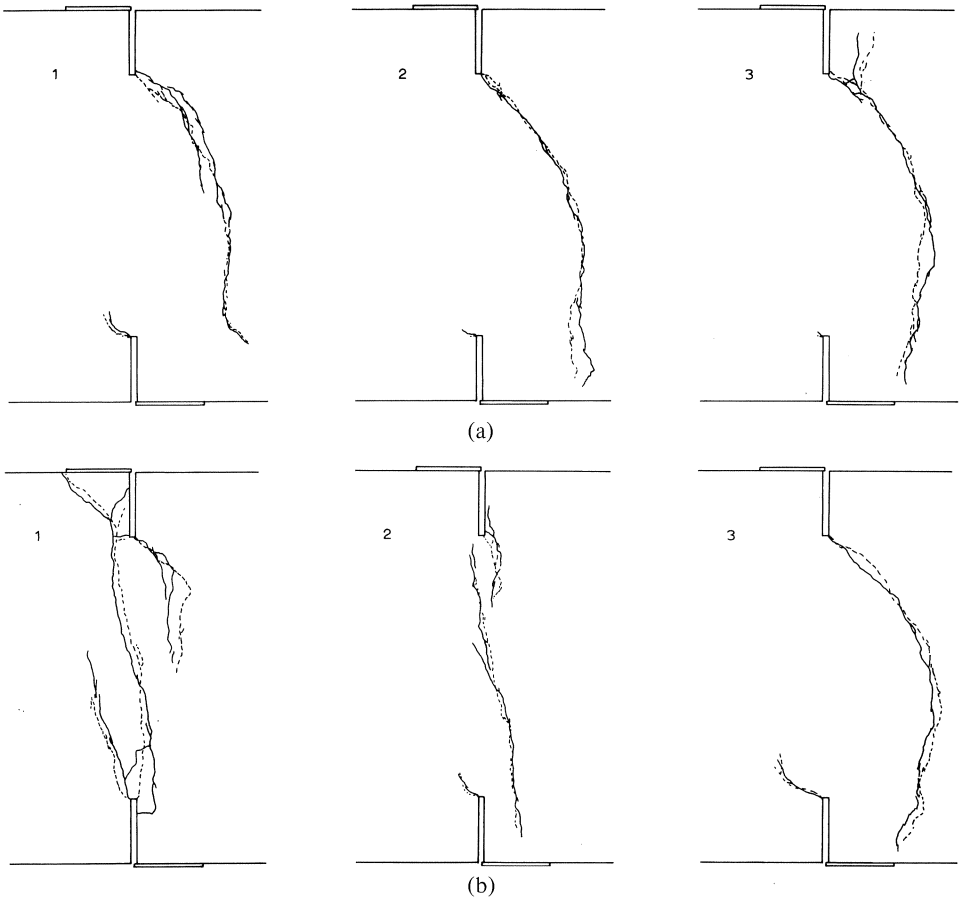

Fig. A3.4 Crack patterns of large DEN beams tested between freely rotating (a) and fixed (b) supports.